

A Computational Fluid Dynamics Investigation of Hemolysis Potential in a Microfluidic
Hemoperfusion Device Designed for Use in Sepsis Treatment

by

Karl N. Myers

A PROJECT

submitted to

Oregon State University

University Honors College

in partial fulfillment of
the requirements for the
degree of

Honors Baccalaureate of Science in Mechanical Engineering

(Honors Scholar)

Honors Baccalaureate of Arts in International Studies

(Honors Scholar)

Presented June 4th 2015
Commencement June 2015

AN ABSTRACT OF THE THESIS OF

Karl N. Myers for the degrees of Honors Baccalaureate of Science in Mechanical Engineering and Honors Baccalaureate of Arts in International Studies presented on June 4th, 2015. Title: A Computational Fluid Dynamics Investigation of Hemolysis Potential in a Microfluidic Hemoperfusion Device Designed for Use in Sepsis Treatment

Abstract Approved: _____

Kendra Sharp

The potential of red blood cell (RBC) and platelet damage was studied for a novel microfluidic hemoperfusion device currently in development at Oregon State University for use in treating sepsis. COMSOL 4.4's computational fluid dynamics (CFD) module was used to examine shear rate profiles in laminar, Newtonian blood flow throughout pre-specified lamina dimensions. The shear rates observed were converted into blood damage statistics using the average residence time and equations that estimates (1) total fraction of hemolysis and (2) critical shear stress at which hemolysis begins to take place.

The resulting hemolysis values for the current flow rate (0.3mL/min) and a hematocrit of 45% were 0.0148% of RBCs and 0.00122% of platelets. For 65% hematocrit, hemolysis values increased to 0.0511% for RBCs and 0.00591% for platelets. In terms of the critical threshold for hemolysis to start occurring, in 45% hematocrit flow, shear stresses applied to RBCs reached only 6.65% of the critical threshold for hemolysis; platelets reached 11.4% of that threshold. At 65% hematocrit, RBCs and platelets reached 11.1% and 18.9% of the critical threshold respectively. Thus, it can be initially concluded that the mechanical stresses in the current lamina design do not produce significant levels of blood hemolysis.

Keywords: cell-depleted layer, computational fluid dynamics, COMSOL, hemolysis, hemoperfusion, microfluidics, sepsis

Corresponding e-mail address: myers.karl@lifetime.oregonstate.edu

©Copyright by Karl N. Myers

June 4th, 2015

All Rights Reserved

Honors Baccalaureate of Science in Mechanical Engineering and Honors Baccalaureate of Arts in International Studies project of Karl N. Myers presented on June 4, 2015.

APPROVED:

Kendra Sharp, Mentor, representing Mechanical Engineering

Adam Higgins, Committee Member, representing Biological Engineering

Nick Fleury, Committee Member, representing the International Degree Program

Toni L. Doolen, Dean, University Honors College

I understand that my project will become part of the permanent collection of Oregon State University, University Honors College. My signature below authorizes release of my project to any reader upon request.

Karl N. Myers

ACKNOWLEDGEMENTS

I greatly appreciate my thesis mentor Dr. Kendra Sharp who gave me the opportunity to work on this amazing project and took the time to help me succeed. Dr. Matthew Ryder was a fantastic research advisor who helped guide me through the thesis process, provided an immense amount of encouragement and was someone I sincerely enjoyed working with. Dr. Adam Higgins also offered me a great deal of insight and kindness as well. Nick Fleury's advice and encouragement kept me motivated to pursue my academic goals throughout my time at Oregon State University. My undergraduate advisor Michelle Eck extended a helping hand throughout the entire time I attended OSU. Dr. Greg Herman allowed me to run simulations on his research computer. Andrew Pfau saved me more than a few times with his technical support. Eden Durant helped me out initially, but suffered a serious knee injury and was not able to assist in the later stages of my thesis.

Thank you so much to my family for cheering me on through all of the insanity over the years, I love you all dearly. A special thanks to my mother who has not only survived two battles with acute myeloid leukemia (AML), but remained strong in faith and in love for our family. She continues to be an inspiration to me and my two sisters, to pursue excellence in all that we do and to trust that God's love is not absent, despite the ever-so-apparent brokenness of this world we live in. And to my father, who lovingly stayed by her side in the face of such adversity. He is my reminder of what loyal, steadfast and selfless love ought to look like.

B.L.A. to Stephan Leung, one of my oldest and dearest friends who has truly been like a brother to me, and throughout the many stages my life. His commitment to medical research

inspires me to push myself harder. A huge mahalos to my roommates and friends who let me excitedly regurgitate my research findings, however momentarily exasperating you must have found it. And to God, who breathes life into all things, and who, despite my failings, inspires me to live in such a way that I can bless the people around me. I hold firmly these words C.S. Lewis wrote, "Faith is the art of holding on to things your reason has accepted in spite of your changing moods" (Mere Christianity).

TABLE OF CONTENTS

INTRODUCTION	1
Significance	1
Objective	2
LITERATURE REVIEW	3
Sepsis.....	3
<i>Sepsis Treatment</i>	<i>5</i>
<i>Global Occurrence of Sepsis</i>	<i>6</i>
<i>Global Mortality and Economic Costs of Sepsis.....</i>	<i>6</i>
Microchannel Hemorheology.....	7
<i>Blood Damage Models</i>	<i>8</i>
<i>Shear Stresses</i>	<i>9</i>
<i>Average Residence Time.....</i>	<i>10</i>
<i>Cell-Depleted Layer.....</i>	<i>10</i>
<i>Blood's Behavior as a Semi-Newtonian Fluid</i>	<i>13</i>
<i>Apparent Viscosity of Blood.....</i>	<i>14</i>
<i>Surface Interaction Related Platelet Activation</i>	<i>16</i>
METHODOLOGY	17
<i>Device Dimensions</i>	<i>17</i>
<i>Laminar Flow Calculations.....</i>	<i>20</i>
<i>Entrance Length Calculations</i>	<i>21</i>
<i>Residence Time Calculations</i>	<i>22</i>
Comsol	22
<i>Model Geometry.....</i>	<i>23</i>

TABLE OF CONTENTS (CONTINUED...)

<i>Mesh</i>	24
<i>Laminar Flow Settings</i>	24
RESULTS	28
<i>Comsol Generated Velocity Profiles</i>	28
<i>Comsol Generated Shear Profiles</i>	29
<i>Comsol Global Values</i>	31
Hemolysis Calculations	33
<i>CDL Effects on Platelet Hemolysis</i>	34
<i>Parametric Sweep Results</i>	35
Validation	37
<i>Validation Model Dimensions</i>	37
<i>Validation Model Mesh</i>	38
<i>Theoretical Pressure Drop Comparison</i>	40
<i>Theoretical Velocity Profile Comparison</i>	41
<i>Final Thoughts on Validation</i>	42
CONCLUSIONS	43
FUTURE WORK	45
REFERENCES	46
APPENDICES:	50

INTRODUCTION

Significance

Sepsis is a serious medical condition defined by the body's inflammatory response to infection, often leading to organ dysfunction, organ failure and death.^{1,2} Despite its obscurity to the general public, every year sepsis afflicts at least 18 million people worldwide. In the US there are about 750,000 cases of sepsis yearly with an estimated 28-50% fatality rate, and sepsis remains the leading cause of death among critically ill patients in non-coronary intensive care units (ICU).¹⁻⁷

Oregon State University is currently developing a promising method of sepsis treatment through the use of a sorbent hemoperfusion device designed to dynamically remove select targets from the blood. This device is planned to be a multilayered, multichannel apparatus composed of a biocompatible polymer coated with an experimental peptide capable of capturing gram-negative bacteria and its fragments known as lipopolysaccharide (LPS), which are a primary cause of sepsis and septic shock.^{1,8} The device bears some similarities to current hemodialysis and hemofiltration technology, but does not require the use of a dialysate or filtrate which means it would not exhaust the blood of nutrients.^{9,10} Consequently, the novel design, if proven effective, has potential to become a preferred method of sepsis treatment.

One innovative aspect of the proposed design is that it takes advantage of a phenomenon in whole blood flow known as the cell-depleted layer (CDL). The CDL

describes the thin, outmost region of blood flow, where red blood cells rarely enter due to their natural tendency to aggregate in the center of a laminar micro-scale flow profile.¹¹⁻¹⁵ The CDL is instead occupied primarily by blood plasma, which in the case of sepsis patients would include blood toxins such as gram-negative bacteria and LPS that get pushed out as a result of RBC migration toward the center of blood flow.¹¹ The significance of the CDL is that it interfaces with the design's proposed peptide coating, maximizing the potential of bacteria and LPS to peptide adsorption. It is important to note that if the design is a success, this method of dynamic blood purification may be expanded beyond the removal of gram-negative bacteria to include the removal of any toxin that could be adsorbed from blood plasma through an applicable surface coating.

Objective

One important consideration for any new hemoperfusion device is potential blood damage. For OSU's new hemoperfusion device to be considered a viable method of sepsis treatment, any significant hemolysis of RBCs is unacceptable, because it can quickly result in patient mortalities.^{16,17} It is also important that the blood platelet integrity is maintained so that the device does not get clogged by platelets, or worse contribute to medical complications for the person being treated.¹⁸ In general, blood integrity is one of the highest concerns.

Therefore, the primary objective of this study was to mitigate any concerns that the mechanical shear stress in the current design will produce an unacceptably high level of harm to RBC and platelet integrity. An investigation of flow rate dependent

shear rates and residence times within the device prototype was conducted using COMSOL 4.4 Computational Fluid Dynamics (CFD). The results from the CFD module were used to predict potential blood damage within the current design specifications using power law equations that estimate blood damage (see equations 1-4)¹⁹⁻²¹ This investigation also compiles a great deal of literature on the subject. It takes into account the potential of the CDL to amplify shear stresses above what the COMSOL model shows. It also accounts for the effect of elevated hematocrit on the apparent viscosity of blood in microchannel flow and its subsequent amplification of shear stresses that contribute to hemolysis.

The secondary objective was to develop a computational fluid dynamics model that could be adapted to the needs of the project as the device is likely to undergo various design iterations. The model developed within COMSOL 4.4 meets this objective as it provides a framework for use in future blood flow investigations. Moreover, all the fundamental settings of the CFD model have been recorded in this study so that even if the original file is misplaced, the results can still be replicated.

LITERATURE REVIEW

Sepsis

Sepsis is a variation of systemic inflammatory response syndrome (SIRS) due to the presence of a bodily infection for which there are three severity levels: sepsis, severe sepsis and septic shock. A patient is diagnosed with SIRS when two out of four of the following medical symptoms manifest: (1) body temperature leaving the range of 36-38° C; (2) heart rate increasing to over 90 beats per minute; (3) tachypnea occurring as indicated by over 20 breaths per minute or hyperventilation, when PaCO₂ drops below 32 mm Hg; and (4) white blood cell count (WBC) leaving the range of 4,000-12,000 per cubic mm.^{1,22} However, SIRS is not always sepsis, as shown in the Venn diagram developed by Bone et al. in figure 1:

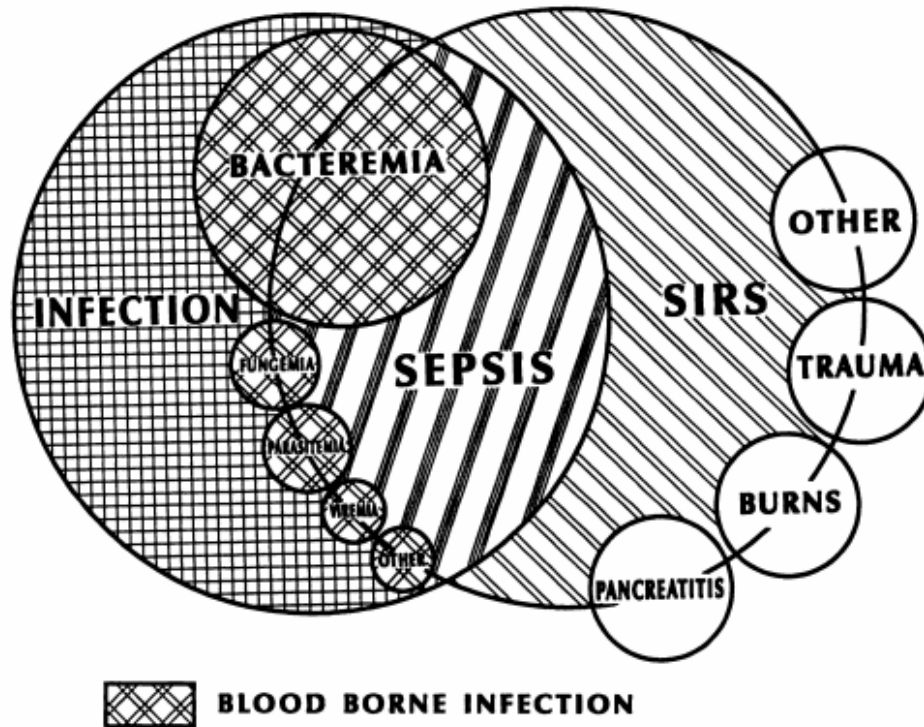


Figure 1: Visualization of the overlap between sepsis and similar conditions. The small text bubbles that reside between infection and sepsis read "fungemia," "parasitemia," "viremia" and "other." Figure from Bone et al.²²

SIRS is recognized to be sepsis as soon as an infection is confirmed.¹⁻³ SIRS in sepsis is brought on by a large number of potential factors, but most often by the presence of bacterial endotoxin (i.e. LPS) that come from the breakdown of gram-negative bacteria and results in the activation of the body's pro-inflammatory cytokines.^{1,23-25} In layman's terms, sepsis manifests as inflammation because of the body's aggressive response to a serious infection.^{2,22,23} Sepsis is considered to be severe sepsis when the symptoms of SIRS are also paired with organ dysfunction, hypoperfusion, or hypotension.^{1,22} This happens when the body's continual production of pro-inflammatory cytokines cause endothelial necrosis – which is the destruction of

the blood vessel wall – causing blood to permeate the vessels and wreak havoc on the organs.²⁴ If severe sepsis persists, it may advance to the last and most fatal stage: septic shock. Septic shock occurs when hypotension continues regardless of adequate fluid resuscitation due to continuous vascular permeability; if septic shock persists, the patient will undergo organ failure and die soon after.^{22,24}

Sepsis Treatment

Presently, sepsis treatment relies on the use of broad-spectrum antibiotics and symptom management using fluid resuscitation and regulation, oxygen therapy, often paired with vasopressors, inotropes and anti-inflammatory agents.^{5,26,27} If possible, the source of the infection may be removed through surgery.²⁶ The primary drawback to treating sepsis with antibiotics is that they take time to enter the bloodstream, and ongoing symptom management is taxing on both the patient and the medical staff.^{26,27} The development of antibiotic resistant bacteria can make treating sepsis especially difficult.¹

Two reasons why hemoperfusion may hold the key to sepsis treatment are (1) it focuses on the removal of gram-negative bacteria molecules, the root cause of harmful SIRS symptoms; and (2) the development of bacterial resistance is not an issue since the hemoperfusion device simply captures bacteria within a peptide coated wall. Hemoperfusion could be used in conjunction with antibiotics for increased effectiveness.

Global Occurrence of Sepsis

Every year sepsis afflicts at least 18 million people worldwide.³ This number is likely too conservative as many developing countries, lack the medical infrastructure to accurately gather and report sepsis incidence and mortality data.⁶ The Global Sepsis Alliance estimates the number of worldwide cases of sepsis to be 30 million, which is probably more accurate.²⁸ In the US, the annual incidence rate is estimated to be 300 per 100,000 people (for an approximate total of 750,000).^{1,3-5,7} Sepsis occurrence appears to be slightly lower in European countries.^{6,7} In a report put together by The Centre for Population Health Sciences of the University of Edinburgh Medical School detailing sepsis incidences worldwide, the reported sepsis occurrence rate across US, Brazil, the UK, Norway and Australia was found to be somewhere between 149 to 240 people per 100,000.⁶ Although limited information exists regarding developing countries, the report also deduced that more than 1 in 1000 people in developing countries develop sepsis each year.⁶ As for the lowest-income countries, there appear to be no studies that assess incidence, prevalence, mortality or morbidity.⁶

Global Mortality and Economic Costs of Sepsis

Across the developed world, sepsis mortality rates can reach 30% for sepsis, 50% for severe sepsis and 80% for septic shock.⁶ Despite the lack of studies in lower income and developing countries, one may assume that the mortality rate is likely to be higher in countries with under-developed medical infrastructures, since sepsis survival is highly dependent on the quality of medical care available.^{26,27} If the loss of life is not

staggering enough, sepsis is a drain on the global economy as well. Data suggests that the annual cost of patients with septicemia is nearly \$17 billion in the US with an average hospitalization stay of 19.6 days.^{1,5} For countries with highly developed healthcare systems the average total cost to the ICU per day in 2003 was anticipated to be about \$1,400 (converted from the Euro at € 1 = \$US1.15).⁷ What is overwhelming about this data is that 70-80% of the cost associated with sepsis is attributed to productivity losses in hospital staff due to patient mortalities.⁷ In less-developed countries, sepsis cannot be quantified in financial cost or even accurate mortality rates, but there is no doubt that the loss of life due to sepsis affects people across the world.

Microchannel Hemorheology

In order for a computational fluid dynamics model to provide a good representation of the damage that whole blood might undergo within a hemoperfusion device, it is important to first understand the power models that estimate blood damage. Next it is important to review the basic equations used to calculate the shear stress values in blood and residence time in the device. Then, the phenomena which affect blood flow will be explored. These phenomena include the cell depleted layer (CDL), shear dependent Casson-to-Newtonian flow transition, the change in apparent viscosity due to the diameter restrictions of microchannel flow, and the other considerations that make determining platelet damage considerably complex.

Blood Damage Models

In order to estimate shear induced damage of both RBCs and platelets in the hemoperfusion device's microchannels, a series of equations will be used. Equations 1 and 2, proposed by German scientist Giersiepen²⁰ derived from a 2D regression analysis based on Wurzinger's experimental data.^{19,29,30} These equations are popular because they overestimate the fraction of RBC and platelet destruction in laminar whole blood flow.¹⁹ Goubergrits et al. confirm that the power contestants used in equations 1 and 2 are accurate because they reflect the mechanical properties of blood cells, but point out that a defective seal in the Wurzinger experiments cause overestimation to be one whole order of magnitude.³⁰

For part of this study, the average shear stresses and residence times of blood in the prototype hemoperfusion channels will be entered into equations 1 and 2 as prescribed by Goubergrits et al. in order to estimate the total fraction of hemolysis.³⁰

$$D_{RBC} = 3.62 * 10^{-5} * t_{res}^{0.785} * \tau_{ave}^{2.416} \quad (1)$$

$$D_{Platelets} = 3.66 * 10^{-6} * t_{res}^{0.77} * \tau_{ave}^{3.075} \quad (2)$$

In equations 1 and 2 damage (D) of both RBCs and platelets is measured as a lysis fraction (0-1), t_{res} is the average residence time within the device in seconds, and τ_{ave} is the average shear stress experienced by the cells in Pascals.²¹

The second set of equations 3 and 4, use the critical threshold approach, or what Goubergrits¹⁹ calls the 'all or nothing' evaluation of blood damage. These equations are

supported by more experimental data than equations 1 and 2¹⁹ and instead use only the residence time of blood to determine the maximum shear stress at which blood cells begin to undergo noticeable damage.¹⁹

For equations 3 and 4, the average residence time of the blood can be entered in order to find the respective hypothetical critical shear stress rates ($\tau_{RBCcrit}$ and τ_{Pcrit} for RBCs and platelets respectively) at which cell integrity would to be destroyed.¹⁹ The maximum shear stress observed in the prototype device will then be compared to the critical shear stress as a measure of how close the device might be to inducing hemolysis.

$$\tau_{RBCcrit} = 88.905 * t_{res}^{-0.3372} \quad (3)$$

$$\tau_{Pcrit} = 54.986 * t_{res}^{-0.3585} \quad (4)$$

Shear Stresses

In this study basic shear stress is calculated using the shear rate values acquired from COMSOL and multiplying them by the apparent viscosity of blood within the device's microchannels. Equation 5 describes this conversion where shear stress is given by τ , shear rate by γ and apparent viscosity by μ_{app} .

$$\tau = \gamma * \mu_{app} \quad (5)$$

Equation 5 will be used to calculate both the average shear stress felt by blood within a microchannel and maximum shear stresses. The average shear stress will be applied to

equations 1 and 2, whereas the maximum will be used to determine if any point in the channel exceeds the critical shear stresses obtained from equations 3 and 4.

Average Residence Time

Since this study examines blood damage as a function of residence time, it is important to review equation 6 which will be used to determine the average residence time within the device. In equation 6, the priming volume describes the volume of space the flow has to fill before it exits the lamina. Thus, in incompressible flow, a constant flow rate can be used to obtain the average residence time for a known priming volume.

$$\text{Average Residence Time} = \frac{\text{Priming Volume}}{\text{Flow Rate}} \quad (6)$$

Equation 6 can be considered a very good measure of the average RBC residences, however, there is some ambiguity surrounding its measure of platelet residence time due to the tendency of platelets to migrate to outside of the flow where the velocity is the lowest. This will be explained in the following section by the presence of the CDL

Cell-Depleted Layer

The formation of the cell-depleted layer (CDL), also called the cell-free layer (CFL), is a phenomenon that takes place in laminar whole blood flow in which RBCs migrate away from the wall and toward the center of the flow channel.¹¹⁻¹⁵ This affinity to gather in the center of flow is a result of the geometry and deformability of RBCs.¹² As a result

of RBC aggregation, other blood constituents are pushed to the outside of flow, creating the CDL, a region of RBC depletion.¹² The CDL has the lowest apparent viscosity within the flow diameter and contains highest concentration of platelets and blood plasma.^{11,12,14,15} The size of this region is dependent on the degree of RBC aggregation, hematocrit, RBC morphology, flow channel diameter, the presence or absence of an endothelial glycocalyx layer, flow rate and laminar flow conditions that allow the CDL to form.^{12,14}

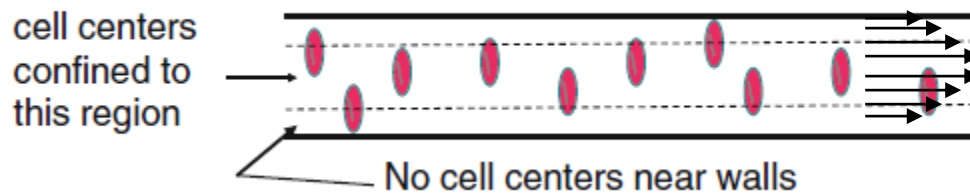


Figure 2: Visualization of the CDL (Cell Depleted Layer). Diagram adapted from Rosell et al.³¹

One important aspect of the RBC aggregation and the resulting CDL to consider is its impact on cell residence time.^{12,14,31} The impact on cell residence time is a result of RBCs monopolizing the center of flow and pushing the other components of blood to the outside of the flow profile. In laminar microchannel flow, the velocity approaches zero near the channel walls. Thus, if platelet rich plasma is pushed to the outer diameter of flow it will move through the channel at a much slower rate than the RBCs.^{12,31} This is extremely relevant because the percent hemolysis and critical shear stress models use the residence time to calculate cell lysis data.^{19,21} There does not appear to be any literature that examines the changes in estimated platelet damage based on the

presence of the CDL; however, by modifying equation 4 it is possible to find the critical residence time of a platelet stuck in the CDL.

$$(t_{res})_{crit} = 7.1378 * 10^4 * \tau_{wall}^{-2.789} \quad (7)$$

The critical residence time, calculated in equation 7, uses the wall shear stress to approximate the length of time a platelet would have to be stuck in CDL before it underwent significant damage.

Another consideration of the CDL is its potential amplification of shear stress. The potential of the CDL to amplify shear stress is due to the low cell concentration as illustrated in figure 3. The low-viscosity region between the RBC layer and the CDL has an impact on the shear stress felt by the plasma in the CDL.

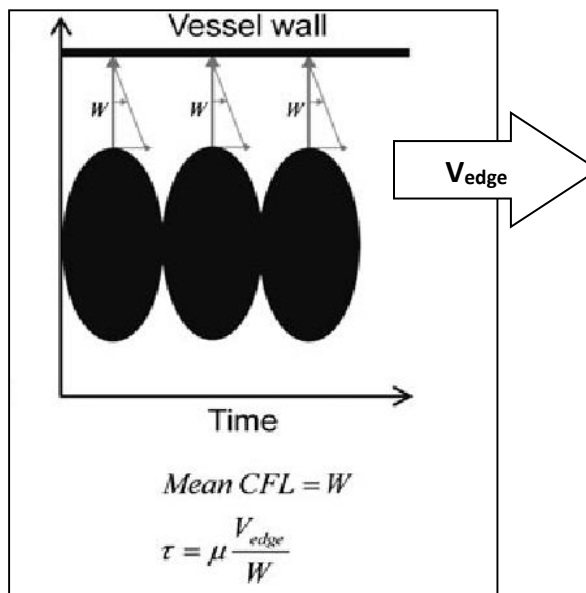


Figure 3: A 2D sketch of red blood cells (marked in black) moving with velocity V_{edge} through a channel, illustrating the effect of the CDL (CFL in the diagram) on wall shear stress. Here τ is shear stress and μ is the plasma viscosity. Diagram adapted from Namgung et al.¹⁴

Figure 3 was developed by Namgung et al.¹⁴ in a study which demonstrated that shear stress could be reduced by increasing the size of the CDL layer. In order to account for this, the near edge velocity of the flow can be used to approximate shear stress. This will be done using equation 8 taken from figure 3.

$$\tau = \frac{\mu_{plasma} V_{edge}}{W} \quad (8)$$

It must be considered that a platelet trapped in the CDL, could experience an amplified shear stress. The maximum shear stress a platelet could experience in the situation described in figure 3 occurs when the width (W) of the CDL is equal to the platelet thickness, or about 1 μm .³² For the edge velocity of the RBCs (V_{edge}) it seems sensible to use the velocity of the RBC center in the flow profile. Remembering that velocity increases towards the center, it will be best to use the velocity of flow 5 μm from a wall. This accounts for the 1 μm width plus the 4 μm radius of an RBC.³³ The calculation can be seen in equation 22 of the results section.

Blood's Behavior as a Semi-Newtonian Fluid

Blood can be considered a semi-Newtonian fluid as it behaves both as a Newtonian and a Casson fluid depending on the flow conditions.³¹ The transition from Casson to Newtonian flow is primarily dependent on the average shear rate of blood which can be determined by the graph in figure 4 (note that the square root of the shear rate has been used by the author for graphing purposes).

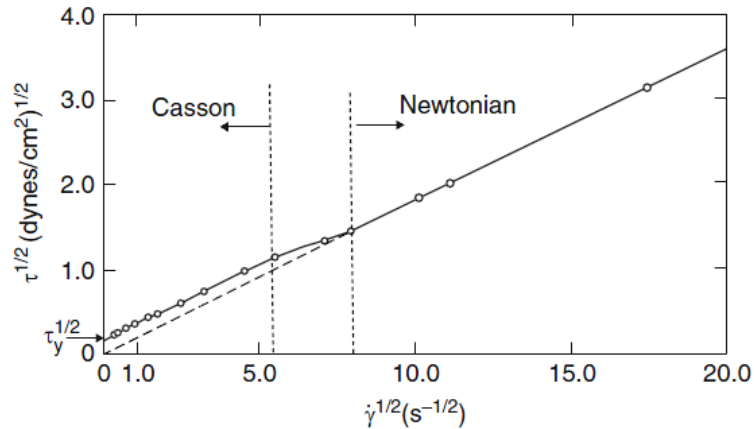


Figure 4: A shear dependent Casson-to-Newtonian transition plot for whole blood, where hematocrit= 40% and temperature is 37°F. Diagram from Roselli et al.³¹

As shown in figure 4, blood behaves as a Newtonian fluid so long as it is acted on by an average square root shear rate above $7 \text{ s}^{-1/2}$. When converted from the average square root shear rate to average shear rate instead, this rate is approximately 50 s^{-1} . Thus, so long as blood in a channel is undergoing an average shear rate over 50 s^{-1} (which happens to be the case) it is reasonable to assume that the blood is behaving as a Newtonian fluid.

Apparent Viscosity of Blood

The dependence of blood's dynamic viscosity on flow channel radius is known as the Fåhræus–Lindqvist effect. The effect is named after Robin Fåhræus and Torsten Lindqvist, the two Swedish scientists who first recorded the effects of forcing blood through glass capillaries with diameters less than $250\mu\text{m}$ under relatively high shear rates ($\gamma_{\text{ave}} \geq 100 \text{ s}^{-1}$).³⁴ The Fåhræus–Lindqvist effect is most applicable to blood flow

while it is behaving as a Newtonian Fluid ($\gamma_{ave} \geq 50 \text{ s}^{-1}$).^{31,35} From the experimental data of Pries et al., figure 5 was generated describing the relative viscosity in laminar flow through various microchannel diameters, where relative viscosity is the ratio between the apparent viscosity observed and the blood plasma's viscosity.

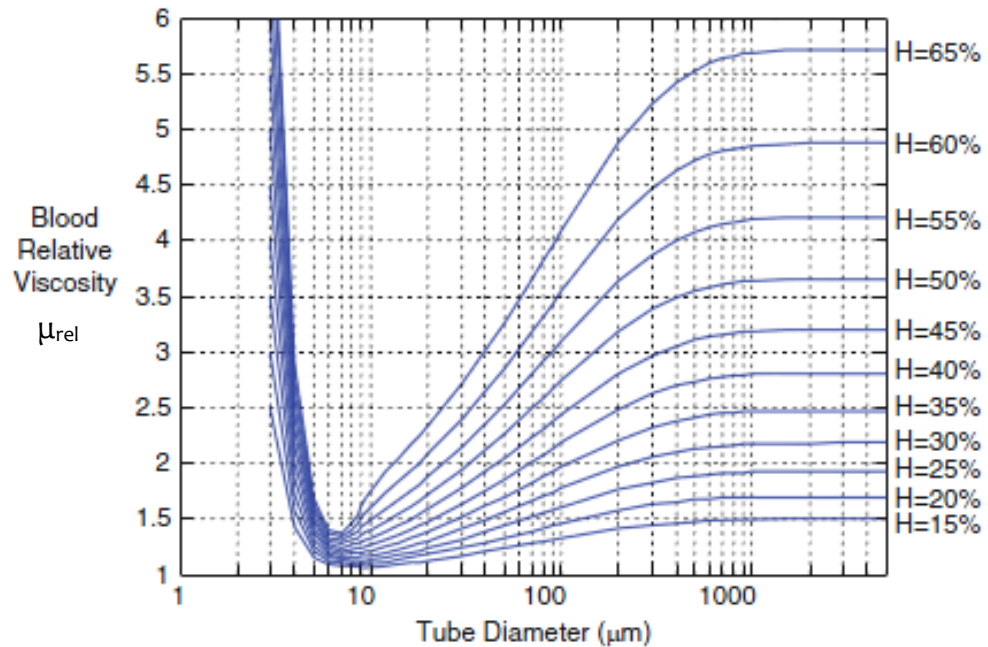


Figure 5: Graph of the relative viscosity (μ_{rel}) in comparison to blood plasma as a result of changing channel diameters of small tubes for various hematocrit percent values (H). Adapted from Roselli et al.³¹

From figure 5 it is possible to determine the relative viscosity of blood based on the hematocrit and hydraulic diameter. This relative viscosity (μ_{rel}) can be transformed into apparent viscosity (μ_{app}) using equation 9. Thus, for an average male adult hematocrit of 45%,³⁶ in a channel with a hydraulic diameter equal to $88.8 \bar{\mu}\text{m}$, the relative viscosity will be approximately 2.4.

$$\mu_{app} = \mu_{rel} * \mu_{plasma} \quad (9)$$

The range of values for the viscosity of plasma at 37°C happens to be quite narrow: 1.10–1.30 mPa-s.³⁷ Plasma viscosity is also independent of age and gender, hematocrit, cell aggregation, and hemoglobin defects (e.g. sickle cell anemia).³⁷ Since the aim of the study is to be conservative, and higher viscosity means higher shear stress (as seen previously in equation 5) 1.30 mPa-s will be chosen to represent the plasma viscosity. By using the plasma value in equation 9 for the previously calculated relative velocity of 2.4 (for a 45% hematocrit and a hydraulic diameter of 88.8 μm) the apparent viscosity is found to equal 3.12mPa-s, as seen in equation 10:

$$\mu_{app} = 2.4 * 1.3mPa \cdot s = 3.12mPa \cdot s \quad (10)$$

This happens to be the apparent viscosity used for the majority of calculations made throughout this study since a 45% hematocrit is a good representation of an average hematocrit in adult males³⁶ and 88.8 μm is the hydraulic diameter in the current prototype lamina channels.

Surface-Interaction Related Platelet Activation

Platelets may activate due to shear stresses, as discussed in the blood damage model section, however there are many more factors at work in platelet activation. Blood contains many hundreds of multifunctional proteins, and the protein fibrinogen has been identified as the primary mediator between biomaterials and surface-induced thrombosis. As blood flows over a biomaterial surface, plasma proteins typically adsorb

to the surface³⁸ and this layer of proteins is likely to encourage platelet adhesion to the walls. This layer of proteins will be problematic if (1) it facilitates clotting within the device or (2) it inhibits the bacteria to peptide adsorption. In general, biomaterial and blood interaction is the biggest contributor to protein adhesion.³⁸⁻⁴⁰ Through testing polymeric surfaces such as poly(methyl methacrylate) (PMMA), polystyrene (PS) and poly(dimethylsiloxane) (PDMS), it has been found that plasma protein adsorption is higher on lower energy substrates.^{39,40} This means that hydrophobic surfaces tend to repel water molecules and adsorb a greater amount of plasma proteins in comparison with hydrophilic surfaces where the water is not so easily displaced. It is apparent that both the material and peptide interactions with blood could have a large role in determining the success of a hemoperfusion device.

METHODOLOGY

Device Dimensions

The present hemoperfusion device is envisioned as a series of peptide-coated biocompatible polymer lamina stacked into layers and housed in a biocompatible plastic casing. Blood infected with gram-negative bacteria and endotoxin is to be pumped out of the body, directly into the device, and then back into the body. The extracorporeal treatment loop itself is comparable to ones currently used by hemodialysis and hemofiltration techniques. The primary difference from a conventional approach is in

the filtration method. As the whole blood interfaces with the plastic lamina, gram-negative bacteria is to be adsorbed by the peptide surface coating. A picture detailing the device can be seen in figure 6.

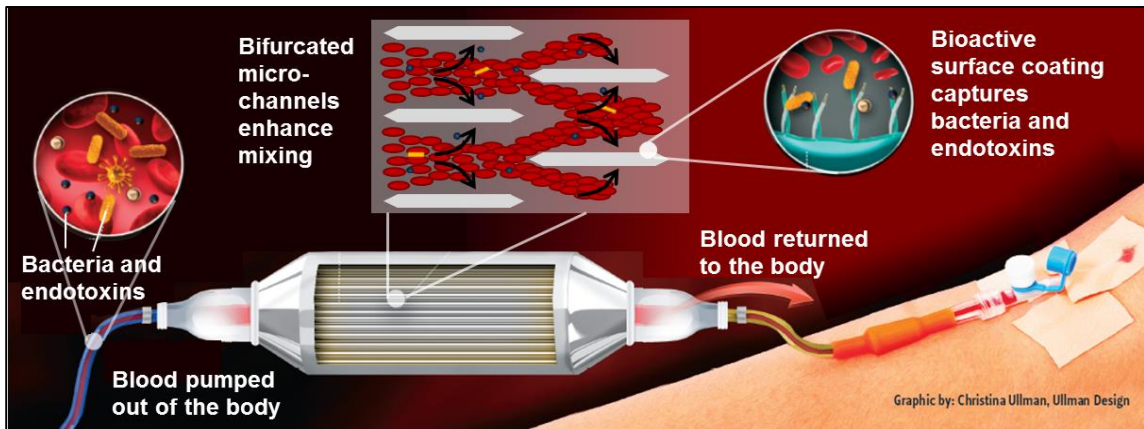


Figure 6: Visual representation of the hemoperfusion device design (image designed by Christina Ullman).⁴¹

Currently, the hemoperfusion device lamina are in the prototyping stage. Individual lamina are manufactured by laser cutting thin sheets of polycarbonate. The dimensions of the channel array are 6 cm long \times 2.5 cm wide with a total priming volume of 0.065 mm. The length of a single channel is 4 mm for a total of 15 channel lengths per device. A visual description of the current geometry is shown in figure 7.

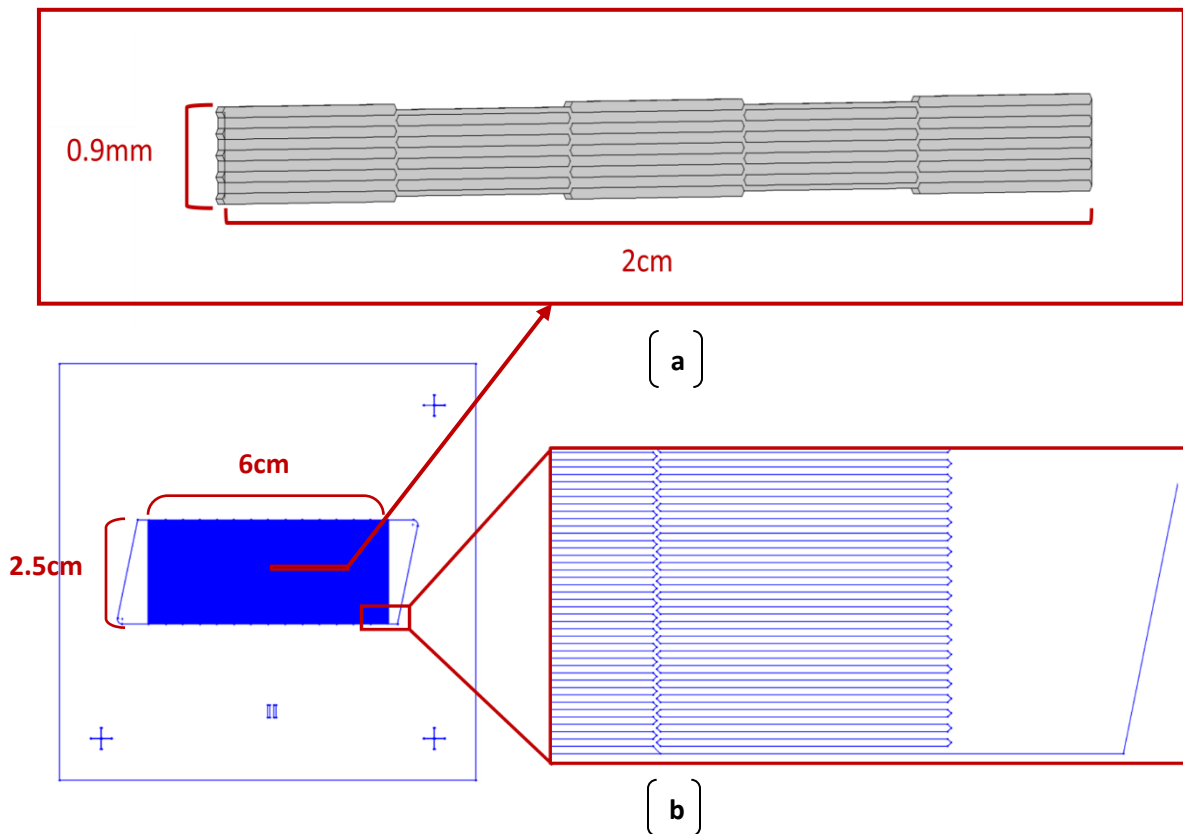


Figure 7: Lamina geometry. (a) is the model created in COMSOL which represents a non-specific portion in the middle of the lamina. (b) is the team's CAD drawing of the current geometry.⁴²

There are 125 channels in the inlet. This number changes to 123 and back to 125 every other bifurcation as can be seen in figure 7b. In a single lamina, each individual channel is $100\ \mu\text{m}$ wide \times $80\ \mu\text{m}$ deep. The material separating each channel shares the same width and depth. Then at the bifurcation, the flow is split into two by right triangle heads as seen in figure 8.

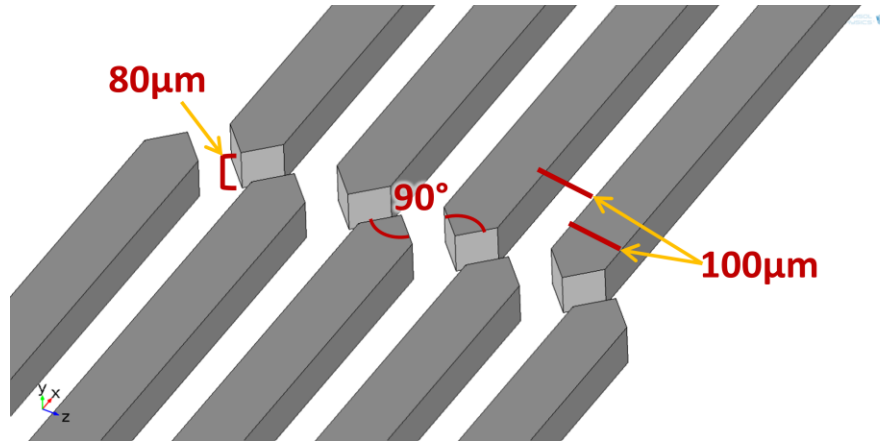


Figure 8: Geometry of the bifurcation region in the lamina, created in COMSOL.

Laminar Flow Calculations

A bulk flow rate of 0.3 mL/min is currently specified for each lamina. When divided by the number of inlets and the cross sectional area of a channel that translates to an average velocity of 0.5 cm/s in the straight channels. In order to confirm that the flow was laminar in the channels, equation 11 was used to calculate the Reynolds number.⁴³

$$Re = \frac{\rho V D_H}{\mu_{app}} \quad (11)$$

In equation 11 Re is the Reynolds number, V is the average velocity of 0.5 cm/s, ρ is 1060 kg/m³ (the density of whole blood at 37°C) and μ_{app} is the apparent viscosity 3.12 mPa-s obtained previously in equation 10 using the channel's hydraulic diameter.^{31,44}

The hydraulic diameter calculation is shown below in equation 12.

$$D_H = \frac{4A}{P} = \frac{4 * 80 * 100}{360} \mu m = 88.\bar{8} \mu m \quad (12)$$

If the values obtained in equations 11 and 12 are entered into equation 13, the Reynolds number can be determined:

$$Re = \frac{1060 * 0.5 * 88.8}{3.12} \frac{kg * cm * \mu m}{m^3 * s * mPa * s} = 1.51 \quad (13)$$

With a Reynolds number of 1.51 it is certain that the flow is laminar. Next, it is important to determine the flow development entrance length to see if it will have an effect on the flow profile.

Entrance Length Calculations

Entrance length was determined using equation 14 which reuses the Reynolds number and hydraulic diameter found in the previous section.⁴⁴

$$l_e = 0.06Re * D_H = 0.06 * 1.51 * 88.8 \mu m = 8.05 \mu m \quad (14)$$

Given an entrance length of 8.05 μm it is safe to neglect the entrance length when considering velocity flow profile, since the average velocity stays constant and the developing flow profile only represents 0.2% of the first 4 mm channel. However, the re-development length after a bifurcation has the potential to be more relevant as the flow must re-develop slightly after every change in diameter. However, after running the COMSOL analysis this was discovered to be approximately 39 μm and only about 1% of a single channel which is still fairly negligible. This re-development length is likely longer than the entrance length calculated because the velocity profile changes significantly in each bifurcation (see the profile developing in Appendix E).

Residence Time Calculations

In order to determine the average residence time of whole blood in the channels the priming volume is divided by the flow rate as seen previously in equation 6. In the current lamina priming volume is equal to 0.065 mL and the flow rate is set to 0.3mL/min such that residence time that will be entered into the blood damage equations 1-4 is equal to 13 seconds. This calculation can be seen below in equation 15:

$$\frac{0.065 \text{ mL}}{0.3 \text{ mL}} \text{ min} * \frac{60 \text{ s}}{\text{min}} = 13 \text{ seconds} \quad (15)$$

COMSOL

The Computational Fluid Dynamics module of COMSOL 4.4 was used for the purpose of analyzing blood flow in the hemoperfusion device's channels, in order to generate numerical solutions for velocity and shear in the filter's chambers and bifurcations, and to generate visual representations of the data. COMSOL uses an iterative method called general minimal residual (GMRES) to solve a nonsymmetric system of linear equations. This method approximates the solution using Krylov subspace with minimum residual and Arnoldi iteration.⁴⁵ It is important to note that GMRES is an approximation, meaning that the exact solution can only be obtained with infinite precision.⁴⁶ Nevertheless, if a reasonably fine mesh is implemented, the answer is considered to be an excellent approximation.

Model Geometry

For the geometry of the lamina it was determined that the dimensions would represent flow in the middle of the channel (seen previously in figure 7). This is indeed a good approximation because the flow conditions are symmetric and consistently laminar in the device and the entrance length is negligible (see equation 14). Although 3D geometries can be imported into COMSOL from computer-aided design (CAD) software, the geometry was built in COMSOL 4.4 itself to avoid any issues with compatibility. The geometry reflects a non-specific region in the inside of the filtration device with a total of 5 channels and 4 bifurcations.

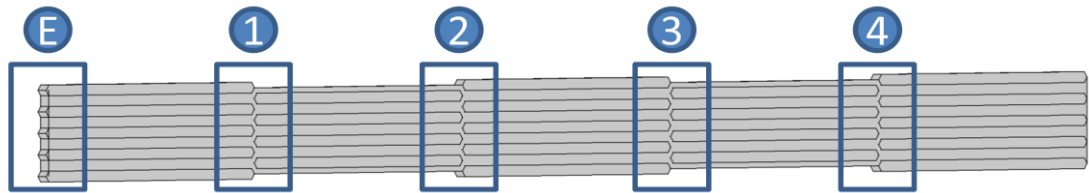


Figure 9: Diagram of the lamina geometry as it appears in COMSOL with the entrance (E) and 4 bifurcations highlighted (1-4). Refer back to figure 7 for a visualization of the channel and bifurcation dimensions.

This geometry was built by sketching one first row and one second row channel divider and then creating an array for each of them. After extruding them, the fluid area was filled in by extruding a simple rectangle across the array. All geometries were finalized using the default "form union" option. Any unnecessary overlapping lines that would affect the mesh were ignored using the virtual operation "ignore vertices" feature in the geometry tab.

Mesh

After the geometry was finalized, the fluid portion of the model was meshed. The mesh size was custom set to a maximum of 8 μm , minimum element size of 0.15 μm , maximum element growth of 1.05, a curvature factor of 0.2 and a setting of 1 for the resolution of narrow region. This created a mesh of 21,370,481 domain elements, 1,176,734 boundary elements and 47,052 edge elements as seen in figure 10.

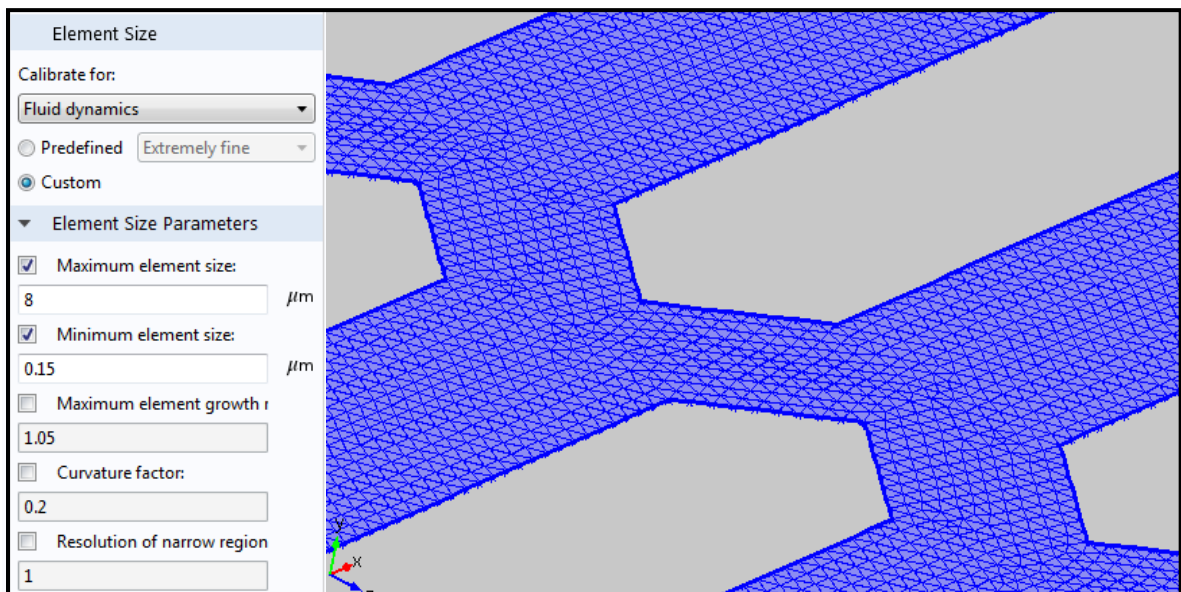


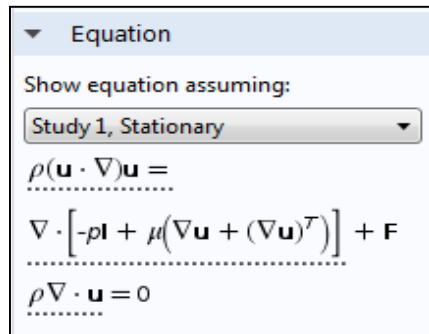
Figure 10: Shows the actual mesh generated in COMSOL to solve for velocity and shear values.

Laminar Flow Settings

In order to aid in the critique or potential reproduction of this study, the exact settings and equations offered in COMSOL CFD are contained in this section. For the extra settings and optional features in COMSOL that were not covered here the default settings of COMSOL 4.4 was applied.

Fluid Properties

For the laminar flow settings, the fluid properties were set to that of blood with an average density of 1060 kg/m³ and an apparent viscosity of 3.12 mPa-s. The apparent viscosity is considered constant because the hydraulic diameter only increases in the bifurcations which make up a mere 2.5% of a channels. Since blood flow in a larger hydraulic diameter would have a lower apparent viscosity, it would also incur lower shear stresses. Thus, keeping the viscosity constant simply serves to increase the safety factor of the calculations. COMSOL uses the Navier-stokes equations as shown in figure 11.



Equation

Show equation assuming:
Study 1, Stationary

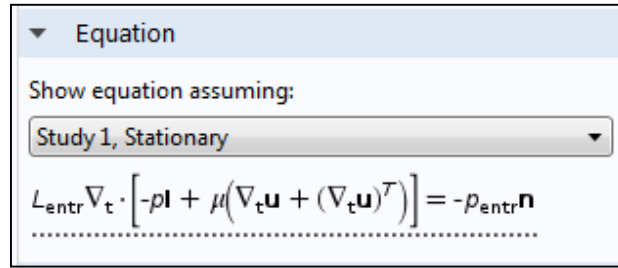
$$\rho(\mathbf{u} \cdot \nabla)\mathbf{u} = \nabla \cdot [-p\mathbf{I} + \mu(\nabla\mathbf{u} + (\nabla\mathbf{u})^T)] + \mathbf{F}$$

$$\rho \nabla \cdot \mathbf{u} = 0$$

Figure 11: COMSOL's Navier-stokes equations shown in the fluid properties section.

Inlet Conditions

The boundary condition was set to laminar inflow. The average velocity option was selected and average velocity was set to 0.5 cm/s. Entrance pressure was set to zero. The entrance length was also set to zero, although it was later learned that re-development after a bifurcation takes 39 μm (see Appendix E). This length equates to about 1% of a channel and has a small impact. The equations for this section are contained in figure 12.



Equation

Show equation assuming:

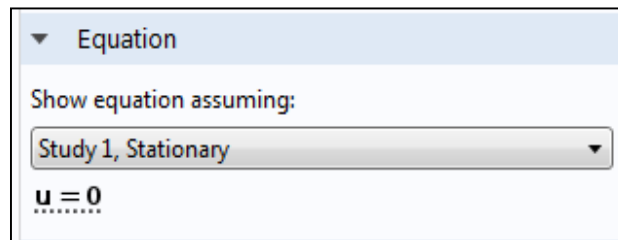
Study 1, Stationary

$$L_{entr} \nabla_t \cdot [-p\mathbf{I} + \mu(\nabla_t \mathbf{u} + (\nabla_t \mathbf{u})^T)] = -p_{entr} \mathbf{n}$$

Figure 12: COMSOL's given equation for the inlet section.

Wall Conditions

The wall conditions were set to no-slip, meaning that the velocity at the channel wall is equal to zero. A no-slip wall condition provides a more conservative estimate because it contributes to higher shear rates due to a more extreme change in the velocity profile. The no-slip equation is represented by $\mathbf{u}=0$ in figure 13.



Equation

Show equation assuming:

Study 1, Stationary

$$\mathbf{u} = 0$$

Figure 13: COMSOL's given equations for a no-slip wall condition.

Outlet Conditions

The outlet boundary conditions were set to laminar outflow. The exit pressure option was chosen and the outlet pressure left at zero. This is not a problem because the model is dependent on an average velocity based inflow, not pressure driven flow. The equation for the outlet section is below in figure 14

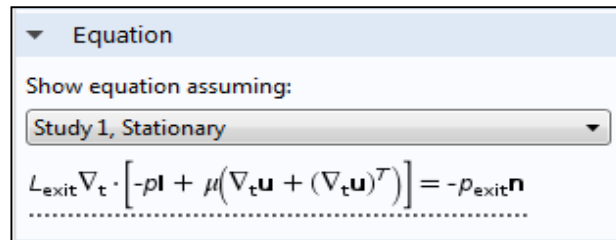


Figure 14: COMSOL's given equation for the outlet section.

Study Settings

The study was set to examine steady-state laminar flow. Lastly, two parametric sweeps were also set up. The first used to vary the flow rate from the current 0.3 mL/min up 100X to 30 ml/min. The second was set up with apparent viscosities that correlated to hematocrits from 45% up to 65% in steps of 5%. After everything was finalized the CFD solver was run on a research server called Harpia. A research computer was a necessity due to the fine mesh calculations requiring a computer with over 16GB of RAM.

RESULTS

This section contains the highlights of the COMSOL findings and their significance to RBC and platelet lysis. Additionally, Appendices A through F contain a fairly exhaustive number of figures detailing velocity and shear rate profiles throughout the COMSOL model of the lamina.

COMSOL Generated Velocity Profiles

The velocity profiles calculated by COMSOL's CFD module along the long portion of each rectangular channel appeared as expected for laminar, Newtonian flow in a rectangular channel. In the flow the velocity profile reaches a maximum of approximately 1.05 cm/s in the center of each long channel as seen in figure 15.

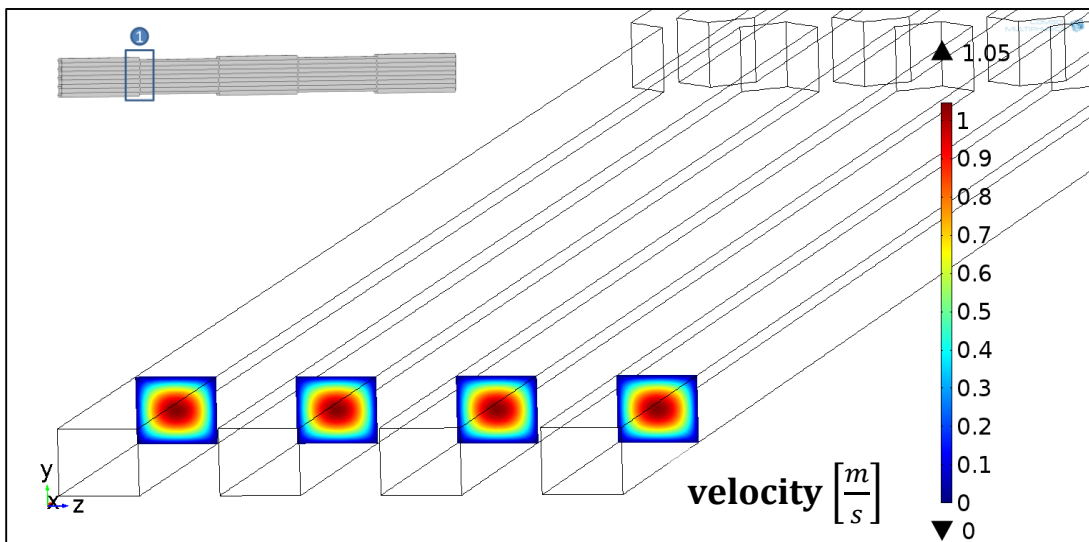


Figure 15: The general velocity profile that can be observed along the vast majority of the each channel.

The maximum flow velocity drops down to 0.74 m/s in each bifurcation as seen in figure 16, and becomes fully re-developed every 39 μm after a channel bifurcation. This process can be observed in Appendix E.

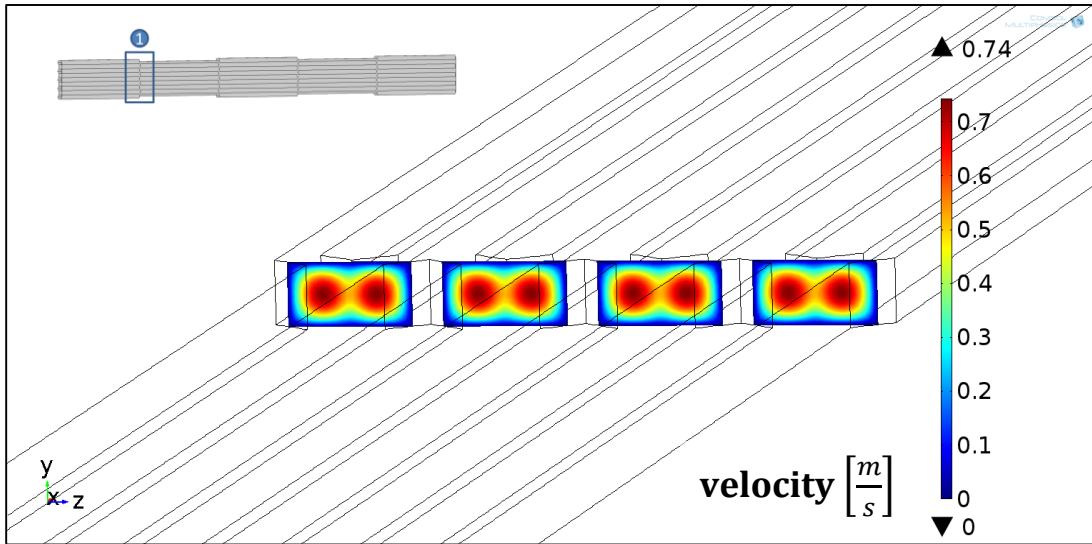


Figure 16: The lowest maximum velocity can be observed in the bifurcations between channels.

COMSOL Generated Shear Profiles

For the current flow rate, the shear rates that blood cells experience in the device are best displayed in figures 17-19. The first figure (figure 17) shows the shear profile in the region where the maximum shear is lowest in the device lamina. These low maximum shear profiles are located in the center of each bifurcation where the hydraulic diameter is the greatest and the flow splits off into two. It is significant to note that the average shear rate is well above 50 s^{-1} such that the whole blood should act Newtonian throughout the whole device lamina. Another aspect worthy of mention is

the near zero value seen at the bottom of the graphs. This is due to the GMRES generating a near zero, but not perfect zero solution.

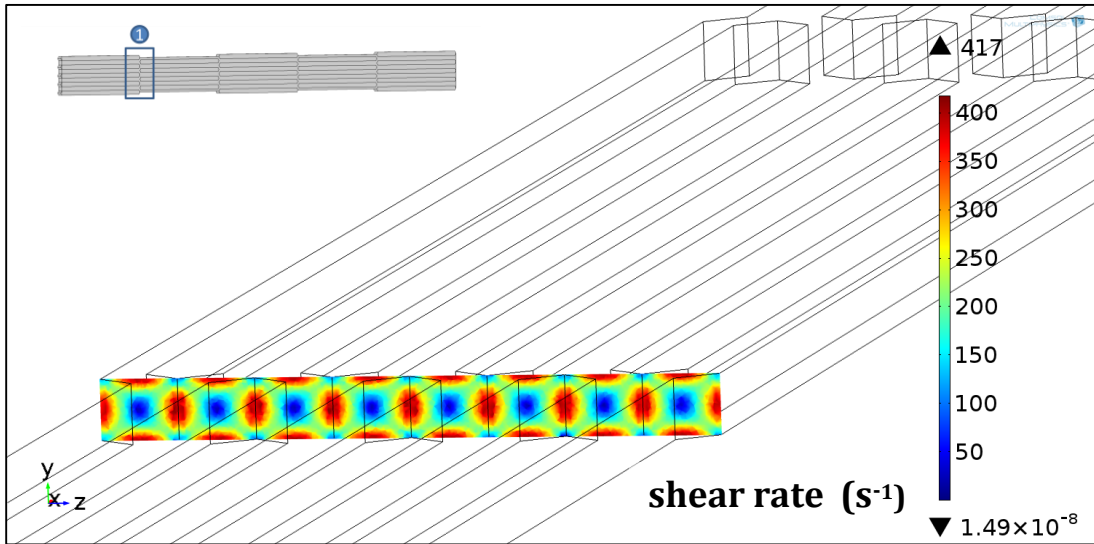


Figure 17: The lowest maximum shear observed occurs Halfway ($50 \mu m$) into each bifurcation.

Next, the highest shear rate profiles that can be observed in the device are displayed in figure 18. Note that this spike of $797 s^{-1}$ is only momentary, and although a shear spike of this sort will have no notable effect on the average shear rate in the device lamina, it may be significant when critical threshold shear is considered.

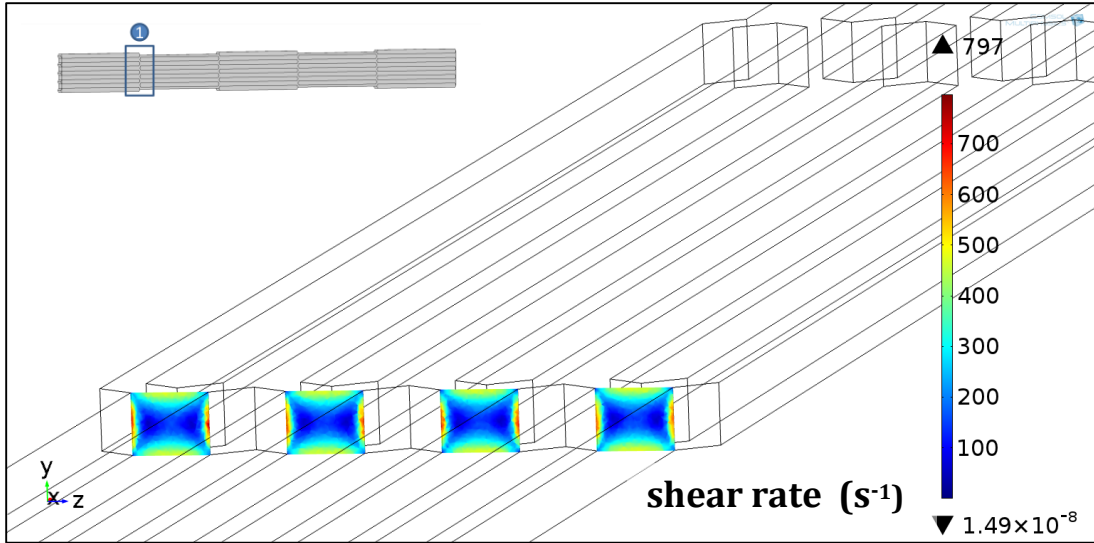


Figure 18: The highest shear rate (797 s^{-1}) can be observed $\sim 1\mu\text{m}$ before each bifurcation and continues for less than a micron in the streamline direction.

Lastly is an analysis of the largest and most consistent section of flow. Just like the velocity profile, the shear profile is consistent from $39 \mu\text{m}$ after every bifurcation until microns before the next bifurcation. A normal shear rate profile can be seen in figure 19:

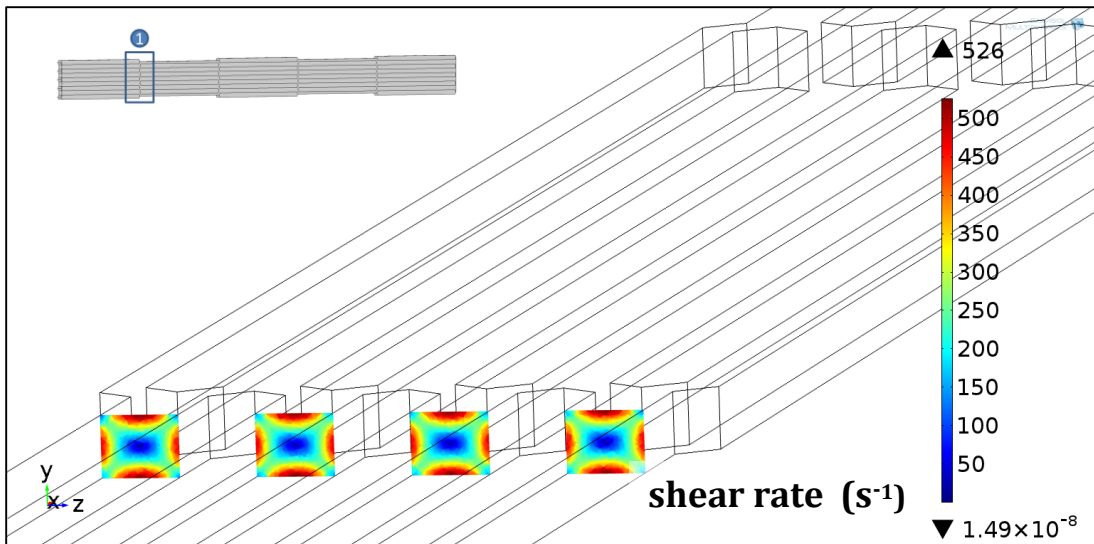


Figure 19: The standard shear profile observed along the vast majority of the each channel.

Here it is important to note that the good, but not perfect resolution causes the max shear rate to fluctuate between 515 and 526 s^{-1} throughout the long channel regions. This fluctuation can be observed in Appendix B.

COMSOL Global Values

COMSOL 4.4's averaging function (which is found in the derived value section) found the average global velocity to be 0.493 cm/s. The fact that it is not exactly 0.5 cm/s makes sense considering that velocity drops temporarily in each bifurcation. Moreover, using COMSOL's maximum function, max global velocity was found to be 1.0537 cm/s. Using the same basic integration functions, the global shear rate average and maximum shear rate were found to be 249.54 and 797 s^{-1} respectively. The global shear profile is best displayed using figure 20, since the greatest shear occurs on the walls and corners of the lamina.

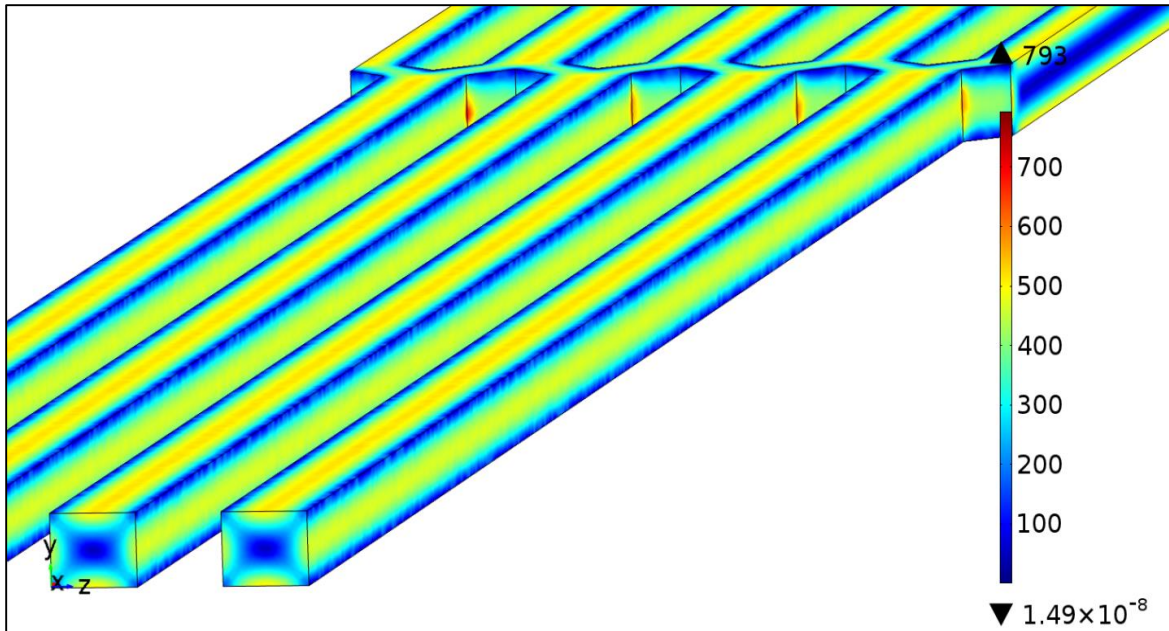


Figure 20: Shear rate profile along the surface of each channel.

Note how briefly the maximum shear rate occurs along the surface which is generally where the highest shear rates occurs due to the velocity layers next to the wall having the largest difference in velocities. Also, along the surface the maximum shear rate is only 793 s^{-1} meaning that the 797 s^{-1} shear rate maximum occurs so briefly in one of the mesh edges that it did not even register along the surface of the COMSOL model. Nevertheless, for a factor of safety, the higher shear rate value of 797 s^{-1} will be used as the maximum value.

Hemolysis Calculations

For an estimate of the percent of damaged RBCs and platelets it makes the most sense to use the average shear and average residence time. This estimation is made bearing in mind that it may not be as good of a model for the platelets due to the

potential of an increased residence time as previously discussed. Complex interactions with biomaterial surfaces and plasma proteins should also be considered. To calculate the percent hemolysis, it is first necessary to convert the average shear rate into the average shear stress using equation 16:²¹

$$\tau_{ave} = \mu_{app}\gamma_{ave} = 3.12mPa \cdot s * 249.54 s^{-1} = 0.779 Pa \quad (16)$$

Through the use of equations 1 and 2 the hypothetical percent of RBC and platelet destruction is:

$$D_{RBC} = 3.62 * 10^{-5} * 13^{0.785} * 0.779^{2.416} = 1.48 * 10^{-4} = 0.0148\% \quad (17)$$

$$D_{Platelets} = 3.66 * 10^{-6} * 13^{0.77} * 0.779^{3.075} = 1.22 * 10^{-5} = 0.00122\% \quad (18)$$

Next, the critical shear threshold residence time is calculated by simply plugging in the average residence time into equations 3 and 4 to get:

$$\tau_{RBCcrit} = 88.905 * 13^{-0.3372} = 37.4 Pa \quad (19)$$

$$\tau_{Pcrit} = 54.986 * 13^{-0.3585} = 21.9 Pa \quad (20)$$

In this case it makes more sense to compare these values to the maximum global stress to see if cells are being damaged as they come into contact with the highest shear available. This calculation is done below in equation 18 to get:

$$\tau_{max} = \mu_{app}\gamma_{max} = 3.12mPa \cdot s * 797 s^{-1} = 2.49 Pa \quad (21)$$

Thus, for the current flow rate, it seems that shear stress levels are well below the critical threshold for both RBC hemolysis to be taking place or for shear stress to be contributing to platelet activation. The maximum shear stress value calculated in equation 21 corresponds to 6.65% of the RBC critical shear threshold and 11.4% of the

platelet critical shear threshold. This means that absolutely no hemolysis should be occurring in the current design specifications.

CDL Effects on Platelet Hemolysis

Platelet Critical Residence Time

It was discussed that there was a notable amount of uncertainty concerning platelet residence time. To determine approximately how long a platelet could reside in the CDL without being damaged, equation 22 was solved (from equation 7) for a wall shear rate equal to 526 s^{-1} which was obtained from figure 19 and represents the highest shear rate observed throughout the majority of the channels. When translated to shear stress this value is equal to 1.64 Pa for a 45% hematocrit.

$$(t_{res})_{crit} = 7.1378 * 10^4 * 1.64^{-2.789} = 17962 \text{ s} = 4.99 \text{ hours} \quad (22)$$

The result was a critical residence time of approximately 5 hours. This value is very encouraging because even given the uncertainty of platelet residence time it is very unlikely that a single platelet will have a residence time over 1000 times greater than the average blood residence time.

Potential Amplification of Shear Stress in the CDL

Referring back to the literature review in the cell-depleted layer section, it was mentioned that shear stresses near the walls can be amplified by the absence of RBCs in the CDL region. This shear stress can be calculated by equation 23 which comes from

the CDL study done by Namgung et al.¹⁴ where μ_{app} for the current flow rate is 3.12 mPa-s, width (W) is 1 μm (a CDL thickness to accommodate a single platelet), the RBC edge velocity V_{edge} is 0.23 cm/s which is the velocity of flow an RBC center 5 μm from the wall (1 μm platelet thickness + 4 μm RBC diameter)^{32,33} as seen in the 2D COMSOL flow profile featured in Appendix L.

$$\tau = \frac{\mu_{plasma} V_{edge}}{W} = \frac{1.30 * mPa * s * 0.23 \frac{cm}{s}}{1 \mu m} = 2.99 Pa \quad (23)$$

The value calculated in equation 23 is interesting because it is only about 17% larger than the shear stress calculated using the maximum observed shear rate. It is still well below the critical threshold for platelet damage (13.7%) and when entered into equation 7, the critical platelet residence time is 56 min. As such, in worst case CDL conditions platelet damage from mechanical stresses are still theoretically negligible.

Parametric Sweep Results

While it is obvious that (1) an increase to the flow rate in steady-state laminar flow should produce identical-looking velocity and shear rate profiles, except with magnitudes that have increased directly proportionally to the change in flow rate; and (2) an increase to viscosity would probably have a very minor affect on the shape of the velocity and shear rate profiles, in the interest seeing if the CFD calculations would deviate from expectations, both sweeps were run. The results of these sweeps behaved exactly as expected, having no noticeable effect on the velocity or shear rate profiles. Flow profiles pictures for 100X flow can be seen in Appendices G and H; the surface

shear data for 100X flow can be seen in Appendix J. Since COMSOL showed that the profile was behaving as expected, the equations for blood damage (1-4) were simply applied again for their relative increases.

An Increased Hematocrit's Contribution to Shear Stress and Hemolysis

The viscosity analysis is very simple since the velocity and shear rate changes were negligible. If blood hematocrit were to be increased from 45% to 65% the results would be a 66% increase in the apparent viscosity and a proportional 66% increase in the observable shear stress. Thus, if blood hematocrit is increased to 65% for the current flow rate (0.3 mL/min) potential hemolysis values increase to 0.0511% for RBCs and 0.00591% for platelets (via Equations 1-2) or 11.1% of the RBC critical shear threshold and 18.9% of the platelets critical shear threshold, which still means that theoretically there is no hemolysis occurring in blood with a higher than average apparent viscosity due to hematocrit or other factors.

An Increased Flow Rate's Contribution to Shear Stress and Hemolysis

Increasing the flow rate proportionally increases the shear stress, but it decreases the residence time in an inversely proportional manner. Figure 21 is a table generated using the same methods as before: equations 1-4 for an apparent viscosity of 3.12mPa-s corresponding to a 45% hematocrit in the current lamina geometry. Entrance lengths must also be recalculated when velocity changes such that figure 21 contains both the entrance length and the L_e/L_c , which is the percent of a single channel in which the flow would be developing.

Flow Rate	Entrance Length (μm)	$\frac{L_e}{L_c}$ Percent	RBC Lysis Percent	Platelet Lysis Percent	Max Shear Stress (Pa)	RBC critical shear stress threshold (Pa)	Platelet critical shear stress threshold (Pa)
1X: 0.3 mL/min	8.05	0.201	0.0148%	0.00122%	2.49	37.4	21.9
2X: 0.6 mL/min	16.1	0.403	0.0459%	0.00605%	4.97	47.3	28.1
4X: 1.2 mL/min	32.2	0.805	0.142%	0.0299%	9.94	59.7	36.0
20X: 6 mL/min	161	4.01	1.96%	1.22%	49.7	103	64.2
50X: 15 mL/min	402.5	10.1	8.75%	10.1%	124	140	89.1
100X: 30 mL/min	805	20.1	27.1%	49.9%	249	177	114

Figure 21: Table of values regarding hemolysis based on different flow rates. The critical shear stresses that are near the maximum stress are marked in orange and those that have been surpassed are marked in red.

VALIDATION

Validation Model Dimensions

For validation purposes a single channel model was built in COMSOL without the bifurcations, as seen in figure 22. The single channel had identical dimensions to that of the long straight channels in the actual lamina. The settings for apparent viscosity due to blood hematocrit at 45%, the current flow rate of 0.3mL/min, and the no-slip condition were all maintained in the validation channel as well.

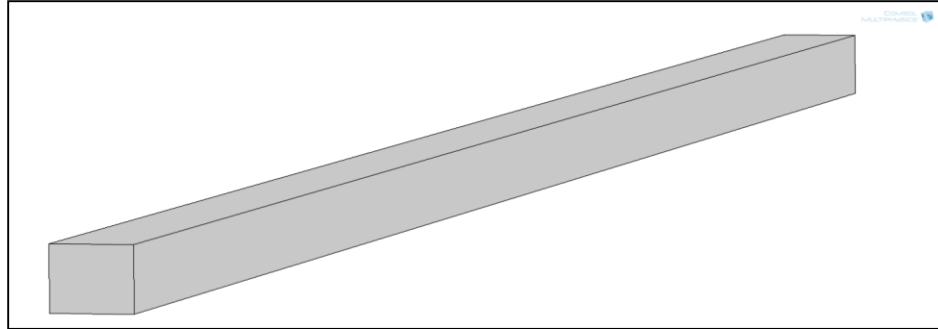


Figure 22: Verification channel created in COMSOL. The channel is $80\ \mu\text{m} \times 100\ \mu\text{m} \times 4\ \text{mm}$ which is identical to the current lamina channels.

Validation Model Mesh

The validation model mesh was made with exact same specifications as the larger bifurcated version as can be seen in figure 23. This created a mesh of 1,034,852 domain elements, 54,742 boundary elements and 2,092 edge elements.

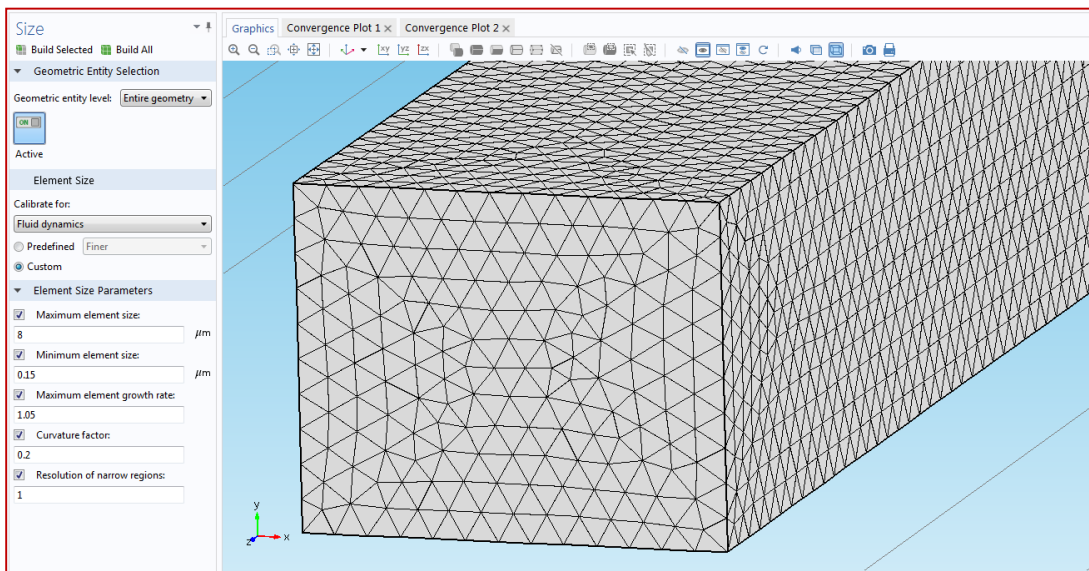


Figure 23: Shows the actual mesh generated in COMSOL for validation of COMSOL results versus known analytical equations.

The overall size of the mesh was proportionally smaller than the large model because of the smaller global volume. Nevertheless, it should provide the same level of accuracy. Figure 24 is a good representation of this since the shear profile looks the same as the shear profiles in the larger model and has the same maximum shear rate. Observe that the non-zero value in the center of the channel is identical to the one in figure 19.

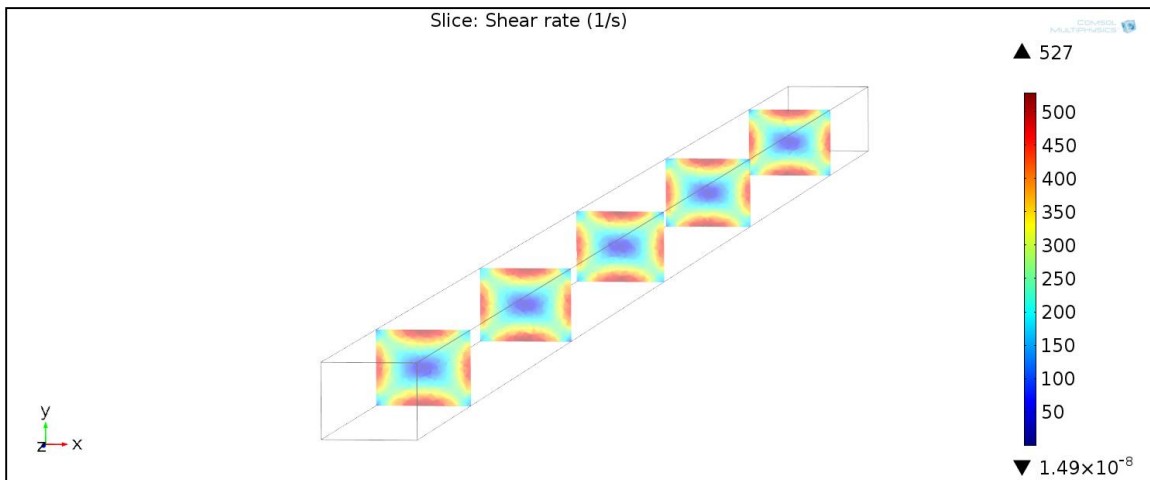


Figure 24: Shows the shear profile for the validation channel as well as the identical non-zero error that the larger version has for shear rate values.

Theoretical Pressure Drop Comparison

As a measure of the COMSOL model's accuracy, the pressure drop of the validation channel was compared to the analytical solution for a rectangular channel, as given in figure 25.

Cross-section	Analytical mean velocity	fRe_{μ}
	$\frac{c^3}{4(1+\varepsilon^2)} \frac{\Delta p}{\mu L}$	$\frac{2\pi\sqrt{\pi}(1+\varepsilon^2)}{\sqrt{\varepsilon E}\sqrt{1-\varepsilon^2}}$
	$\frac{\Delta p c^2}{\mu L} \left[\frac{1}{3} - \frac{64\varepsilon}{\pi^5} \tanh \frac{\pi}{2\varepsilon} \right]$	$\frac{12}{\left(1 - \frac{192}{\pi^5} \varepsilon \tanh \frac{\pi}{2\varepsilon}\right) (1+\varepsilon)\sqrt{\varepsilon}}$
	$\frac{1}{60} \frac{\Delta p a^2}{\mu L}$	$\frac{20}{3^{1/4}} = 15.197$
	$\frac{\Delta p a^2}{\mu L} g(\phi)^{11}$	$\frac{\phi\sqrt{\phi}}{(1+\phi)g(\phi)^{11}}$
	$\frac{\Delta p b^2}{8\mu L} \left[\varepsilon^2 - 1 + \frac{2\ln(1/\varepsilon) + \varepsilon^2 - 1}{\ln(1/\varepsilon)} \right]$	$\frac{8\sqrt{\pi}(1-\varepsilon)\sqrt{1-\varepsilon^2}}{\left(\varepsilon^2 - 1 + \frac{2\ln(1/\varepsilon) + \varepsilon^2 - 1}{\ln(1/\varepsilon)}\right)}$
$^{11}g(\phi) = \frac{\tan(2\phi) - 2\phi}{16\phi} - \frac{128\phi^3}{\pi^5} \sum_{n=1}^{\infty} \frac{1}{(2n-1)^2 (2n-1+4\phi/\pi)^2 (2n-1-4\phi/\pi)}$		$\varepsilon = \frac{c}{b}$

Figure 25: Analytical solutions for mean velocity and fRe of various cross section. Figure from Bahrami et al.⁴⁷

$$u_m = \frac{\Delta p c^2}{\mu L} \left(\frac{1}{3} - \frac{64\varepsilon}{\pi^5} \tanh \left[\frac{\pi}{2\varepsilon} \right] \right) \quad (24)$$

$$\Delta p = u_m * \frac{\mu L}{c^2} \left(\frac{1}{3} - \frac{64\varepsilon}{\pi^5} \tanh \left[\frac{\pi}{2\varepsilon} \right] \right)^{-1} \quad (25)$$

$$0 \leq \varepsilon = \frac{c}{b} \leq 1 \quad (26)$$

By rearranging equation 24 into equation 25 the average velocity can be used to solve for the change in pressure throughout the channel. Where μ is μ_{app} of 3.12 mPa-s, L is the 4 mm length of a channel, c is the 80 μm height of the channel, b is the 100 μm width and ε is the ratio of height to width shown in figure 25 and in equation 26 which is equal to 4/5.

Evaluating equation 25:

$$\Delta p = \frac{0.5 * 3.12 * 4 \text{ cm} * \text{mPa} * \text{s} * \text{mm}}{40^2} \frac{\text{s} * \mu\text{m}^2}{\text{s} * \mu\text{m}^2} \left(\frac{1}{3} - \frac{64 * .8}{\pi^5} \tanh \left[\frac{\pi}{2 * .8} \right] \right)^{-1}$$

$$\Delta p = .0039 * \frac{10^{-2} * 10^{-3} * 10^{-3}}{10^{-12}} 5.79746 Pa$$

$$\Delta p = .0039 * 10^4 * 5.79746 Pa$$

$$\Delta p = 226.1 Pa$$

In comparison, the COMSOL single channel test model with the exact same mesh properties, channel dimensions and flow settings as the full size model, calculated a pressure drop of 229.1 Pa. Visual depictions of this pressure drop can be found in Appendix K. This translates to an error of 1.32% as seen in equation 27 and is noticeable deviation from the expected value, but not serious enough to warrant concern about the validity of the results.

$$\%Error = \left| \frac{Actual - Experimental}{Actual} \right| = \left| \frac{226.1 - 229.1}{226.1} \right| = 1.32\% \text{ error} \quad (27)$$

Theoretical Velocity Profile Comparison

Next, in order to validate that the theoretical velocity profile generated by COMSOL was accurate, it was compared to the analytical solution given by equation 28.⁴⁸

$$u(y, z) = \frac{16a^2}{\mu\pi^3} \left(-\frac{dP}{dx} \right) \sum_{n=1,3,5}^{\infty} \frac{(-1)^{\frac{n-1}{2}}}{n^3} \left[1 - \frac{\cosh\left(\frac{n\pi}{2a}z\right)}{\cosh\left(\frac{n\pi b}{2a}\right)} \right] \cos\left(\frac{n\pi}{2a}y\right) \quad (28)$$

This equation was entered into a series of MATLAB scripts all located in Appendix N. The first script was used to simply calculate max velocity in the middle of the rectangular channel (at position 0,0) which was found to equal 1.1986 cm/s, which

when compared to the COMSOL value of 1.0537 cm/s has an error of about 12%. The second script was used to calculate the average velocity using both a 2,000 X 2,000 and a 10,000 X 10,000 grid that calculated the velocity magnitude in equal steps across the whole cross section and then averaged the values. For the 2,000 X 2,000 grid that average velocity value was found to be 0.4977 cm/s and for the 10,000 X 10,000 grid it was found to be 0.4978 cm/s. COMSOL's global velocity average in the validation channel was found to be 0.4970 resulting in an error less than 0.2% which was excellent to see since it verified both that the MATLAB file was calculating values for the analytical equation well.

Since the 10,000 X 10,000 grid had miniscule effect on the solution accuracy the third script used only the 2,000 X 2,000 grid to calculate and graph the velocity profile across the Z and Y axes. These were compared to the validation channel graphs across the same Z and Y axes. There is some noticeable difference in slope between the two, but overall they appear very similar the COMSOL velocity profile graphs which can be seen in Appendix L and the MATLAB profiles can be seen in Appendix M.

Final Thoughts on Validation

Since the mesh used for the calculations was limited by the RAM of computers available to regular students (i.e. 16GB) on the Oregon State Campus. There was no way to perform a mesh study with finer meshes. However, the above data combined with introspection of Appendices A to F show fairly good resolution and consistent values

when taking small steps across the mesh and in different locations. This certainly lends to credibility of the results, although ideally one would run a mesh study, as well, to further verify the data's validity.

Conclusions

The primary objective of this study was to mitigate concerns that the current hemoperfusion lamina design will cause significant harm to RBCs and platelets due to mechanical shear stresses. To that end, the COMSOL study performed indicates that within the specified flow rate of 0.3 mL/min in the current lamina geometry there should be no appreciable contribution to blood hemolysis. For an average hematocrit of 45% the anticipated percent hemolysis is 0.0148% for RBCs and 0.00122% for platelets. For a 65% hematocrit that number increased up to 0.0511% for RBCs and 0.00591% for platelets, remaining reasonably insignificant.

In terms of the shear stresses approaching the critical threshold for mechanically induced hemolysis to start occurring, for blood hematocrit values of 45%, the shear stresses applied to the RBCs reached only 6.65% of the critical threshold for hemolysis and platelets reached 11.4% of their respective critical threshold. If hematocrit was increased to 65% the RBCs and platelets still only experience 11.1% and 18.9% of the critical threshold respectively. Thus, it could be initially concluded that the mechanical

stresses in the current lamina design do not produce any reasonable level of blood hemolysis.

Some ambiguity surrounds the exact residence times of platelet in the channel flow which depends on platelet interactions with the RBCs and CDL. Nevertheless, the critical residence time of a platelet trapped in the CDL with the highest average shear rate of 526 s^{-1} was approximately 5 hours. Even considering the worst case scenario for an amplified shear stress within the CDL due to RBC depletion, the critical residence time was still nearly 1 hour. This means that platelets would have to get stuck in high shear regions for nearly an hour before there was any reasonable suspicion of potential damage. This strongly supports the notion that no mechanically induced platelet damage will occur within the current design parameters. However, platelet interactions with biomaterials are complex and more testing will be required to ensure that platelets are not being harmed by the blood's interaction with the hemoperfusion device's biomaterials.

Lastly, after running a parametric sweep to evaluate how shear stress and resultant blood damage change based on increasing the flow rate it was found that it may be possible to increase the flow rate without causing significant changes to hemolysis. Whether or not it would be beneficial would require more research. For ease of reference, Appendix O contains tables of useful values pertaining to the results discussed.

Future Work

There are still many studies that have to be done moving forward to validate the safety and efficacy of OSU's potential hemoperfusion device. The most obvious follow-up to this study would be an experimental study of actual hemolysis values found in the prototype lamina to verify that values found using the CFD model and equations 1-4 accurately represent the actual blood damage that takes place. This study could also suggest potential correction factors for any inconsistencies. Another future study could look into the average residence times of platelets in the current lamina and the resulting effect on platelet activation. Another study that would be beneficial would be one that looks into the influences of manufacturing imperfections on shear stresses in blood and its resulting effect on mechanical blood damage. Lastly, the current CFD model could be adapted to look at how the bifurcations and the CDL are influencing the potential for adsorption of gram-negative bacteria onto the peptide surface coatings.

Finally, it seems relevant to note that although the validation of the COMSOL CFD model created seems to point toward the mesh being sufficient for the study done. It would be quite beneficial to use a research computer with more than 16GB of RAM in order to run a mesh convergence study to see if there is any notable deviations from the results obtained in this study.

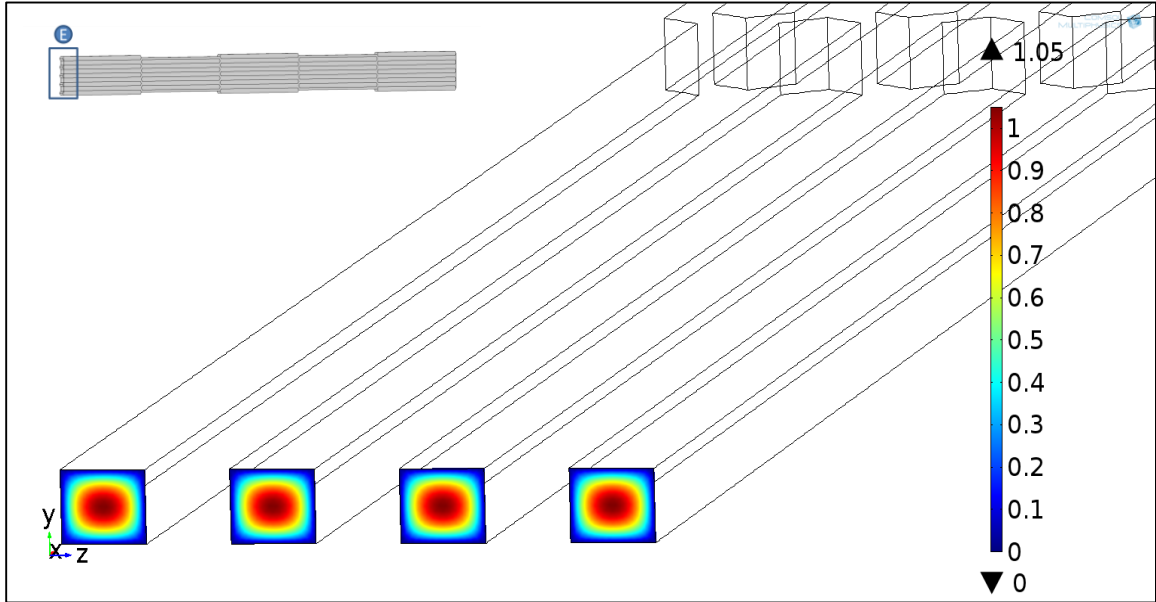
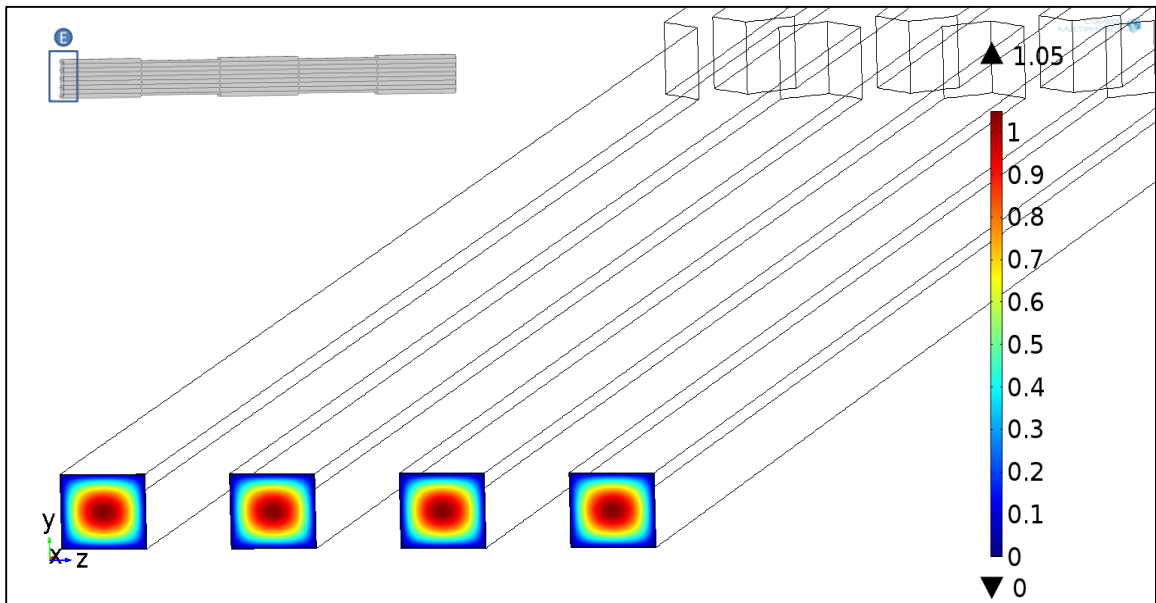
REFERENCES

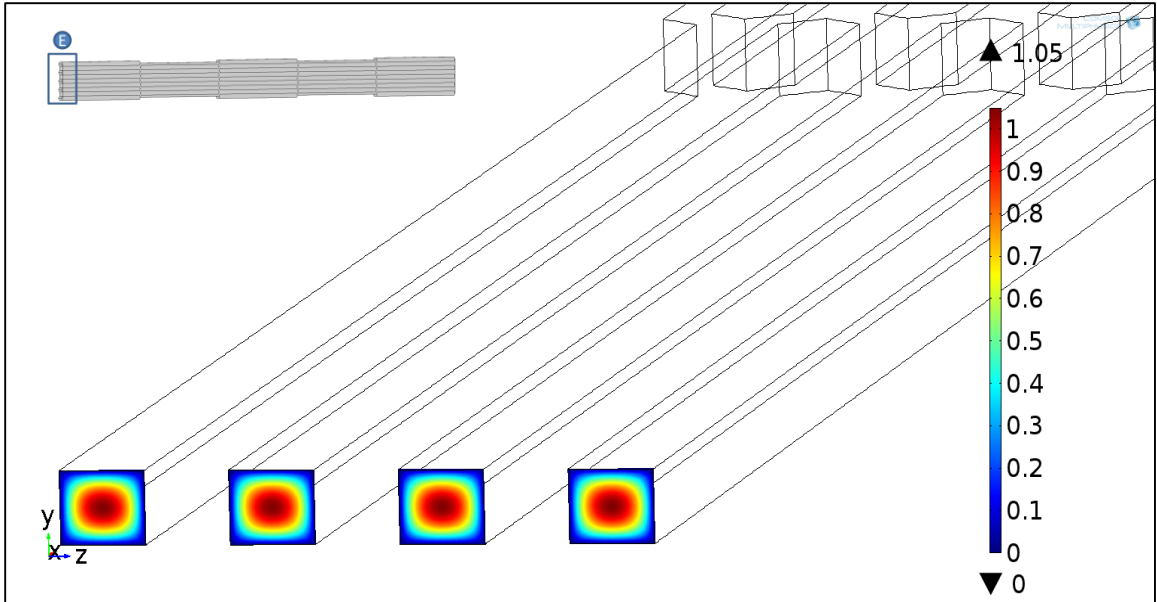
1. Florian BM, Sachin Y, Derek CA. Epidemiology of severe sepsis. *Virulence*. 2014;5(1):4-11. doi: 10.4161/viru.27372.
2. Czura CJ. "Merinoff Symposium 2010: Sepsis"—Speaking with One Voice. *Medicine*. 2011;17(1-2):2.
3. Lyle NH, Pena OM, Boyd JH, Hancock RE. Barriers to the effective treatment of sepsis: antimicrobial agents, sepsis definitions, and host-directed therapies. *Annals of the New York Academy of Sciences*. 2014;1323(1):101-114. doi: 10.1111/nyas.12444.
4. Dombrovskiy VY, Martin AA, Sunderram J, Paz HL. Rapid increase in hospitalization and mortality rates for severe sepsis in the United States: A trend analysis from 1993 to 2003*. *Critical care medicine*. 2007;35(5):1244-1250.
5. Wood KA, Angus DC. Pharmacoeconomic implications of new therapies in sepsis. *Pharmacoeconomics*. 2004;22(14):895-906.
6. Issrah J, Ivana L, Snorri BR. Assessing available information on the burden of sepsis: global estimates of incidence, prevalence and mortality. *Journal of Global Health*. 2012;2(1):010404. doi: 10.7189/jogh.02.010404.
7. Burchardi H, Schneider H. Economic aspects of severe sepsis. *Pharmacoeconomics*. 2004;22(12):793-813.
8. Abe R, Oda S, Sadahiro T, Nakamura M, Hirayama Y, Tateishi Y, Shinozaki K, Hirasawa H. Gram-negative bacteremia induces greater magnitude of inflammatory response than Gram-positive bacteremia. *Critical Care*. 2010;14:R27. doi:10.1186/cc8898.
9. Jhamb M, Weisbord SD, Steel JL, Unruh M. Fatigue in Patients Receiving Maintenance Dialysis: A Review of Definitions, Measures, and Contributing Factors. *Am J. Kidney Dis*. 2008;52(2):353–365. doi:10.1053/j.ajkd.2008.05.005.
10. Wolfson M. Management of Protein and Energy Intake in Dialysis Patients. *J Am Soc Nephrol*. 1999;10:2244–2247.
11. Fedosov DA, Caswell B, Popel AS, Karniadakis GEM. Blood Flow and Cell-Free Layer in Microvessels. *Microcirculation*. 2010;17(8):615-628.
12. Sherwood JM, Dusting J, Kaliviotis E, Balabani S. The effect of red blood cell aggregation on velocity and cell-depleted layer characteristics of blood in a bifurcating microchannel.

- Biomicrofluidics*. 2012;6(2):24119. doi: 10.1063/1.4717755.
13. Sollier E, Cubizolles M, Fouillet Y, Achard JL. Fast and continuous plasma extraction from whole human blood based on expanding cell-free layer devices. *Biomedical Microdevices*. 2010;12(3):485-497. doi 10.1007/s10544-010-9405-6.
 14. Namgung B, Ong PK, Johnson PC, Kim S. Effect of Cell-Free Layer Variation on Arteriolar Wall Shear Stress. *Annals Of Biomedical Engineering*. 2011;39(1):359-366.
 15. Aarts PA, van den Broek SA, Prins GW, Kuiken GD, Sixma JJ, Heethaar RM. Blood Platelets Are Concentrated near the Wall and Red Blood Cells, in the Center in Flowing Blood. *Arteriosclerosis*. Nov-Dec 1988;8(6):819-824.
 16. Duffy R, Tomashek K, Spangenberg M, Spry L, Dwyer D, Safranek TJ, Ying C, Portesi D, Divan H, Kobrenski J, Arduino M, Tokars J, Jarvis W. Multistate outbreak of hemolysis in hemodialysis patients traced to faulty blood tubing sets. *Kidney Int*. 2000;57(4):1668-1674.
 17. Spry L. The diagnosis of hemolysis during hemodialysis. *Seminars in Dialysis*;12(3):205.
 18. Borgdorff P. Migraine: : Possible Role of Shear-Induced Platelet Aggregation With Serotonin Release. *Headache: The Journal Of Head & Face Pain*. 2012;52(8):1298-1318.
 19. Goubergrits L. Numerical modeling of blood damage: current status, challenges and future prospects.(Editorial). *Expert Review of Medical Devices*;3(5):527-531.
 20. Giersiepen, M. Ermittlung von Strömungsprofilen und Schubspannungen am Hertzklappenprothesen mit Hilfe der Laser-Doppler-Anemometrie in pulsatiler Strömung. *in: Ph.D. thesis. Helmholtz Institute for Biomedical Engineering, Aachen, F.R.G.* 1988.
 21. Polaschegg H. Red Blood Cell Damage from Extracorporeal Circulation in Hemodialysis. *Seminars in Dialysis*. 2009;22(5):524-531.
 22. Bone RC, Balk RA, Cerra FB, Dellinger RP, Fein AM, Knaus WA, Schein RM, Sibbald WJ. Definitions for sepsis and organ failure and guidelines for the use of innovative therapies in sepsis. *Chest*. 1992;101:1644-1655.
 23. Matsuno N, Ikeda T, Ikeda K, Hama K, Iwamoto H, Uchiyama M, Kozaki K, Narumi Y, Kikuchi K, Degawa H. Changes of cytokines in direct endotoxin adsorption treatment on postoperative multiple organ failure. *Therapeutic Apheresis*. 2001;5(1):36-39.
 24. Baumgartner JD, Calandra T. Treatment of Sepsis: Past and Future Avenues. *Drugs*. 1999;57(2):127-132.

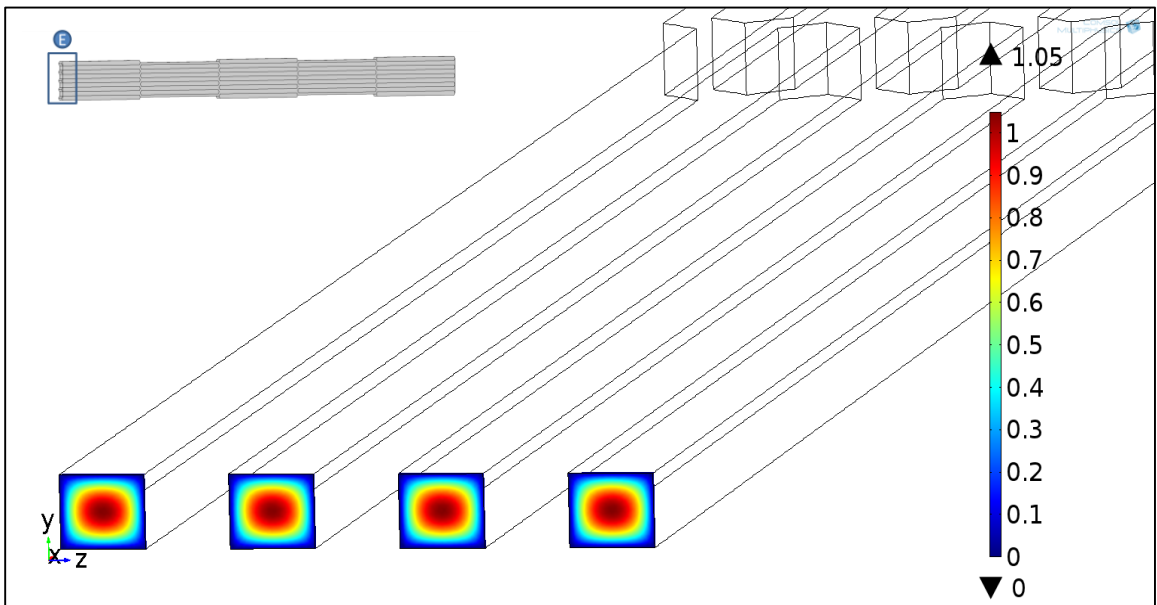
25. Kilár A, Dörnyei Á, Kocsis B. Structural characterization of bacterial lipopolysaccharides with mass spectrometry and on-and off-line separation techniques. *Mass Spectrometry Reviews*. 2013;32(2):90-117.
26. McClelland H, Moxon A. Early identification and treatment of sepsis. *Nurs Times*. Jan 2014;110(4):14-17.
27. Dellinger RP, Levy MM, Carlet JM, Bion J, Parker MM, Jaeschke R, Reinhart K, Angus DC, Brun-Buisson C, Beale R. Surviving Sepsis Campaign: international guidelines for management of severe sepsis and septic shock. *Intensive care medicine*. 2008;34(1):17-60.
28. Fact Sheet Sepsis. Accessed May 12, 2015. http://www.world-sepsisday.org/CONTENTPIC/2015_WSD_FactSheet_long_English.pdf.
29. Wurzinger LJ, Opitz R, Eckstein H. Mechanical blood trauma: an overview. *Angeiologie*. 1986;38,81-97.
30. Goubergrits L, Affeld K. Numerical estimation of blood damage in artificial organs. *Artif Organs*. 2004 May;28(5):499-507. May 2004;28(5):499-507.
31. Roselli JR, Diller KR. Rheology of Biological Fluids. In: *Biotransport principles and applications*. Springer; 2011:107-166.
32. Inglis DW, Morton KJ, Davis JA, Zieziulewicz TJ, Lawrence DA, Austin RH, Sturm JC. Microfluidic device for label-free measurement of platelet activation. *Lab on a Chip*. 2008;8(6):925-931.
33. Diez-Silva M, Dao M, Han J, Lim CT, Suresh S. Shape and Biomechanical Characteristics of Human Red Blood. *MRS Bull*. May 2010;35(5):382-388.
34. Fahraeus R LT. The viscosity of the blood in narrow capillary tubes. *The American Journal of Physiology*. 1931;96:562–568.
35. Pries AR, Neuhaus D, Gaehtgens P. Blood viscosity in tube flow: dependence on diameter and hematocrit. *Am J Physiol - Heart Circ Physiol*. 1992;263(6):H1770–H1778.
36. Purves, WK, Sadava D, Orians GH, Heller HC. *Life: The Science of Biology*. 7th ed. Sunderland: Sinauer Associates; 2004.
37. Késmárky G, Kenyeres P, Rábai M, and Tóth K. Plasma viscosity: A forgotten variable. *Clinical Hemorheology and Microcirculation*. 2008;39(1):243–246. doi 10.3233/CH-2008-1088.
38. Xu, LC, Bauer JW, Siedlecki CA. Proteins, platelets, and blood coagulation at biomaterial

- interfaces. *Colloids and Surfaces B: Biointerfaces*. 2014;124:49-68.
doi:10.1016/j.colsurfb.2014.09.040.
39. Black J. *Biological Performance of Materials: Fundamentals of Biocompatibility*, Third Ed. CRC Press;1999:166-170 ISBN 978-1-4200-5197-1.
40. Comelles J, Estévez M, Martínez E, Samitier J. The role of surface energy of technical polymers in serum protein adsorption and MG-63 cells adhesion. *Nanomedicine: Nanotechnology, Biology, and Medicine*. 2010;6(1):44-51.
41. Higgins A. Personal Communication, 2015.
42. Ryder M. Personal Communication, 2015.
43. Munson BR, Young DF, Okiishi TH. *Fundamentals of Fluid Mechanics*, 4th Ed. John Wiley and Sons Inc; 2002:448,459-461.
44. Cutnell J, Johnson K. *Physics*, Fourth Ed. Wiley and Sons Inc; 1998:308.
45. Saad Y, Schultz MH. GMRES: A generalized minimal residual algorithm for solving nonsymmetric linear systems. *SIAM J. Sci. Stat. Comput.* 1986;7:856-869.
doi:10.1137/0907058.
46. Ryaben'kii VS, Tsynkov SV. *A Theoretical Introduction to Numerical Analysis* CRC Press; 2006. ISBN 978-1-4200-1116-6.
47. Bahrami M, Yovanovich MM, Culham JR. Pressure Drop of Fully-Developed, Laminar Flow in Microchannels of Arbitrary Cross-Section. *Journal Of Fluids Engineering- Transactions Of The Asme*. 2006;128(5):1036-1044.
48. J-Y Jung, H-Y Kwak. Fluid flow and heat transfer in microchannels with rectangular cross section. *Heat and Mass Transfer*. 2008;44(9):1041-1049.

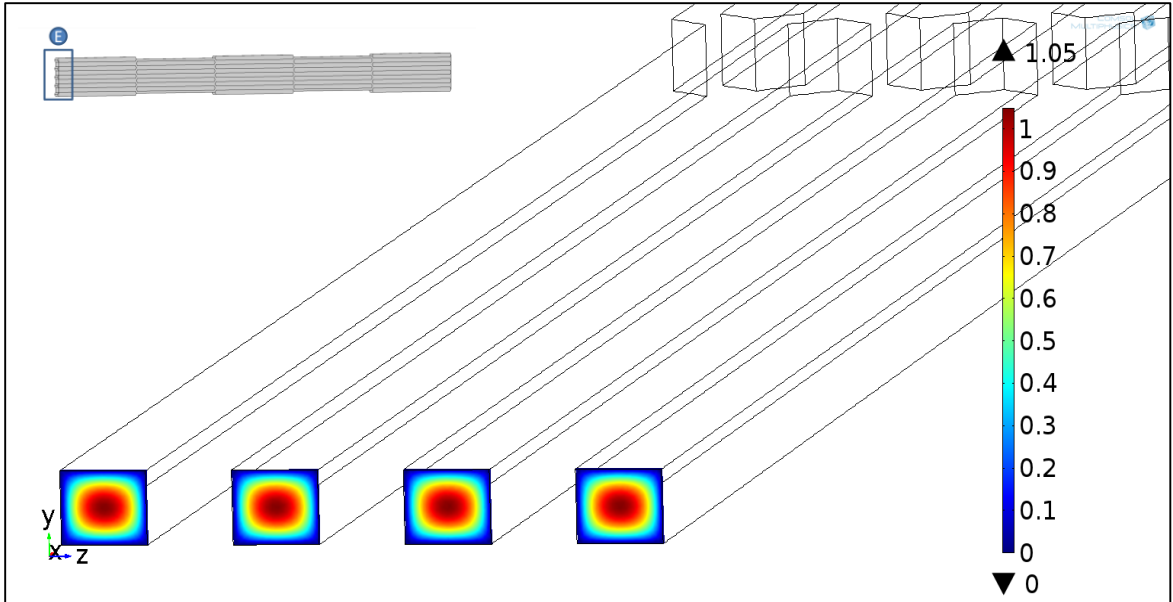
APPENDIX A: INLET VELOCITY PROFILES**FLOW RATE = 0.3ML/MIN****Velocity (cm/s) - Inlet****Velocity (cm/s) - 1 μ m from the Inlet**



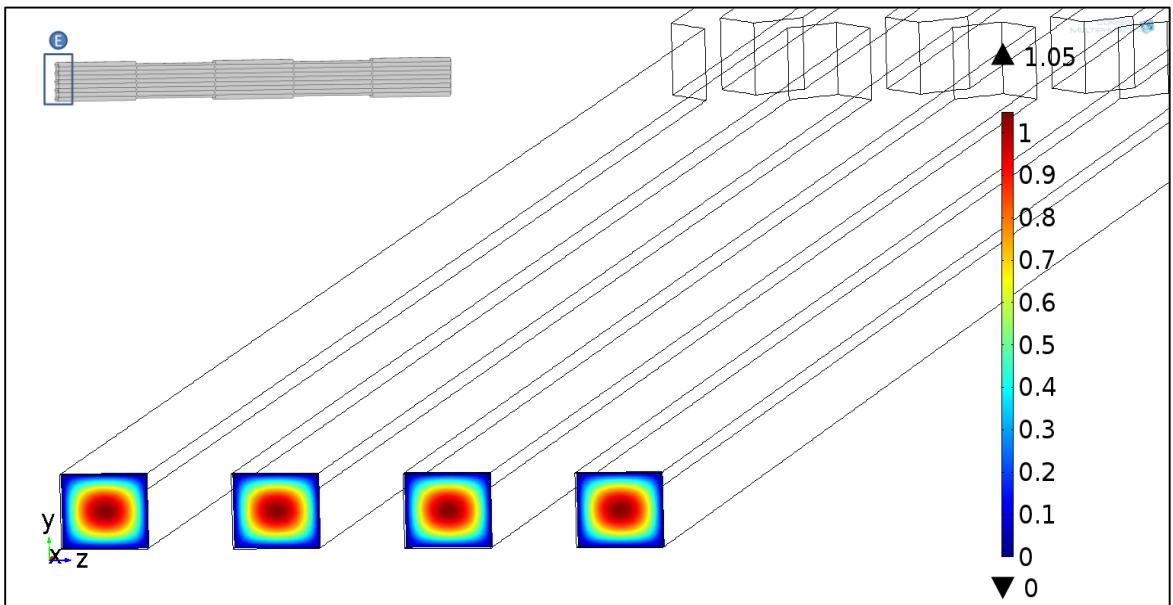
Velocity (cm/s) - 2 μ m from the Inlet



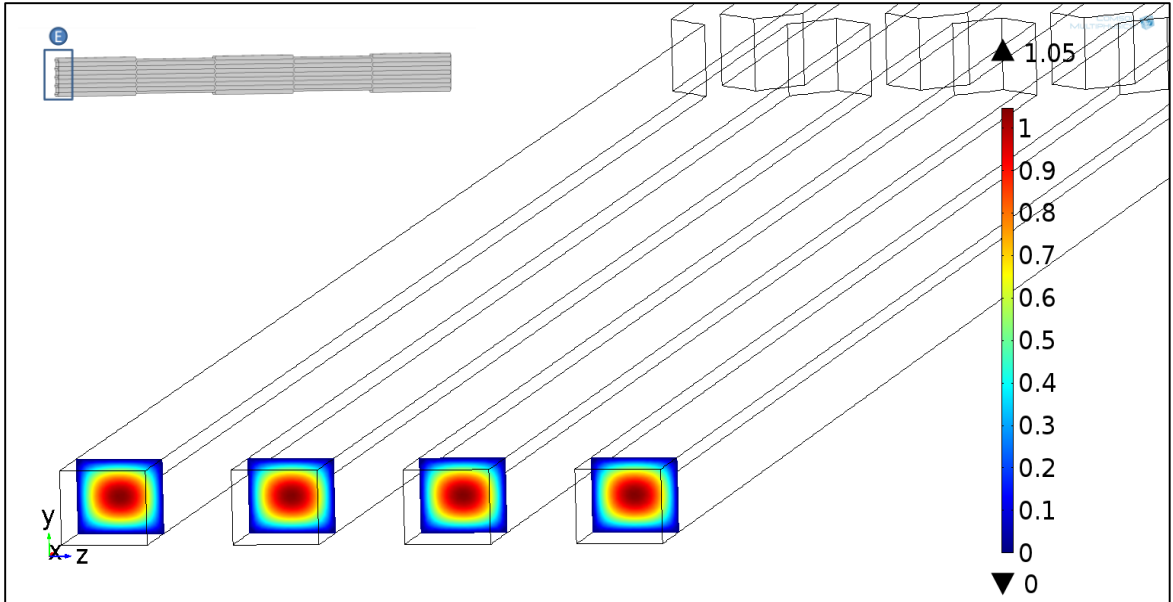
Velocity (cm/s) - 3 μ m from the Inlet



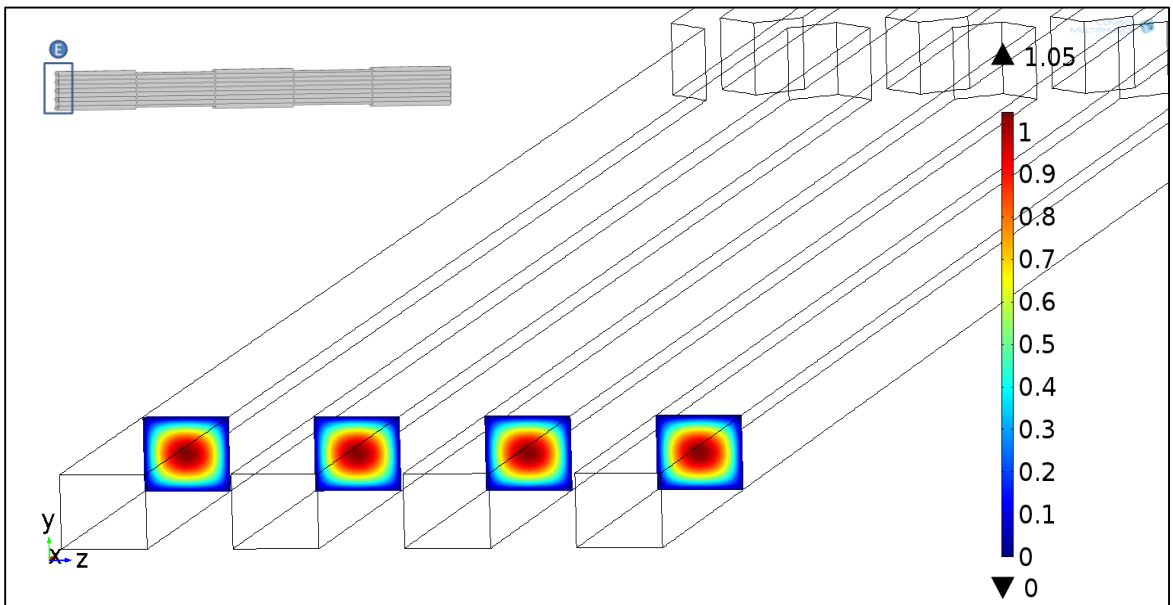
Velocity (cm/s) - $4\mu\text{m}$ from the Inlet



Velocity (cm/s) - $5\mu\text{m}$ from the Inlet

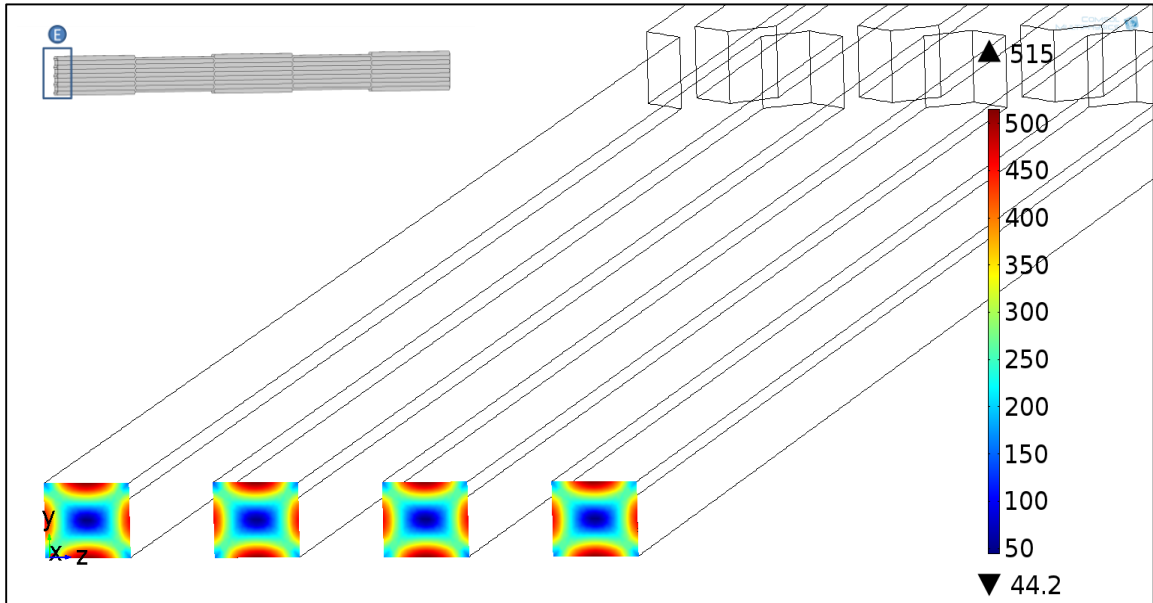


Velocity (cm/s) - 100 μ m from the Inlet

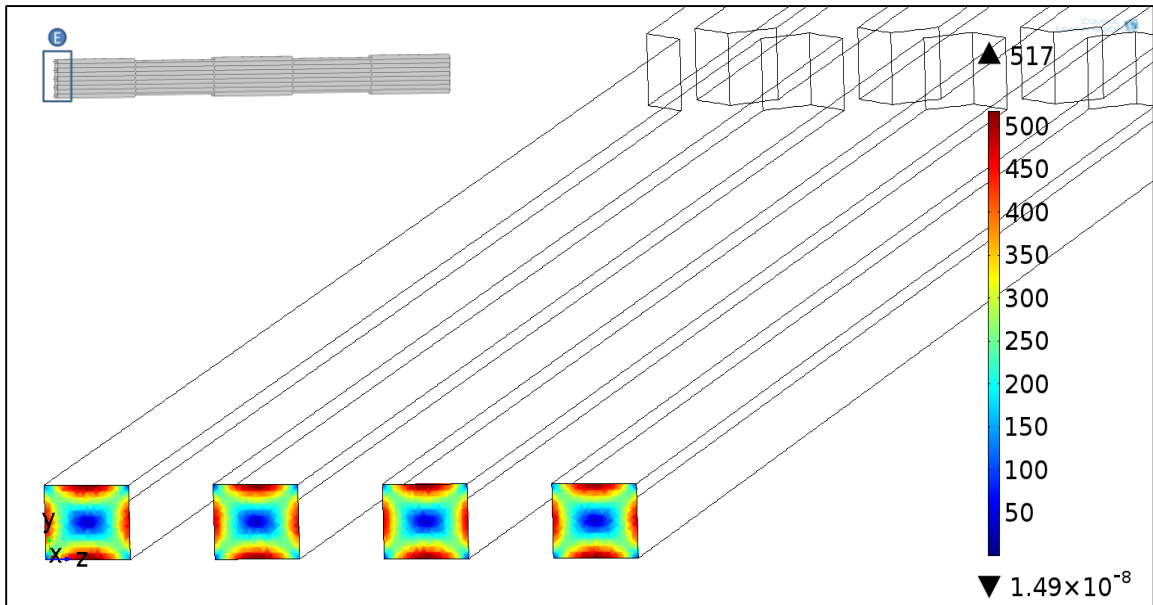


Velocity (cm/s) - 500 μ m from the Inlet

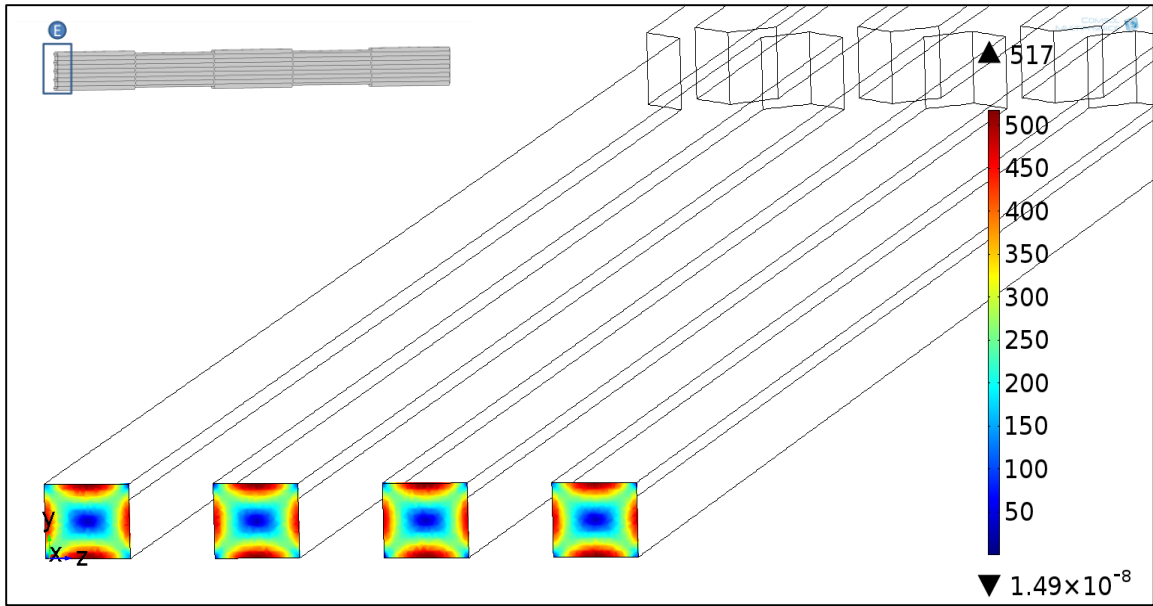
APPENDIX B: INLET SHEAR RATE (s^{-1}) PROFILES



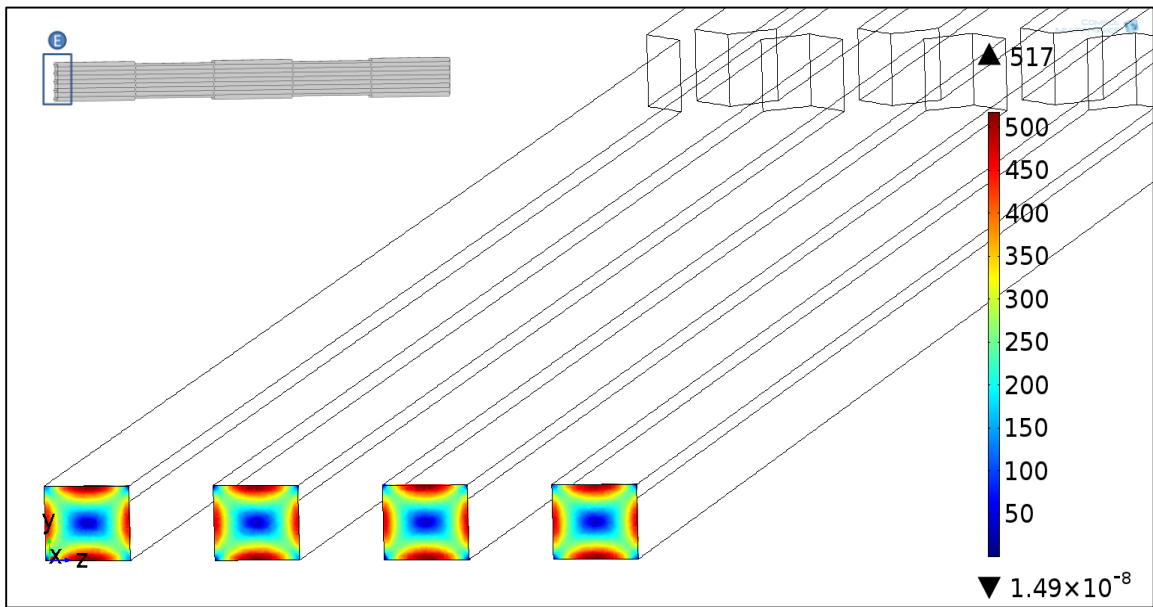
Shear rate (s^{-1}) - Inlet



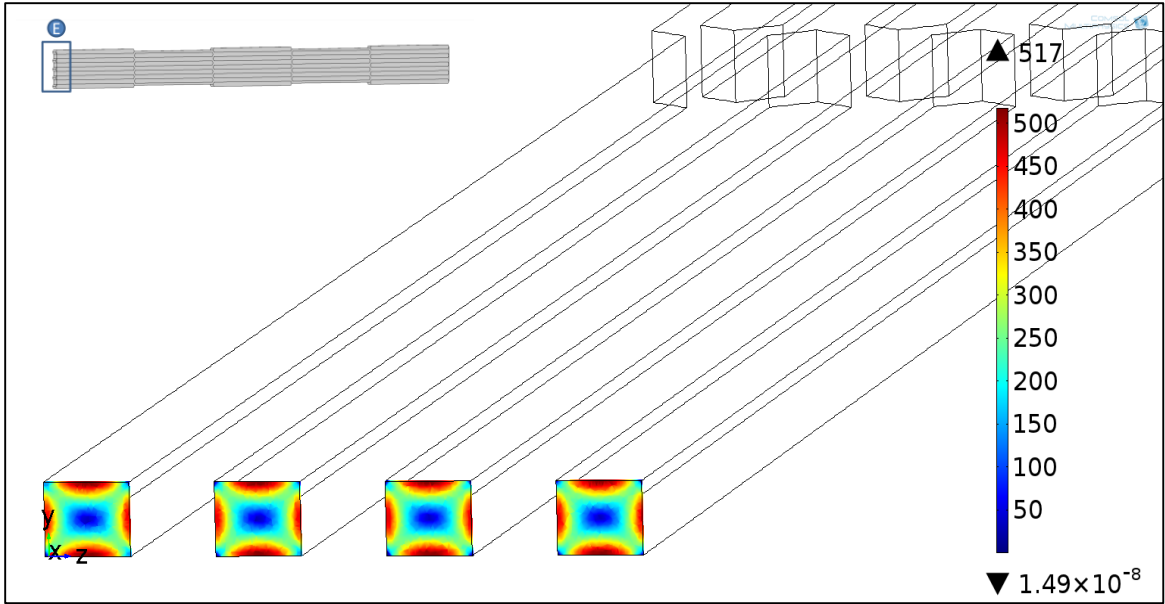
Shear rate (s^{-1}) - $1\mu m$ from the Inlet



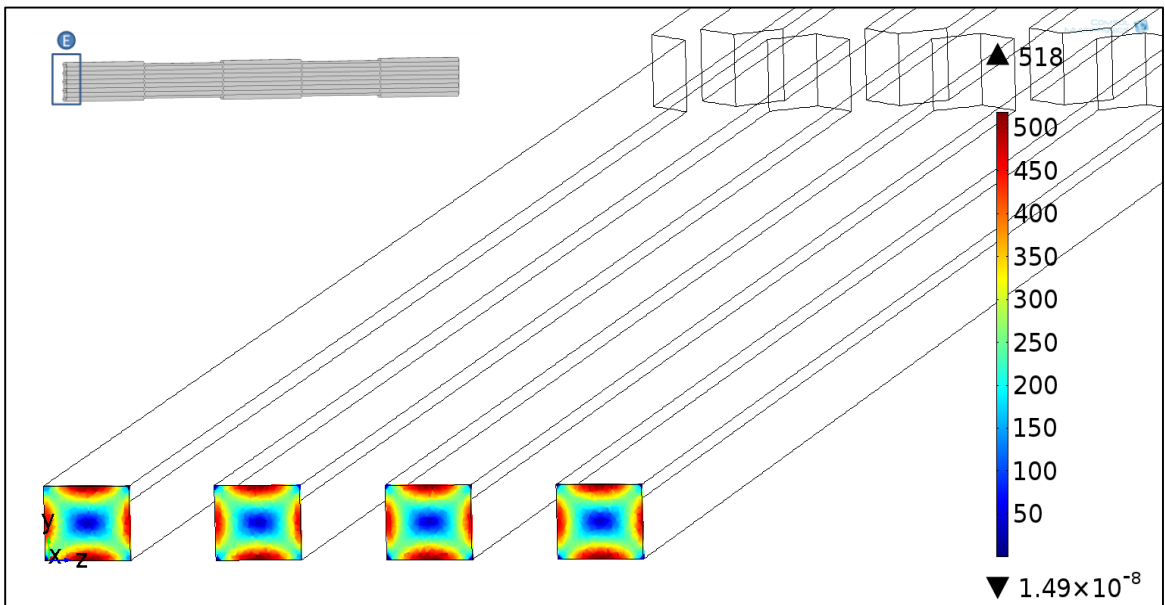
Shear rate (s^{-1}) - $2\mu m$ from the Inlet



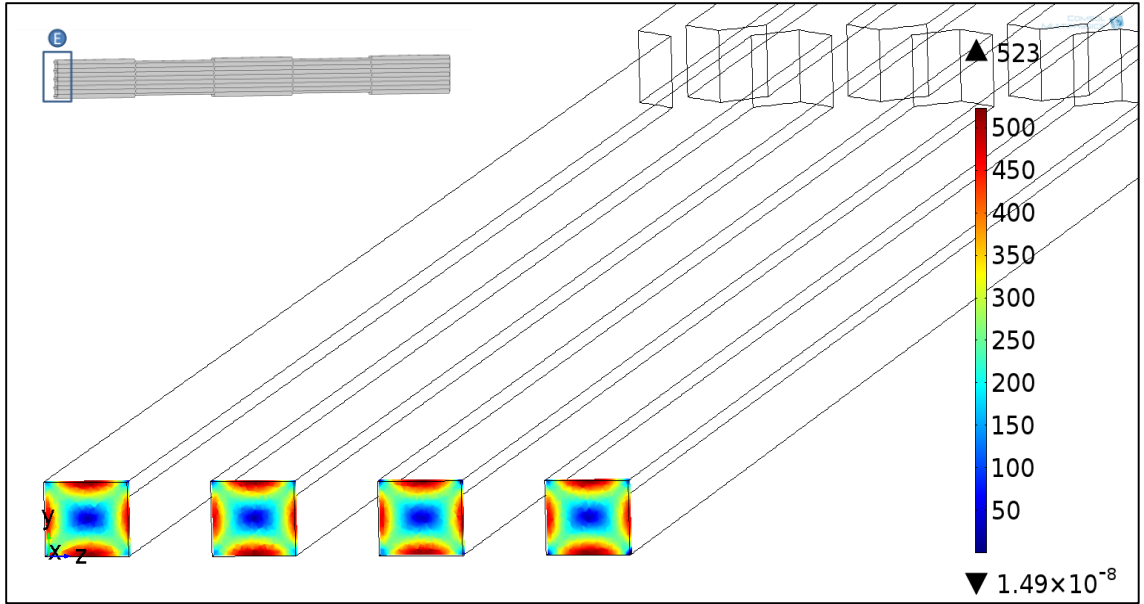
Shear rate (s^{-1}) - $3\mu m$ from the Inlet



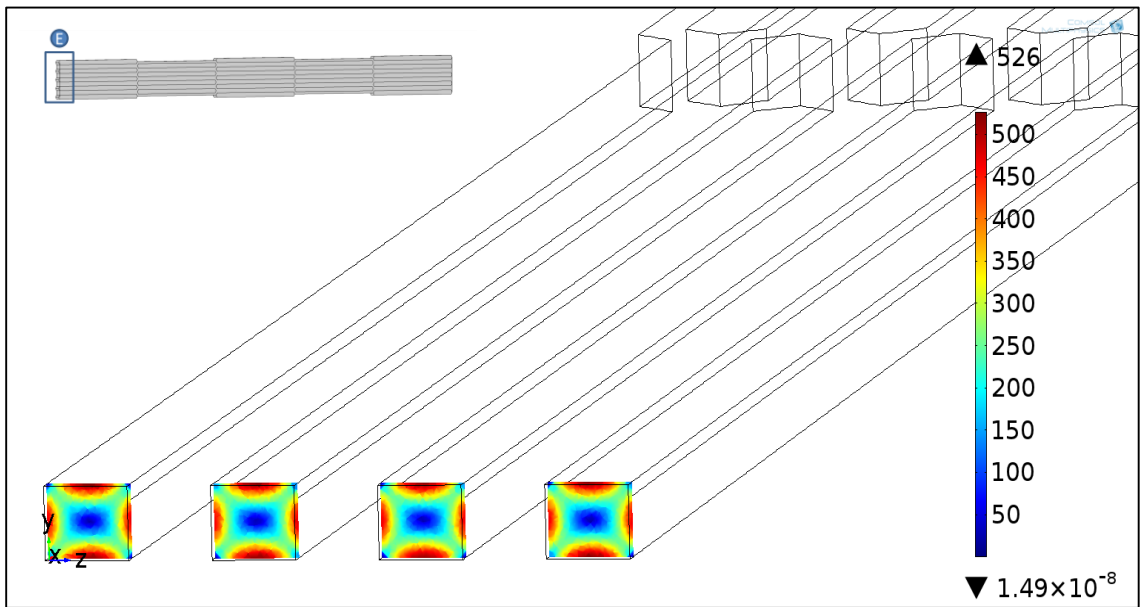
Shear rate (s^{-1}) - $4\mu\text{m}$ from the Inlet



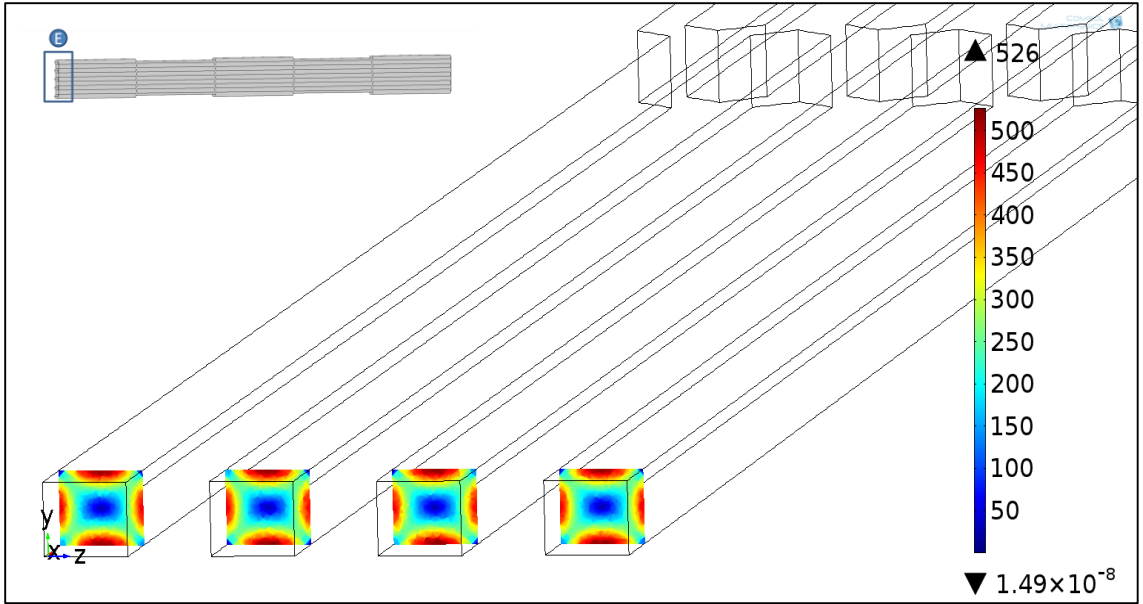
Shear rate (s^{-1}) - $5\mu\text{m}$ from the Inlet



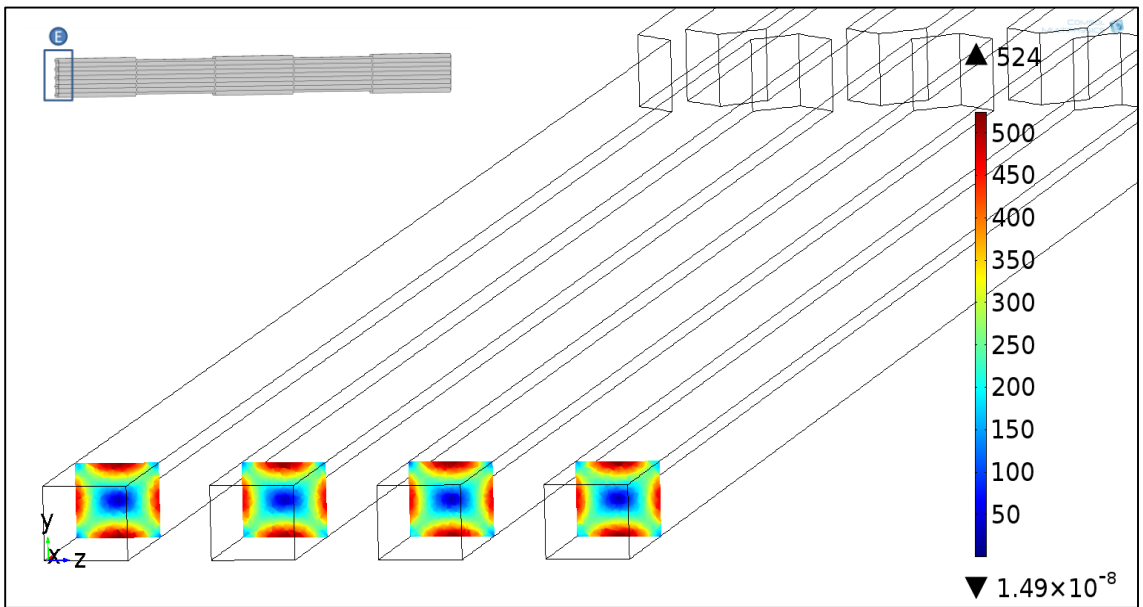
Shear rate (s^{-1}) - 10 μm from the Inlet



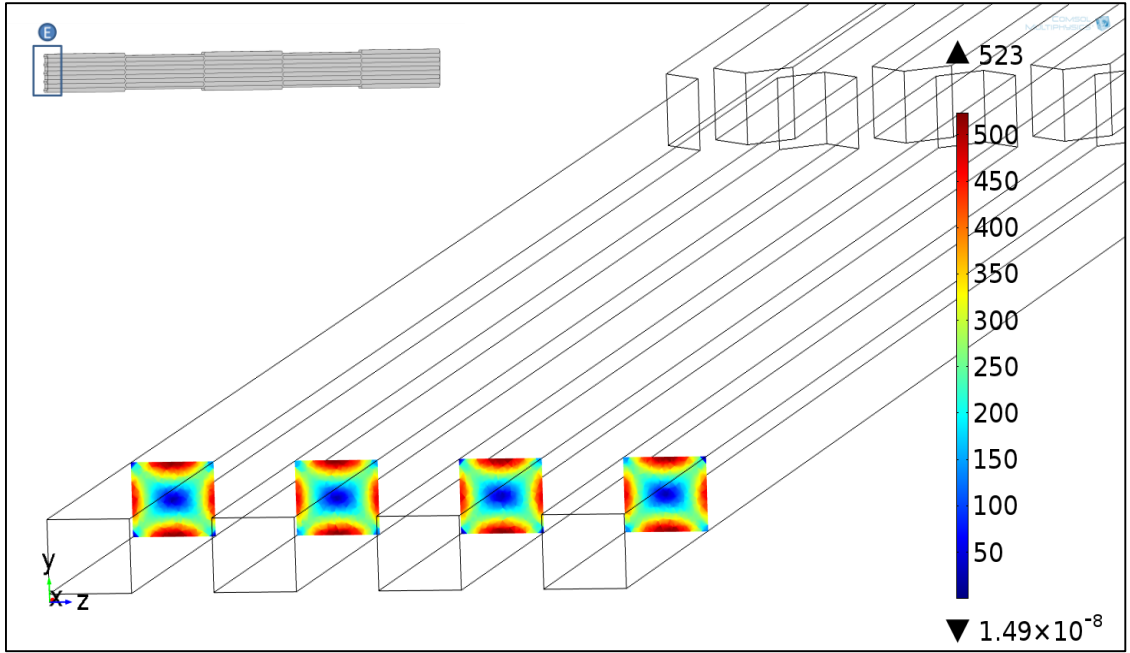
Shear rate (s^{-1}) - 20 μm from the Inlet



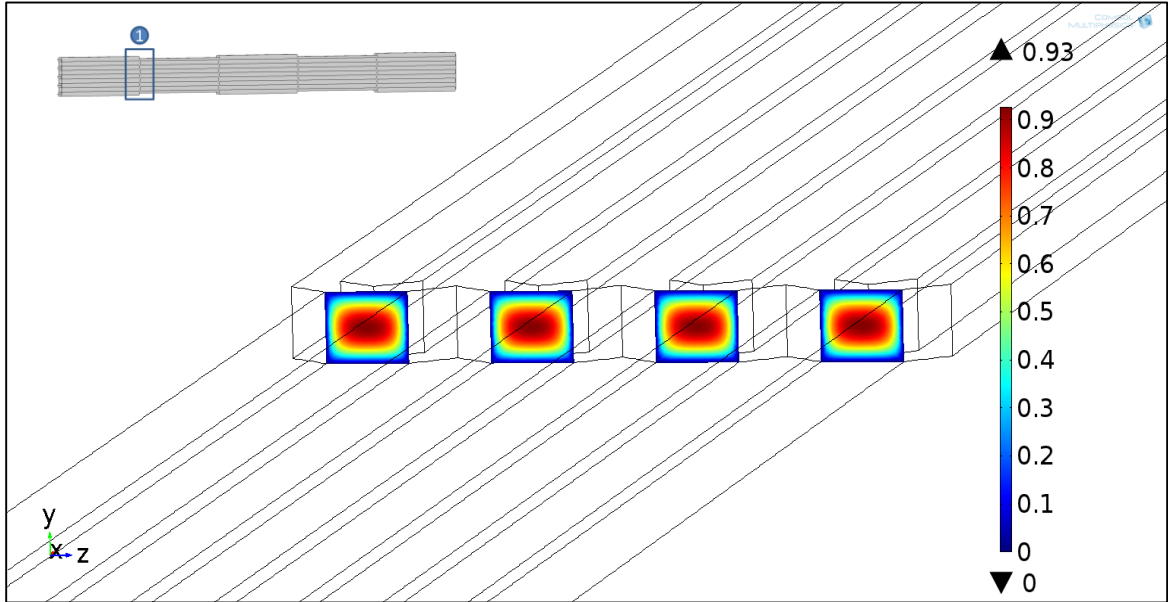
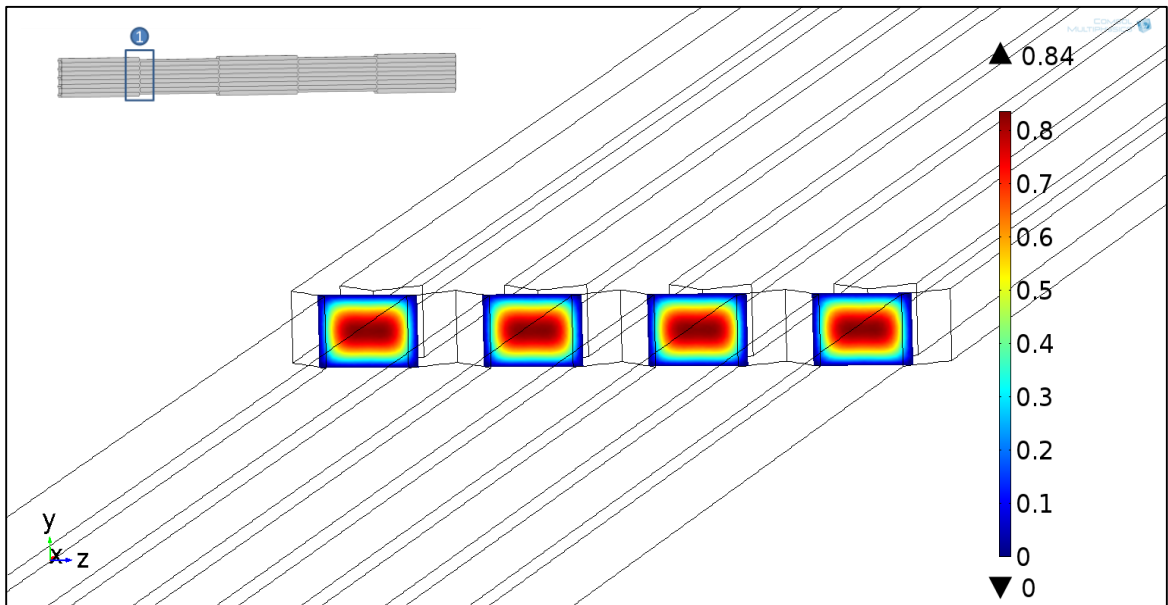
Shear rate (s^{-1}) - 50 μ m from the Inlet

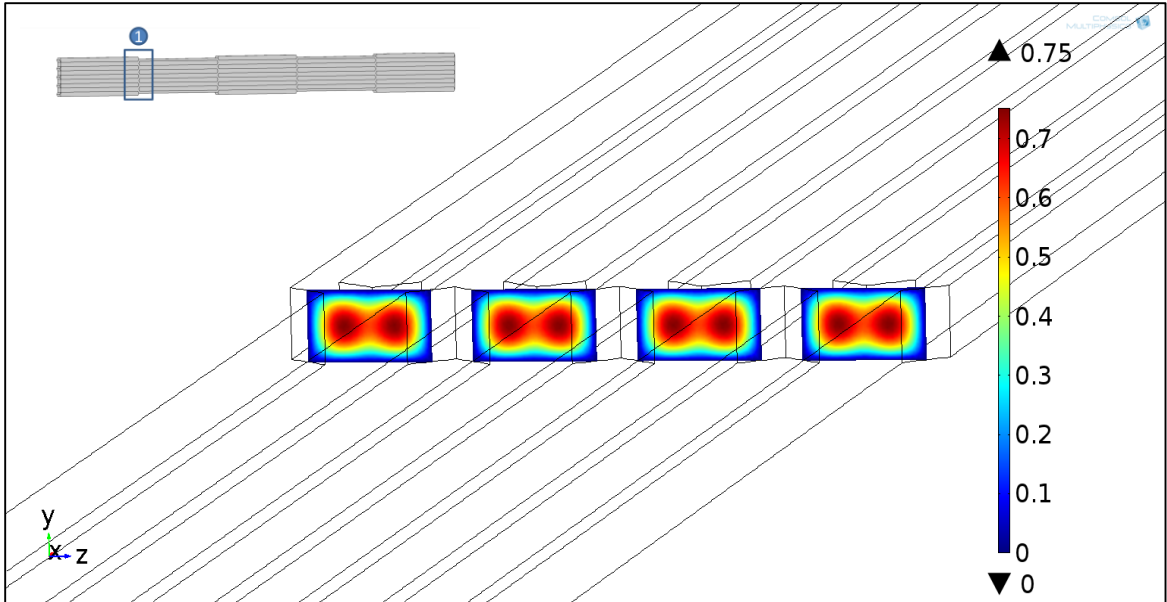


Shear rate (s^{-1}) - 100 μ m from the Inlet

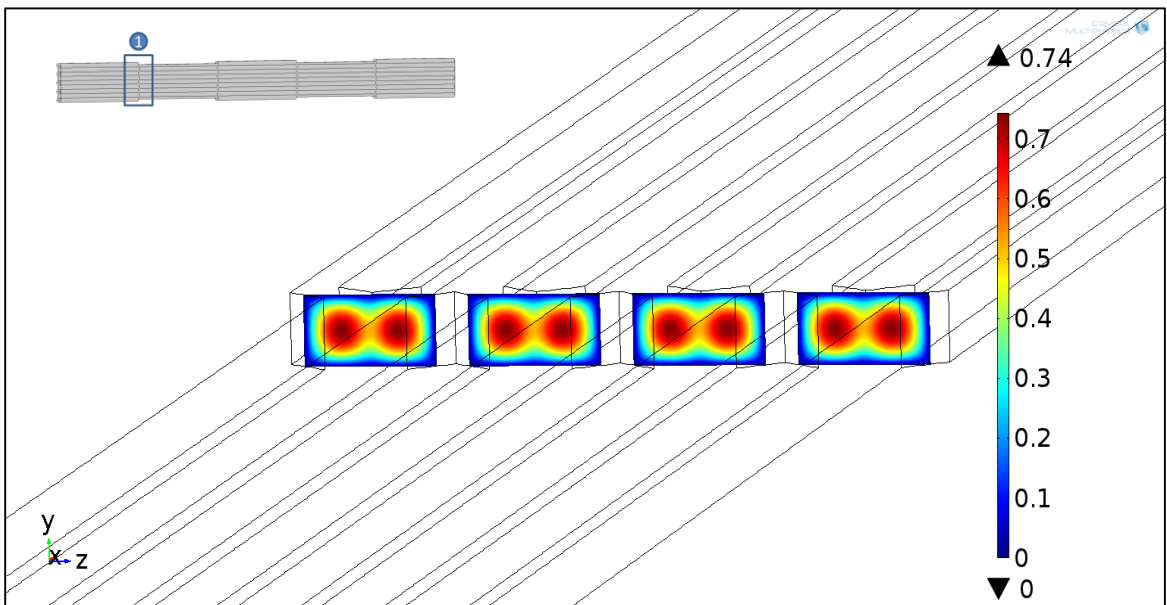


Shear rate (s^{-1}) - 500 μm from the Inlet

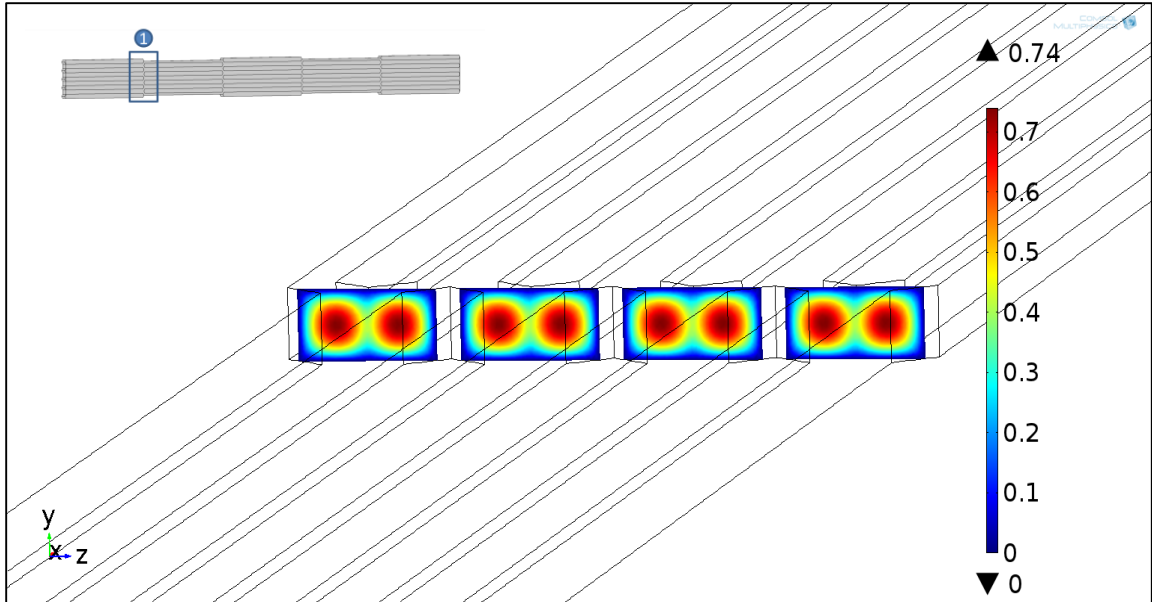
APPENDIX C: 1ST BIFURCATION VELOCITY PROFILES**FLOW RATE = 0.3ML/MIN****Velocity (cm/s) - Entrance of 1st bifurcation****Velocity (cm/s) - 10 μ m into 1st bifurcation**



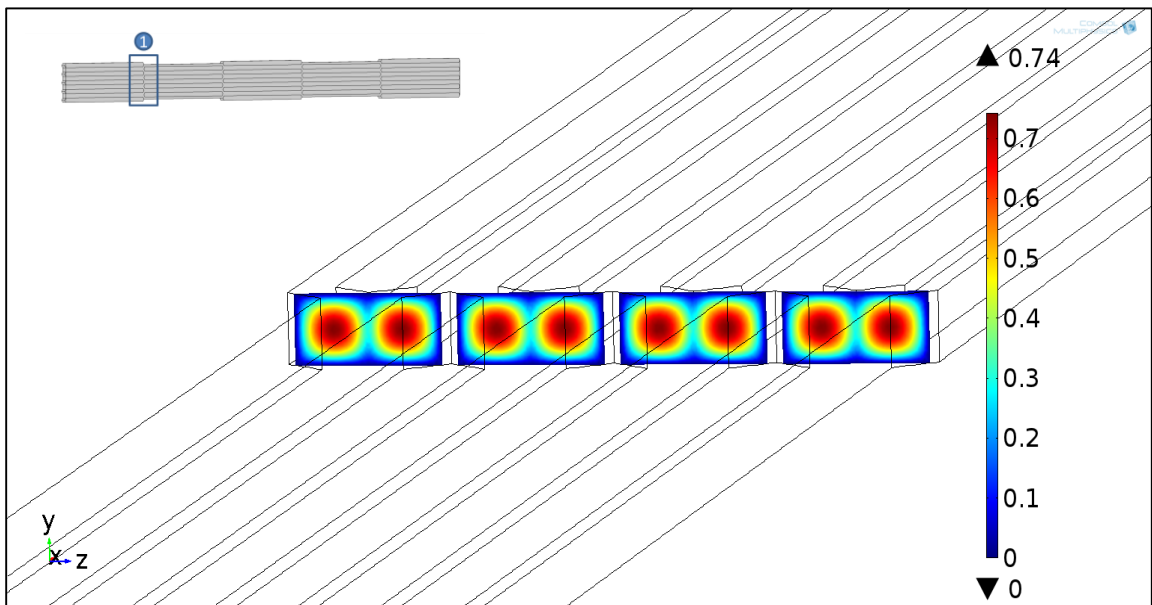
Velocity (cm/s) - One Quarter (25 μm) into 1st bifurcation



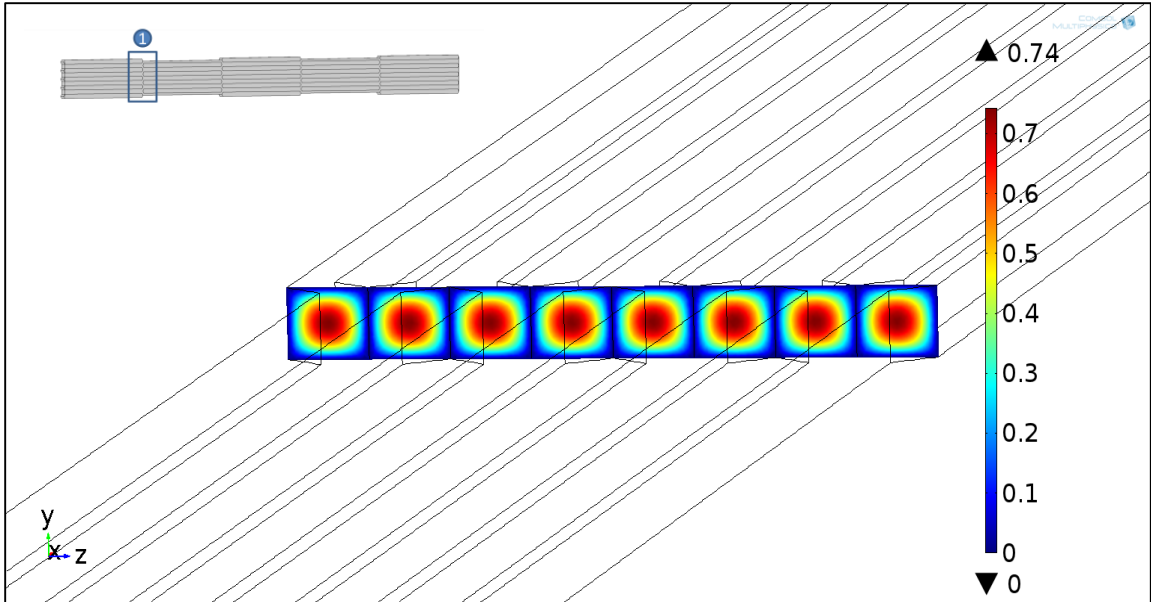
Velocity (cm/s) - 30 μm into 1st bifurcation



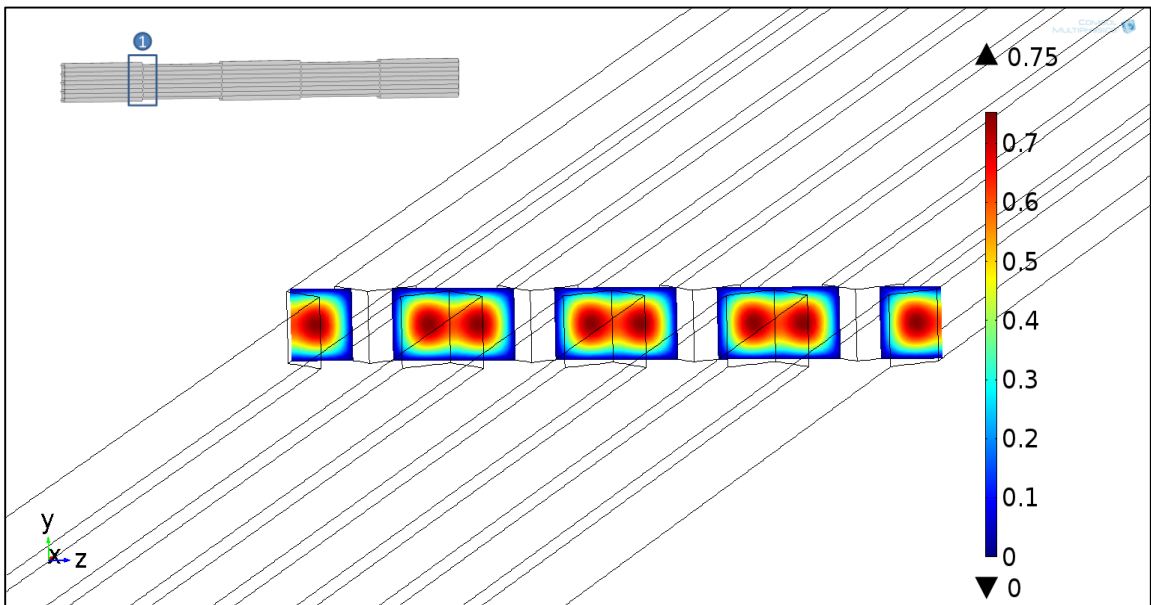
Velocity (cm/s) - 35 μm into 1st bifurcation



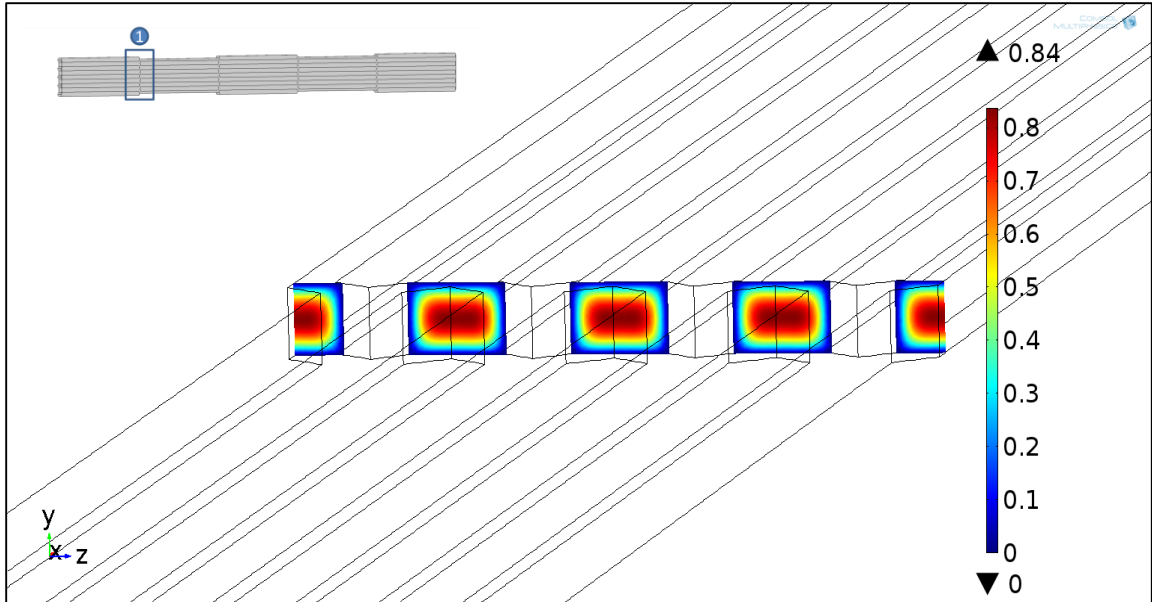
Velocity (cm/s) - 40 μm into 1st bifurcation



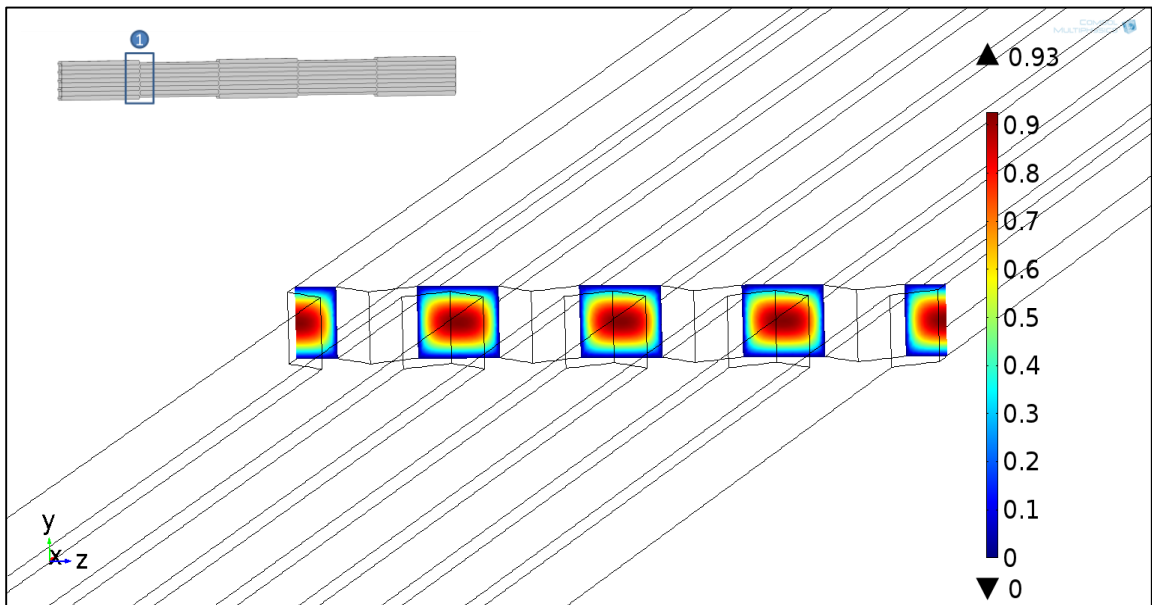
Velocity (cm/s) - Halfway (50 μm) into 1st bifurcation



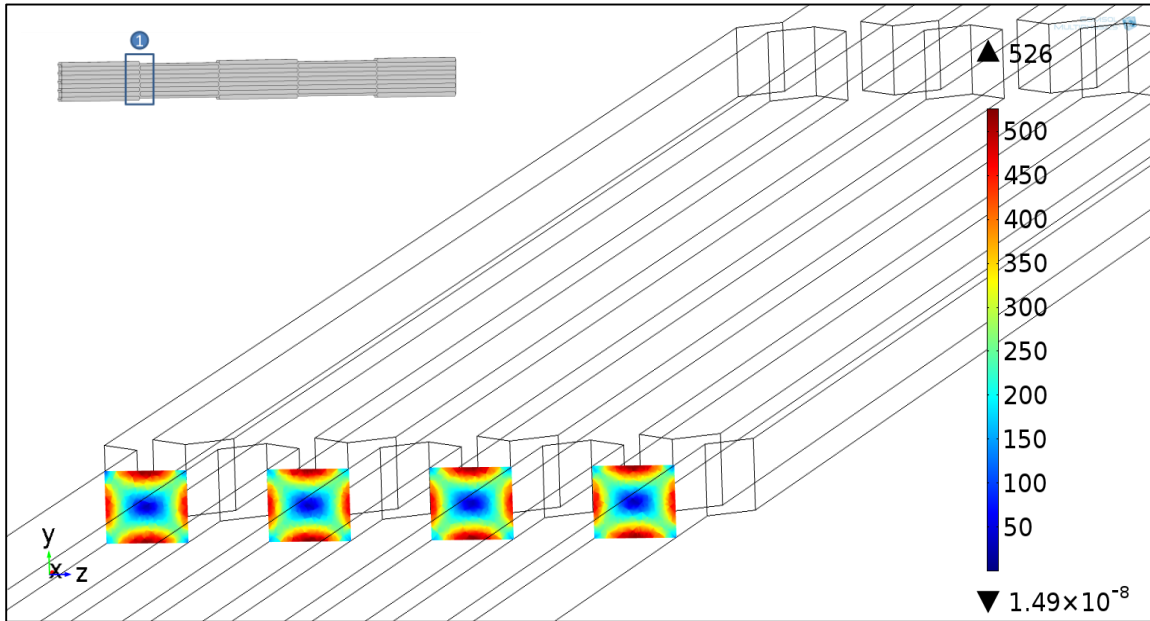
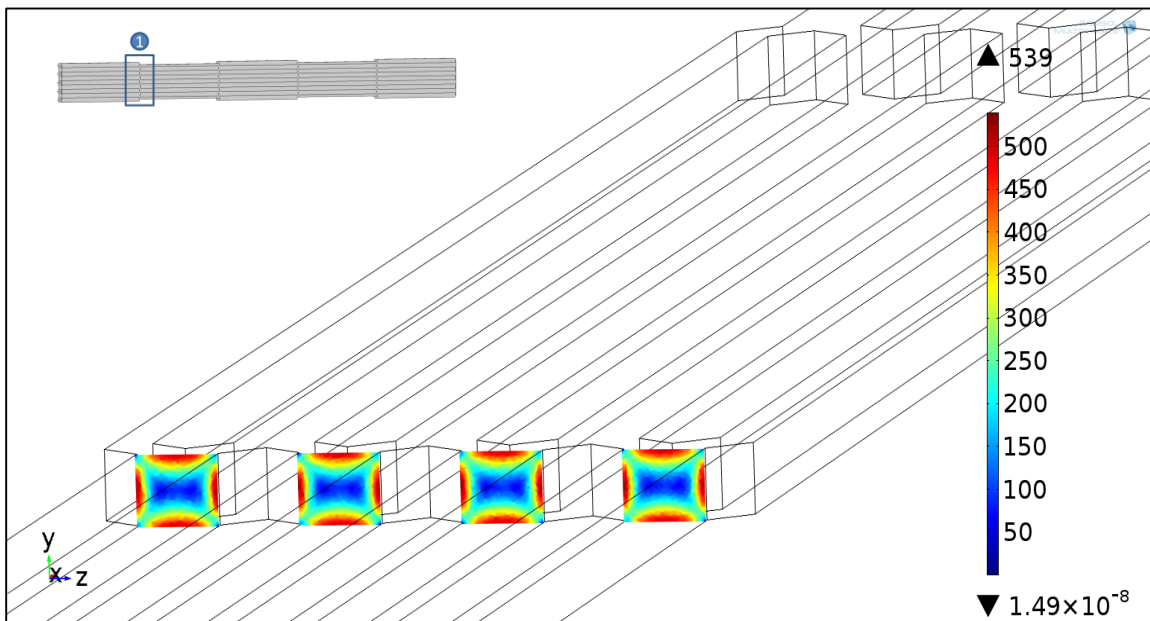
Velocity (cm/s) - Three Quarters (75 μm) into 1st bifurcation

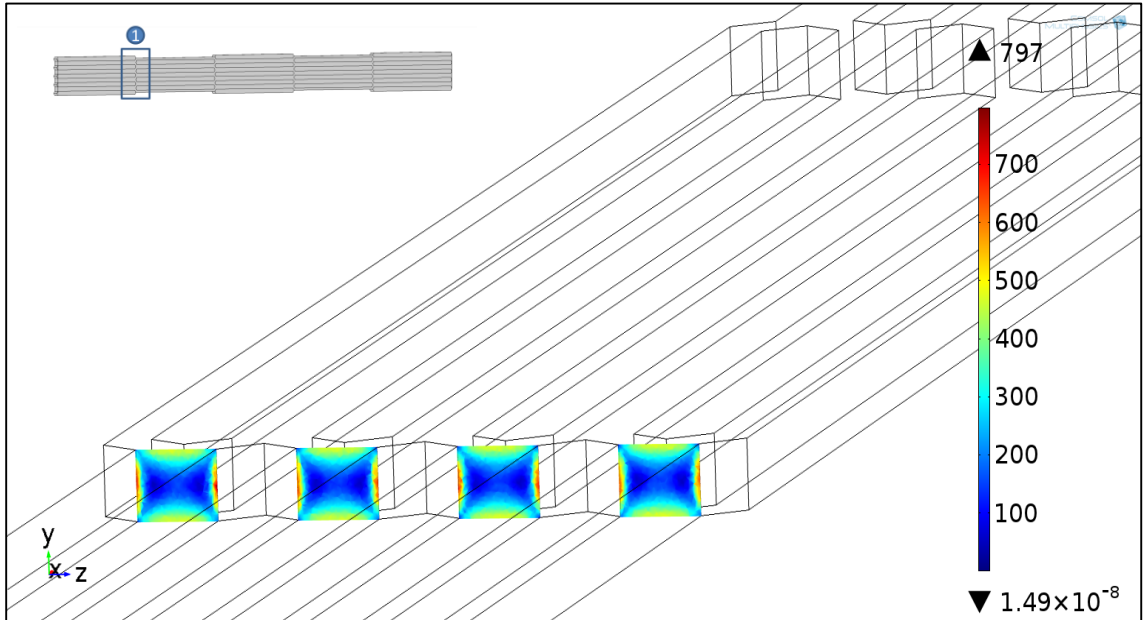


Velocity (cm/s) - 90 μm into 1st bifurcation

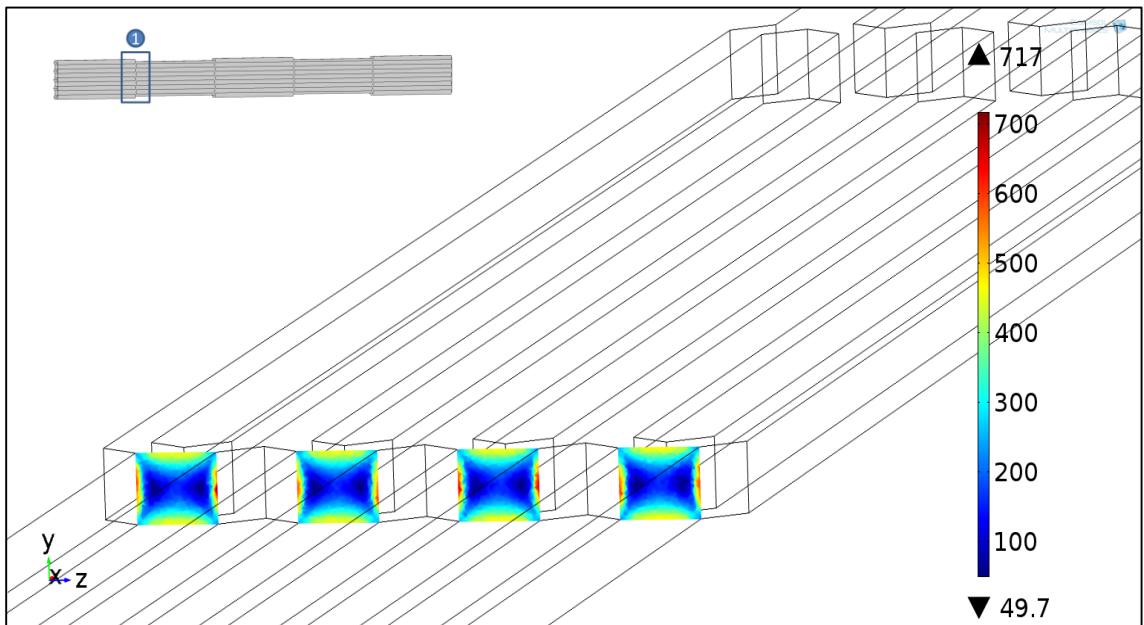


Velocity (cm/s) - End (100 μm) of 1st bifurcation

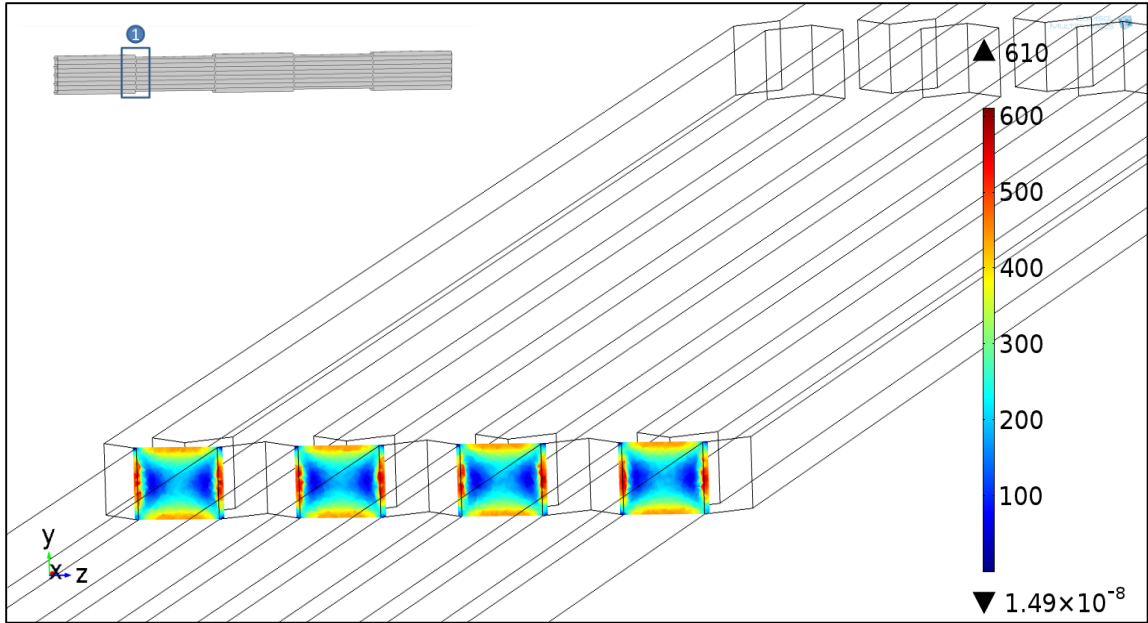
APPENDIX D: 1ST BIFURCATION SHEAR RATE PROFILES**FLOW RATE = 0.3ML/MIN****Shear rate (s^{-1}) - 200 μm before 1st bifurcation****Shear rate (s^{-1}) - 5 μm before 1st bifurcation**



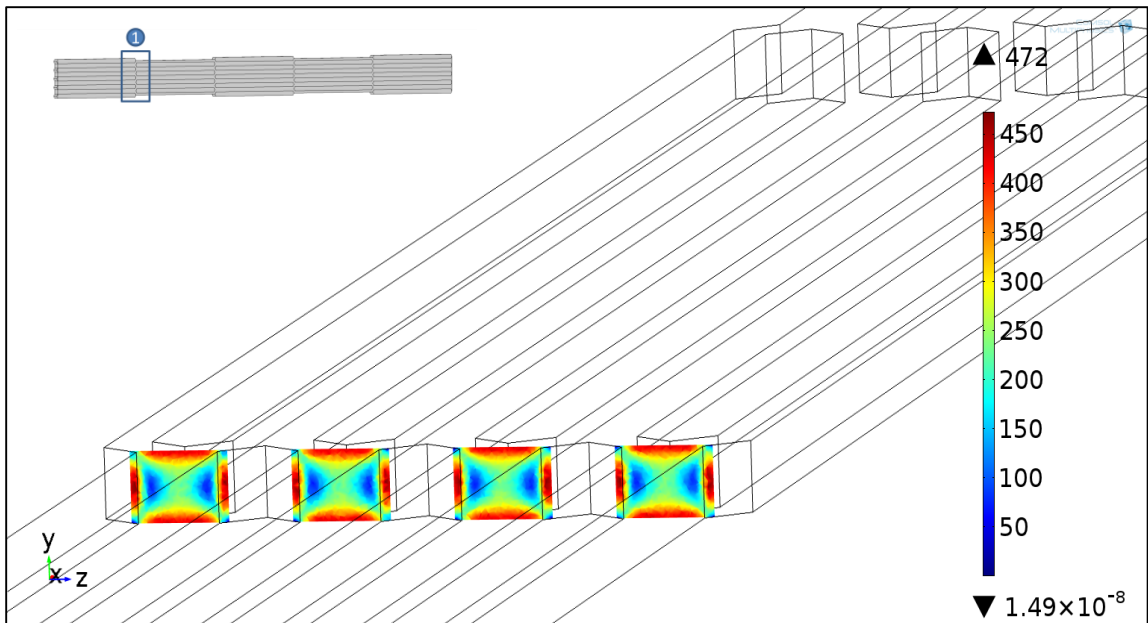
Shear rate (s^{-1}) - 1 μm before 1st bifurcation



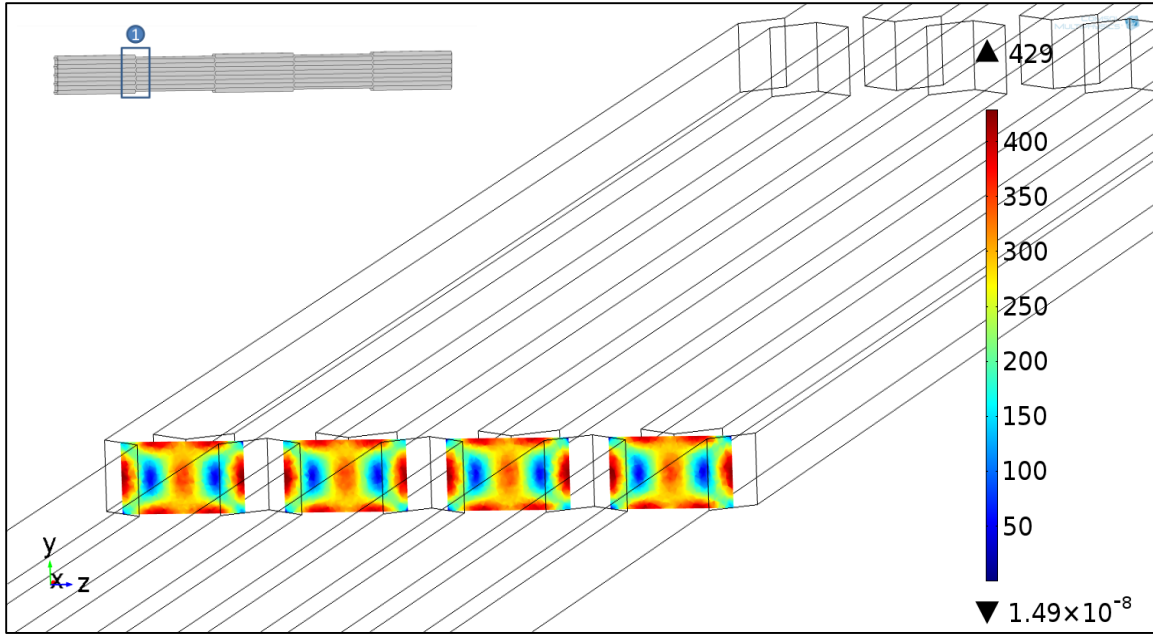
Shear rate (s^{-1}) - Entrance of 1st bifurcation



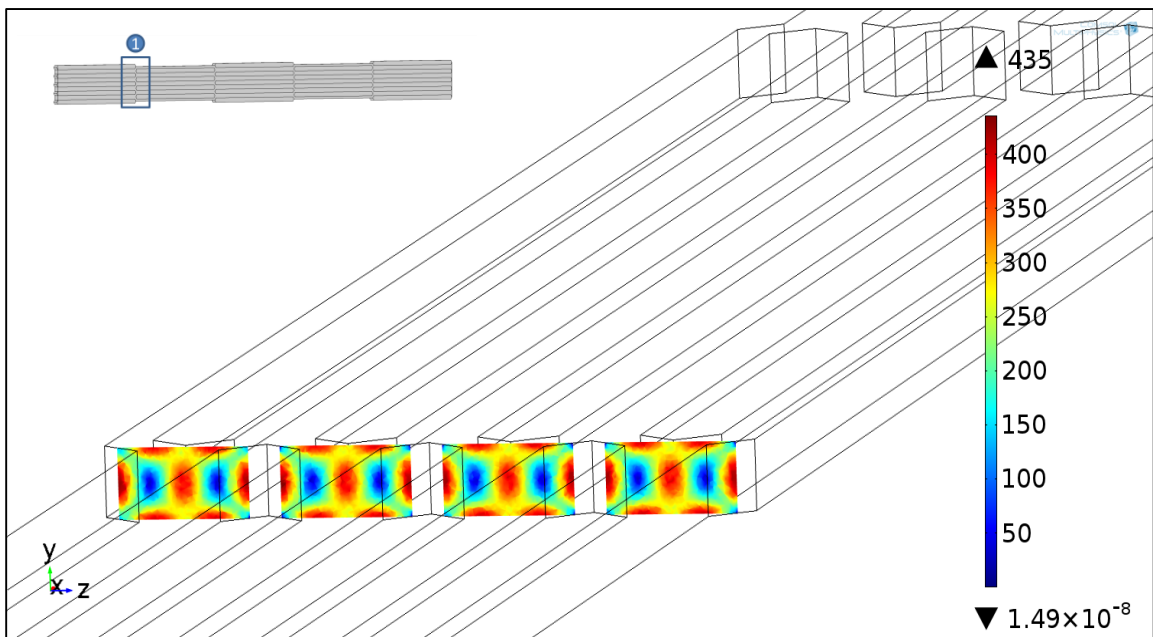
Shear rate (s^{-1}) - 5 μm into 1st bifurcation



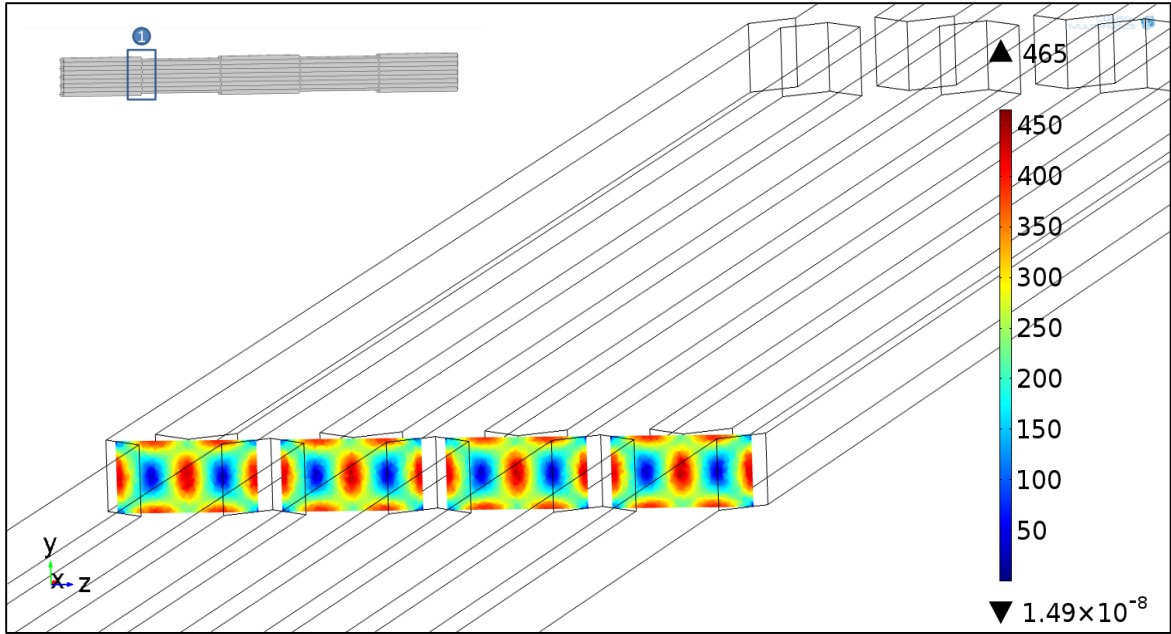
Shear rate (s^{-1}) - 10 μm into 1st bifurcation



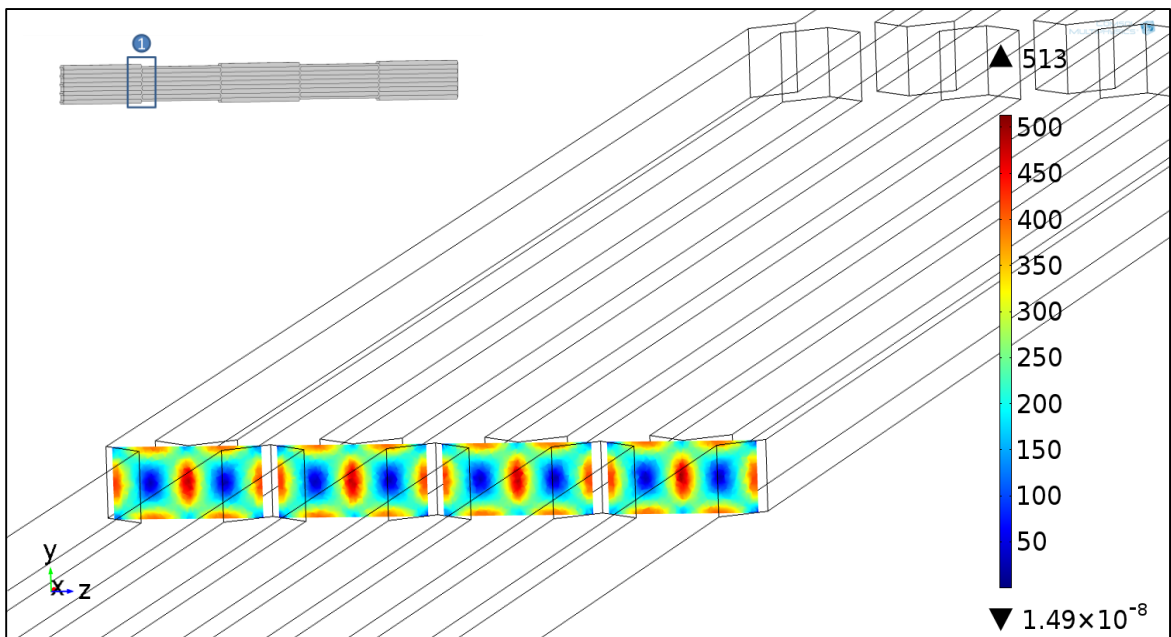
Shear rate (s^{-1}) - One Quarter (25 μm) into 1st bifurcation



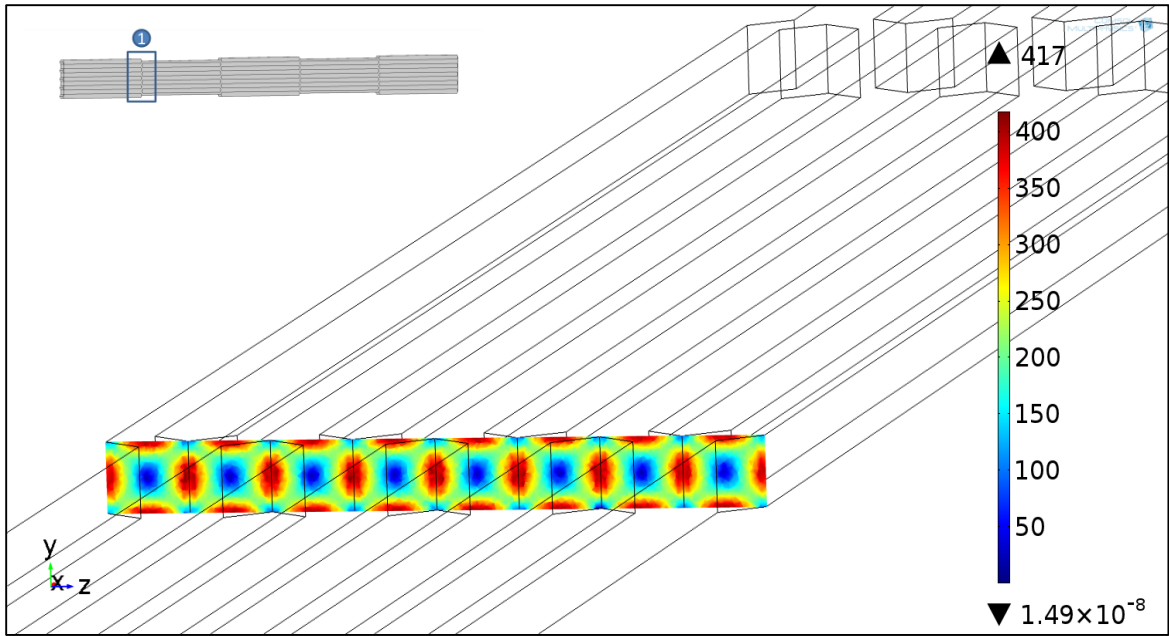
Shear rate (s^{-1}) - 30 μm into 1st bifurcation



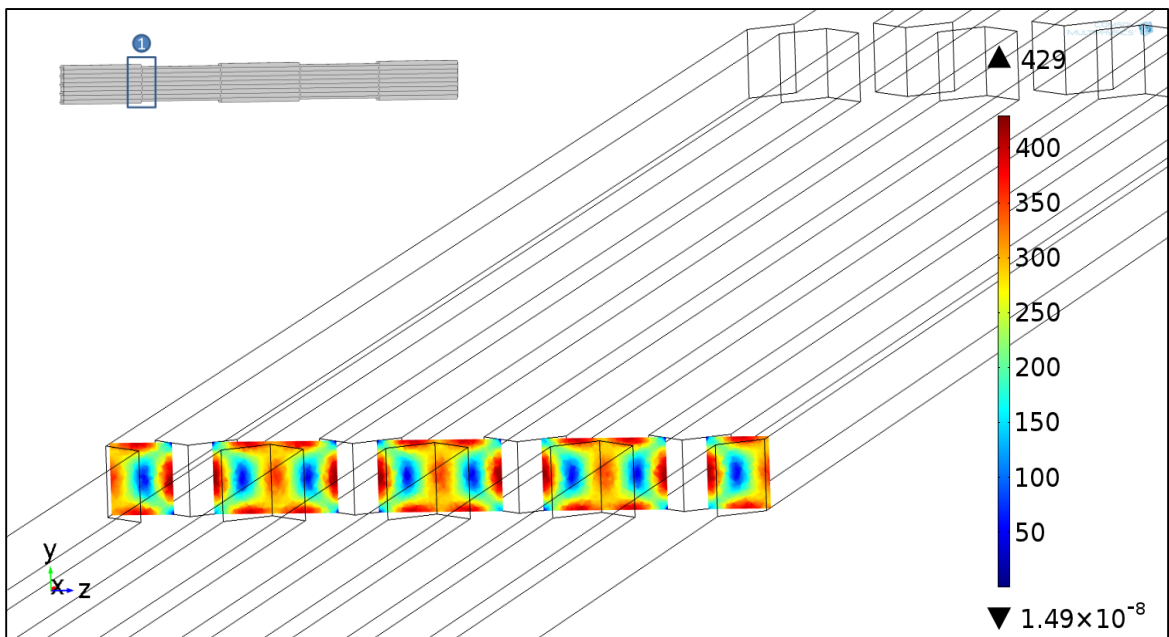
Shear rate (s^{-1}) - 35 μm into 1st bifurcation



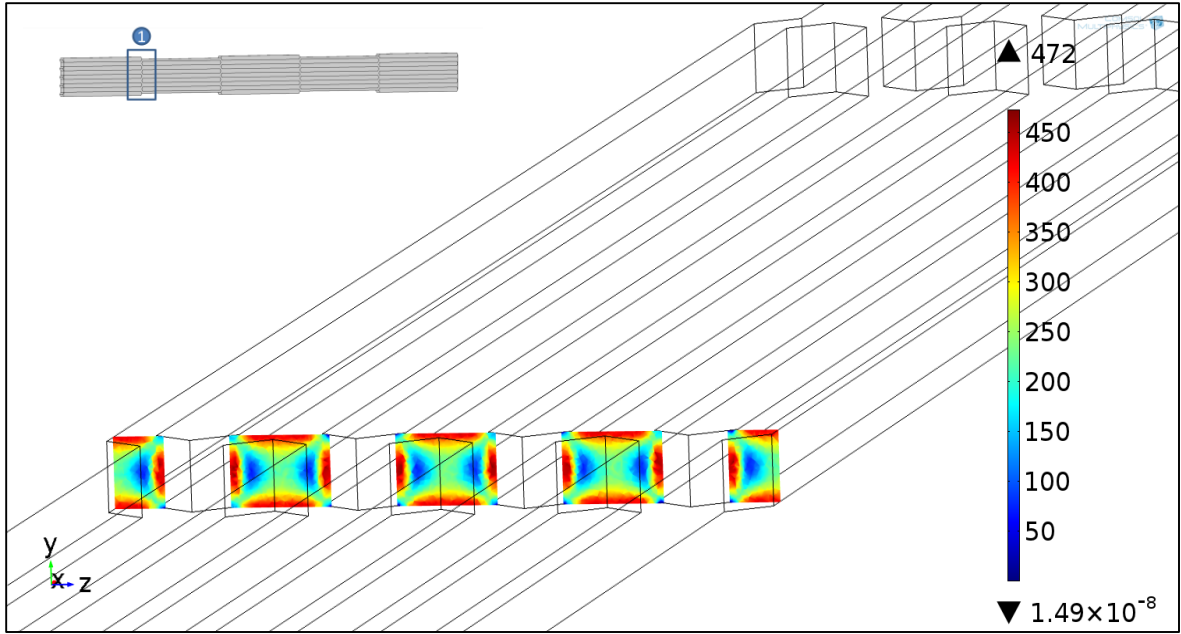
Shear rate (s^{-1}) - 40 μm into 1st bifurcation



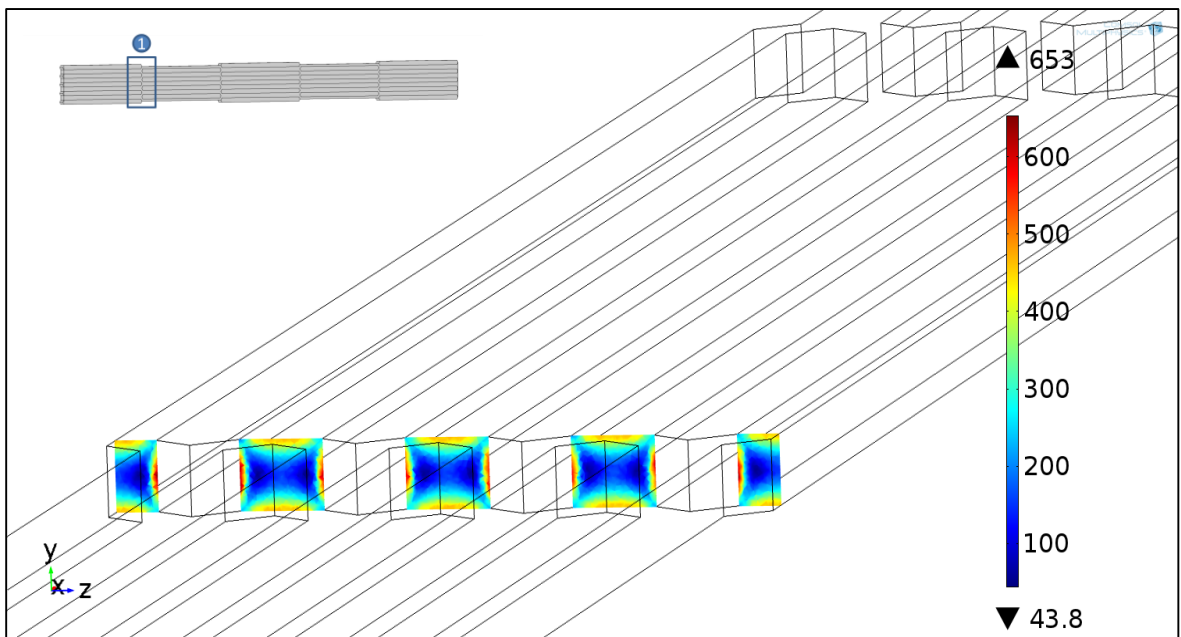
Shear rate (s^{-1}) - Halfway ($50 \mu\text{m}$) into 1st bifurcation



Shear rate (s^{-1}) - Three Quarters ($75 \mu\text{m}$) into 1st bifurcation



Shear rate (s^{-1}) - 90 μm into 1st bifurcation

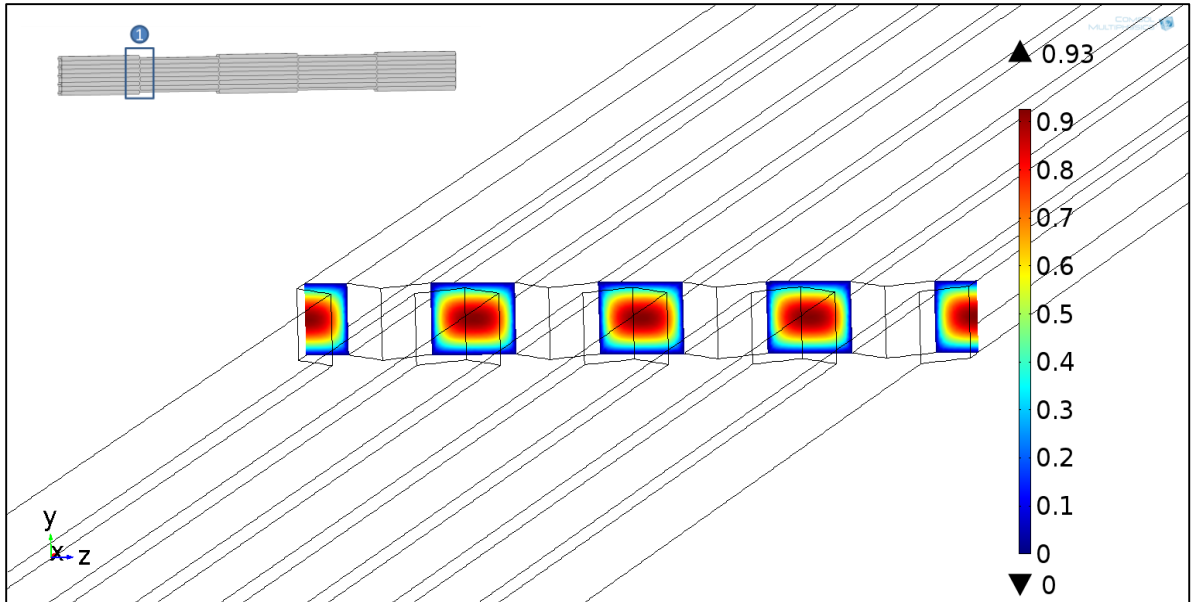


Shear rate (s^{-1}) - End (100 μm) of 1st bifurcation

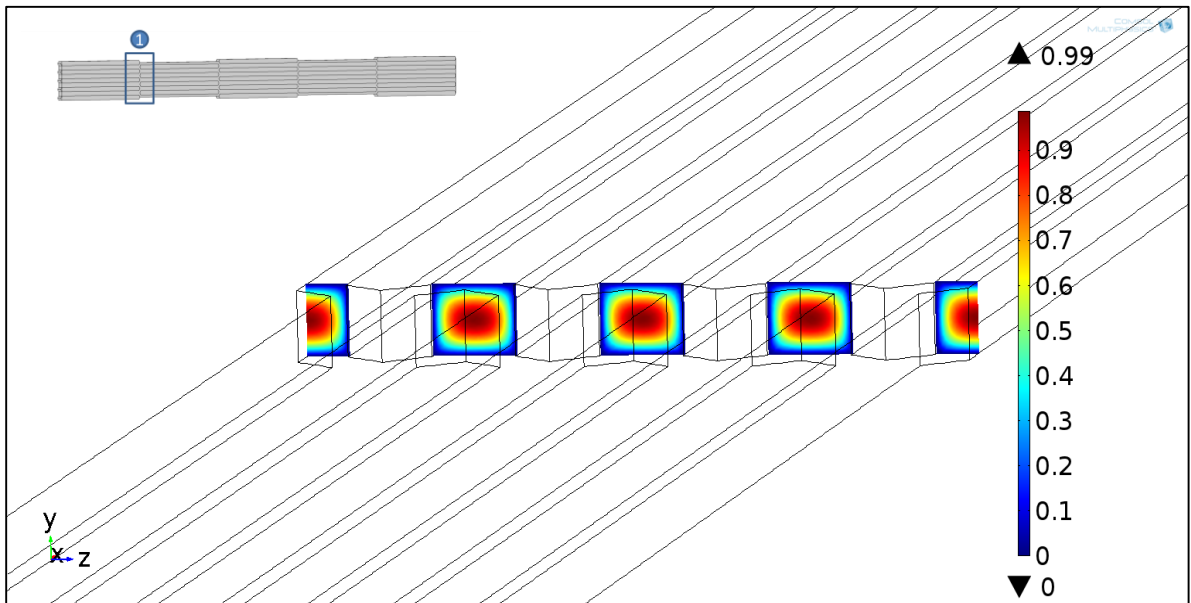
APPENDIX E: *DEVELOPMENT AFTER 1ST BIFURCATION*

VELOCITY PROFILES

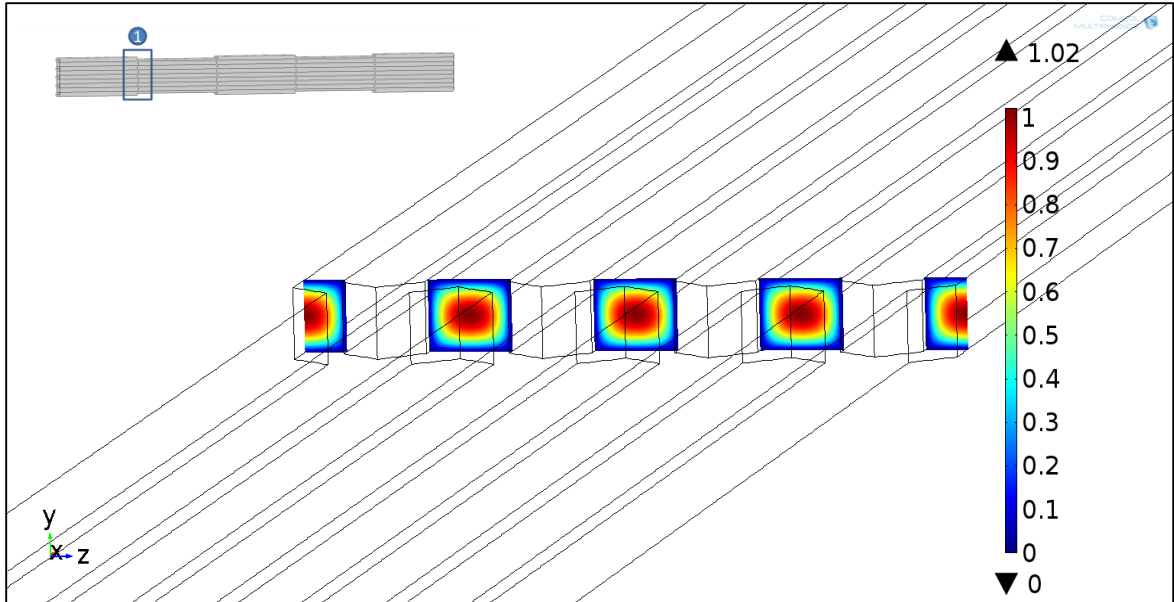
FLOW RATE = 0.3ML/MIN



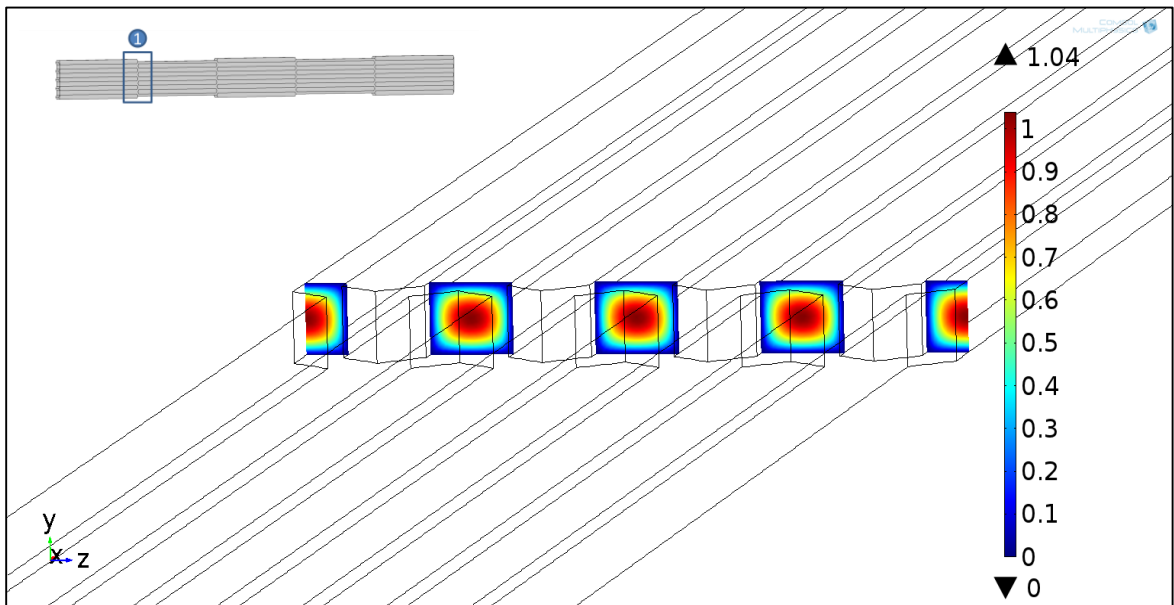
Velocity (cm/s) - End of 1st bifurcation / Beginning of Next Channel



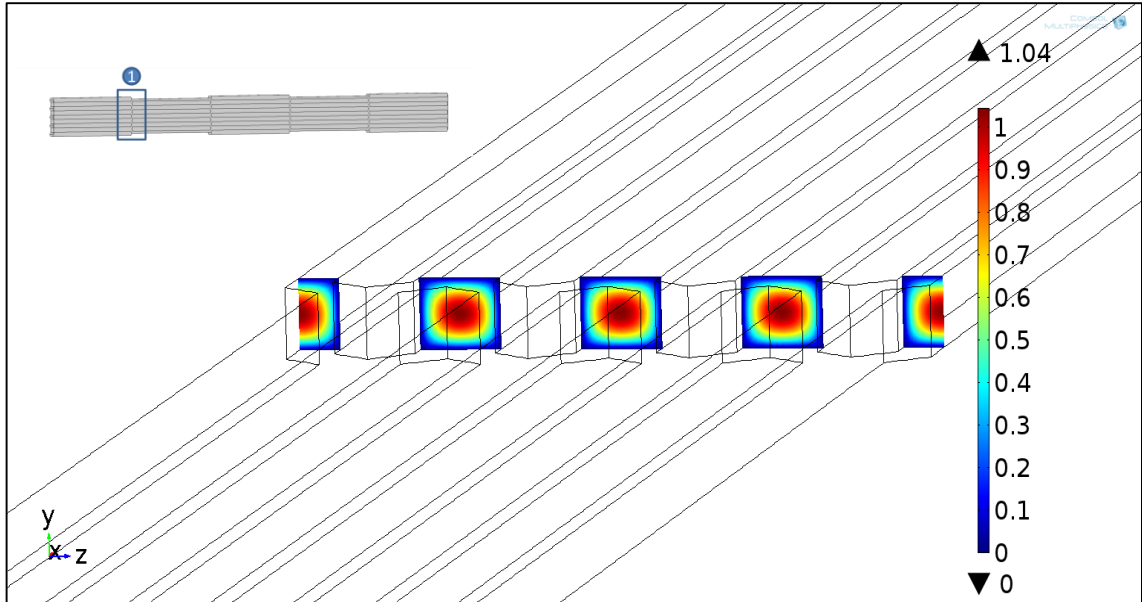
Velocity (cm/s) - 10 μ m After 1st Bifurcation



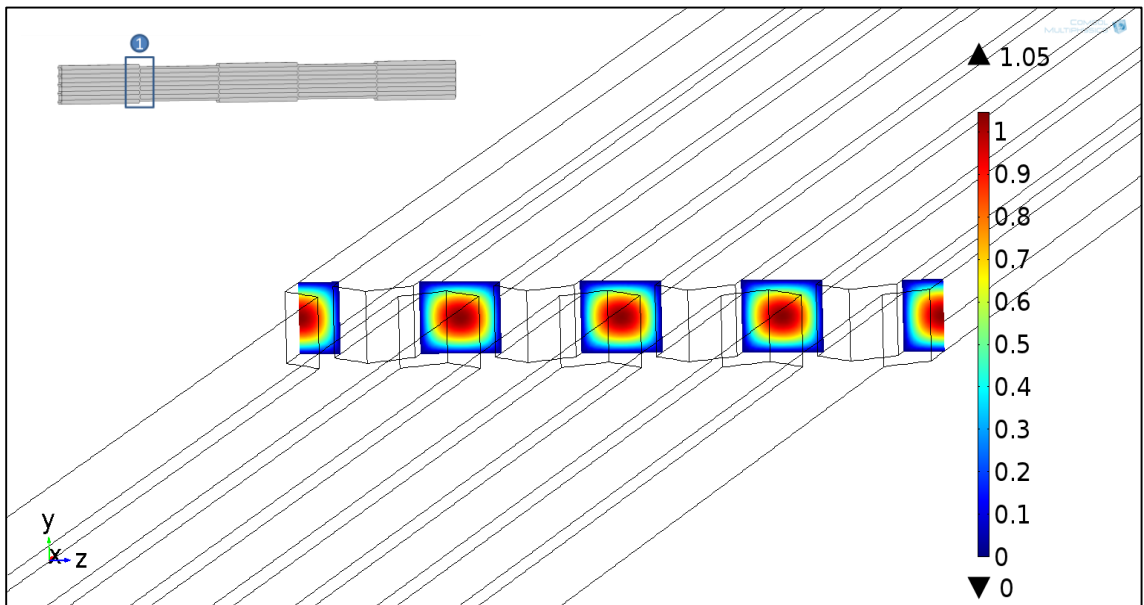
Velocity (cm/s) - 20 μm After 1st Bifurcation



Velocity (cm/s) - 30 μm After 1st Bifurcation

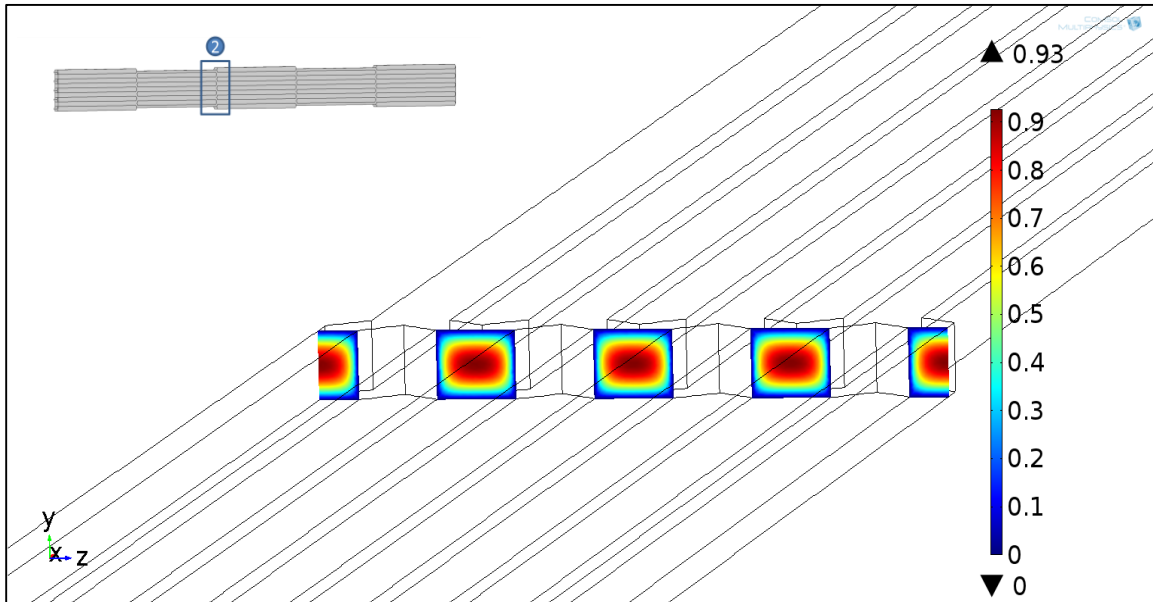
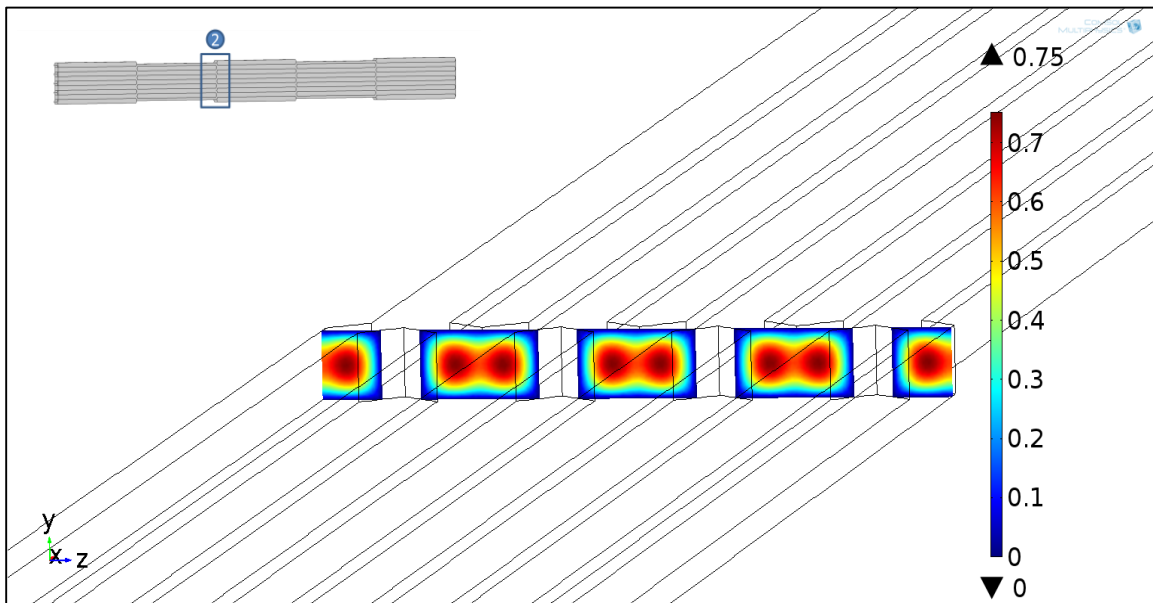


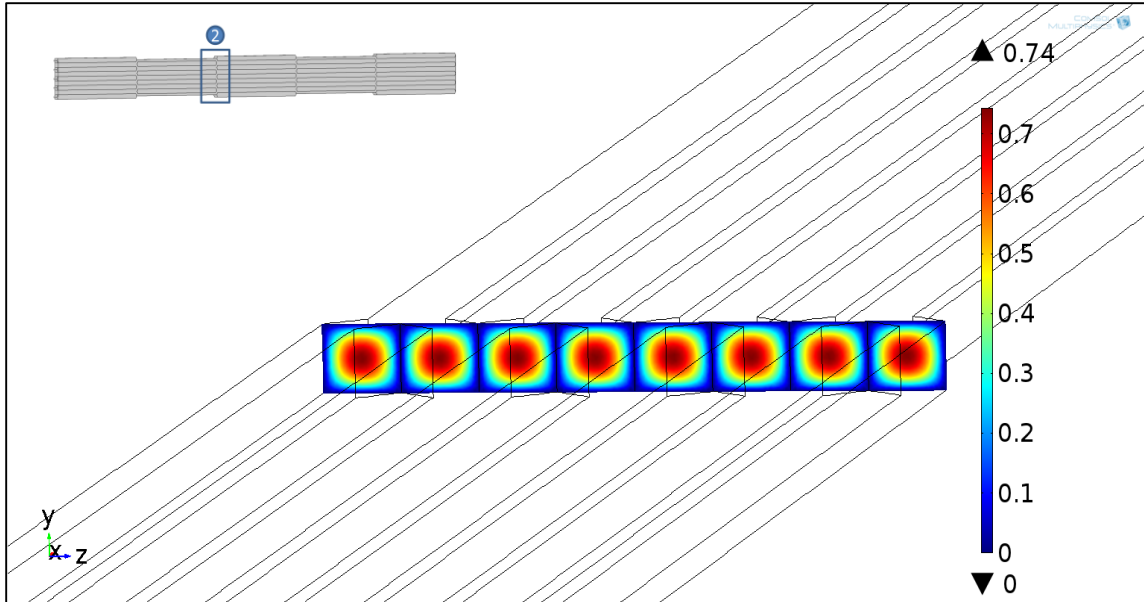
Velocity (cm/s) - 38 μm After 1st Bifurcation



Velocity (cm/s) - 39 μm After 1st Bifurcation

Note: Flow finishes re-developing at 39 μm

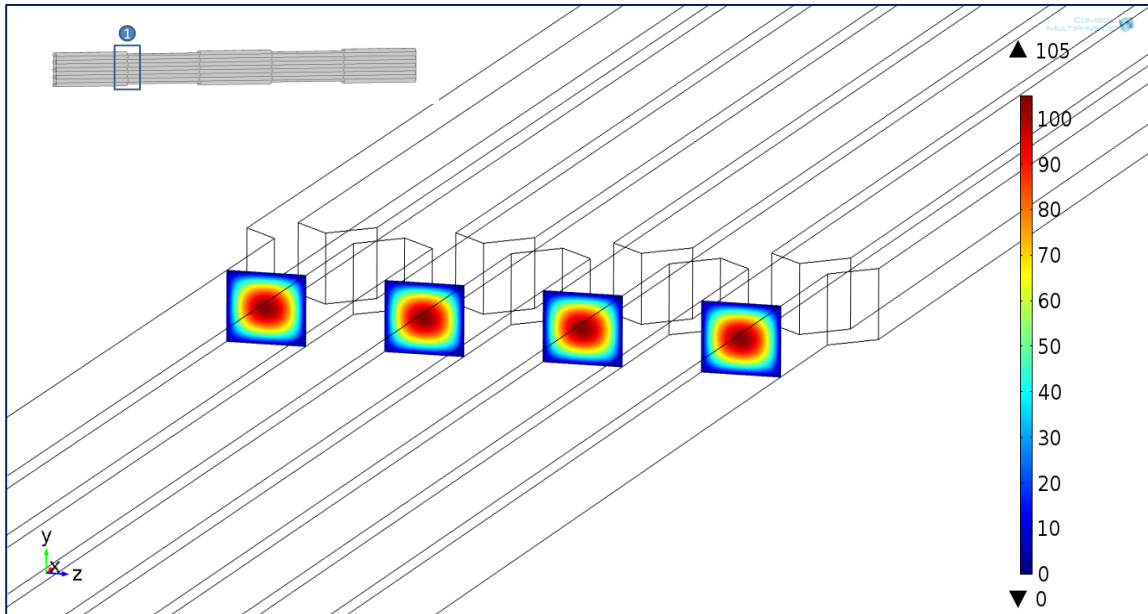
APPENDIX F: 2ND BIFURCATION VELOCITY PROFILES**FLOW RATE = 0.3ML/MIN****Velocity (cm/s) - Entrance of 2nd bifurcation****Velocity (cm/s) - One Quarter (25 μm) into the 2nd bifurcation**



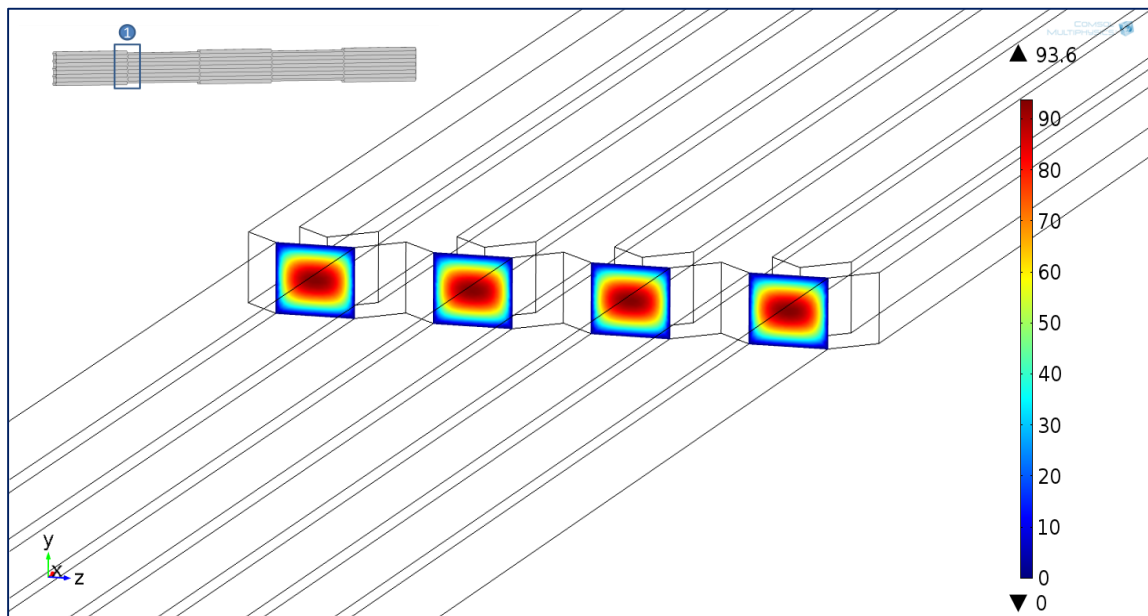
Velocity (cm/s) - Halfway (50 μm) into 2nd bifurcation

APPENDIX G: 100X FLOW RATE
1ST BIFURCATION VELOCITY PROFILES

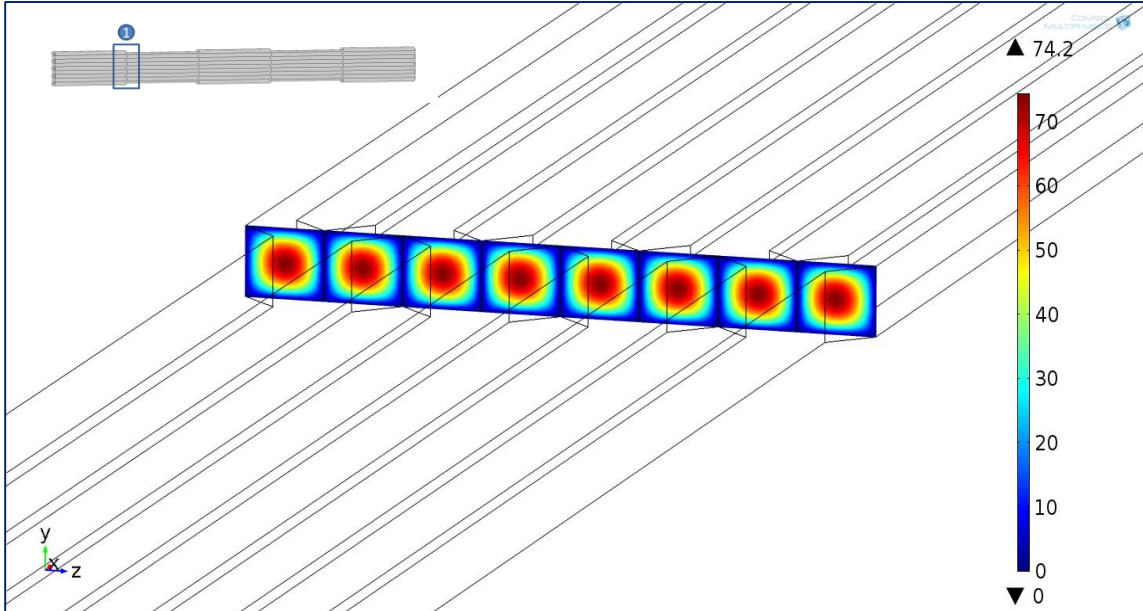
FLOW RATE = 30ML/MIN



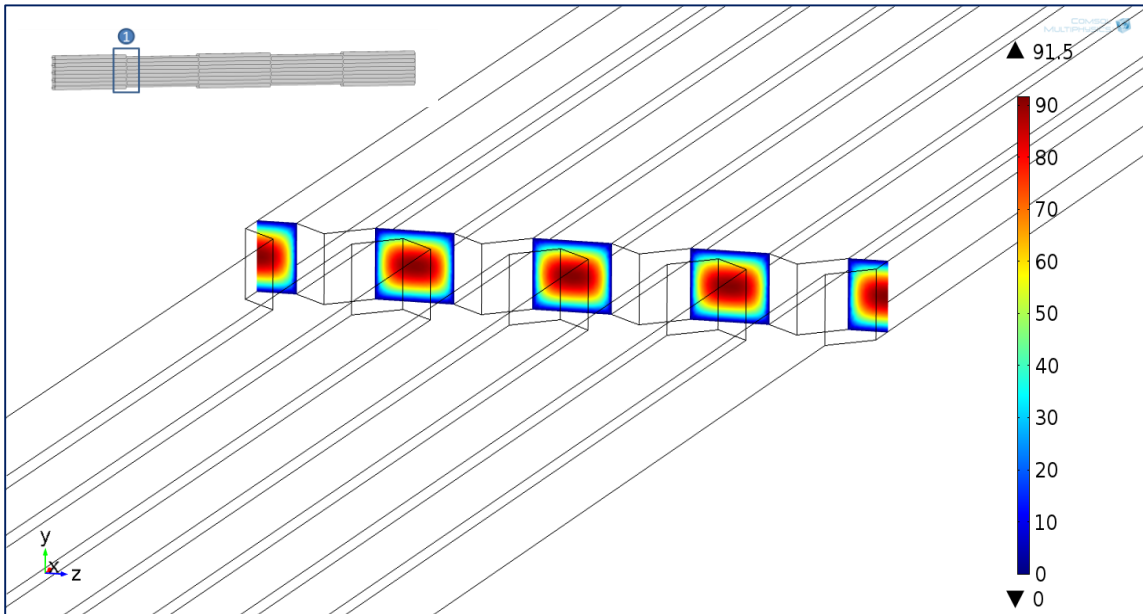
Velocity (cm/s) - 200 μ m before 1st bifurcation



Velocity (cm/s) - Entrance of 1st bifurcation



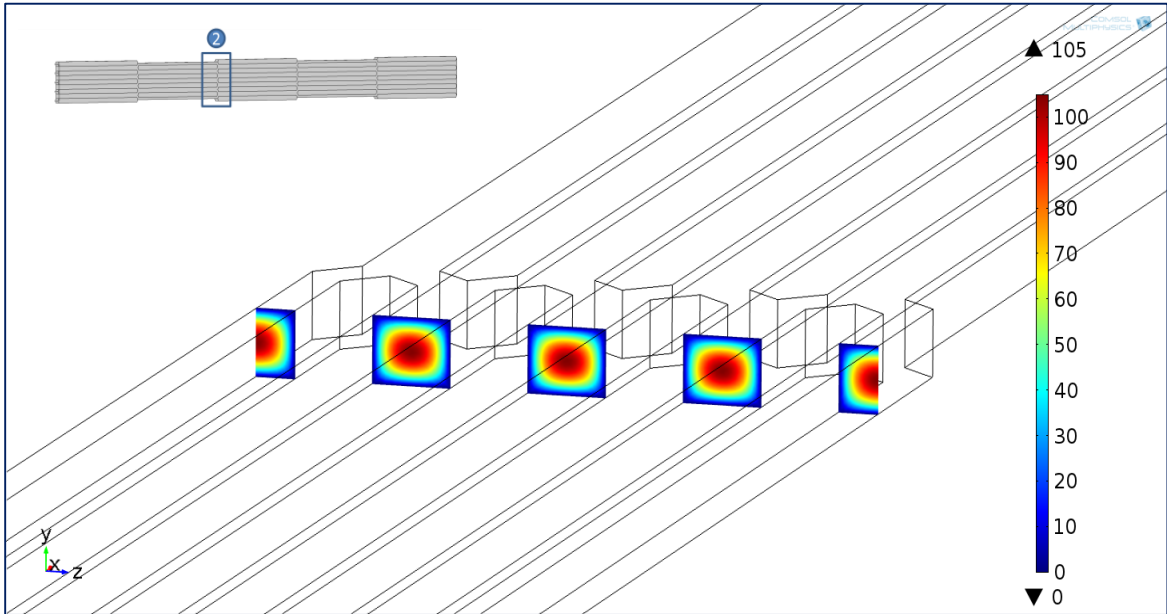
Velocity (cm/s) - Halfway (50 μm) into 1st bifurcation



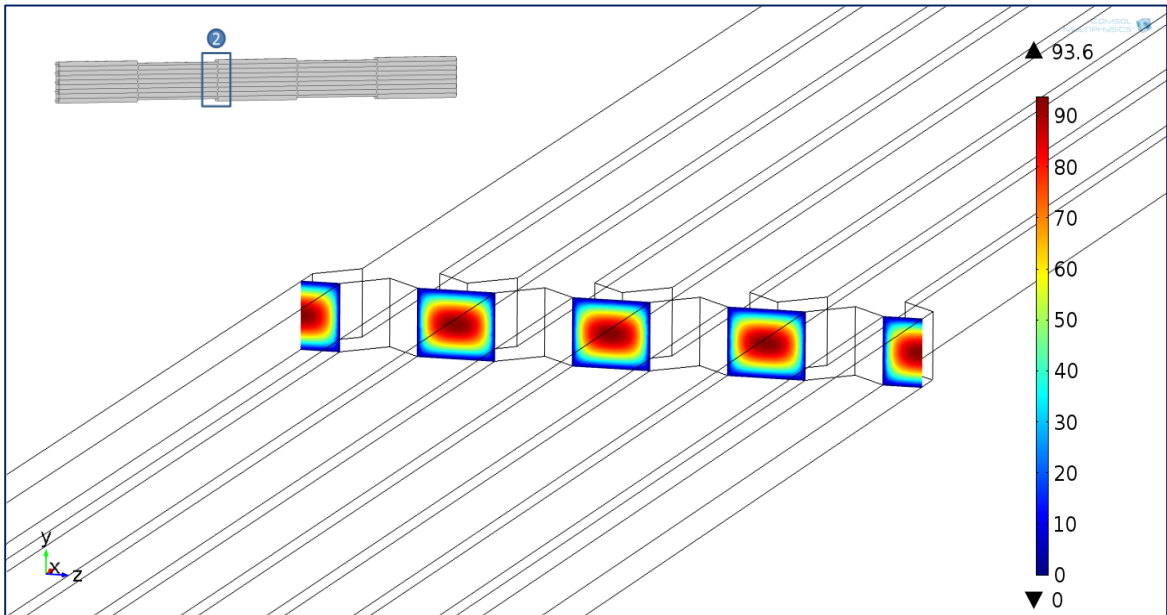
Velocity (cm/s) - End of 1st bifurcation / Beginning of Next Channel

APPENDIX H: 100X FLOW RATE
2ND BIFURCATION VELOCITY PROFILES

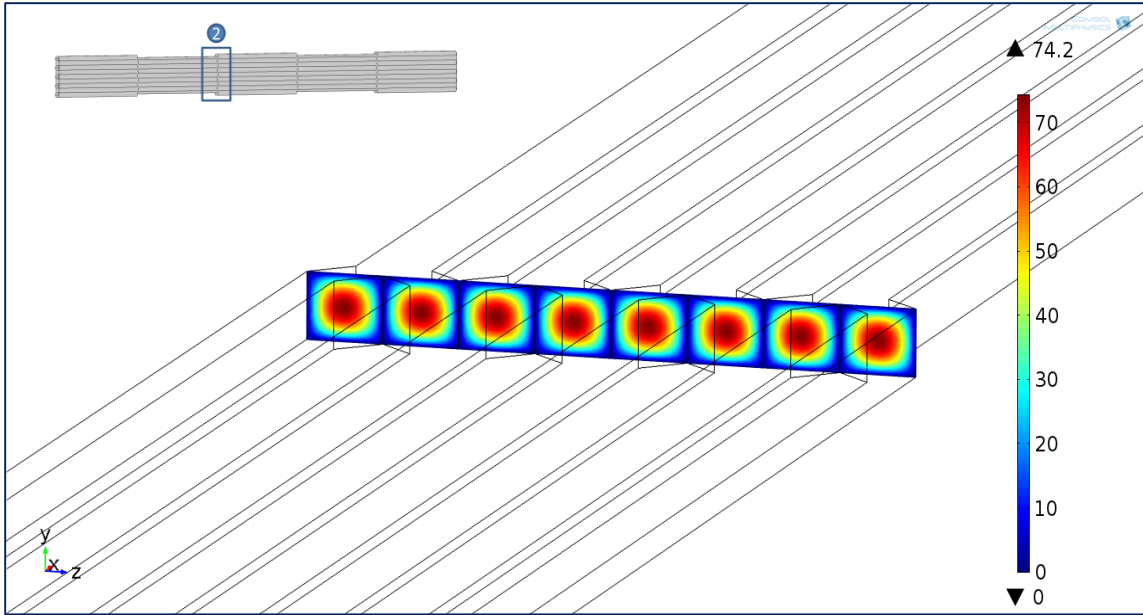
FLOW RATE = 30ML/MIN



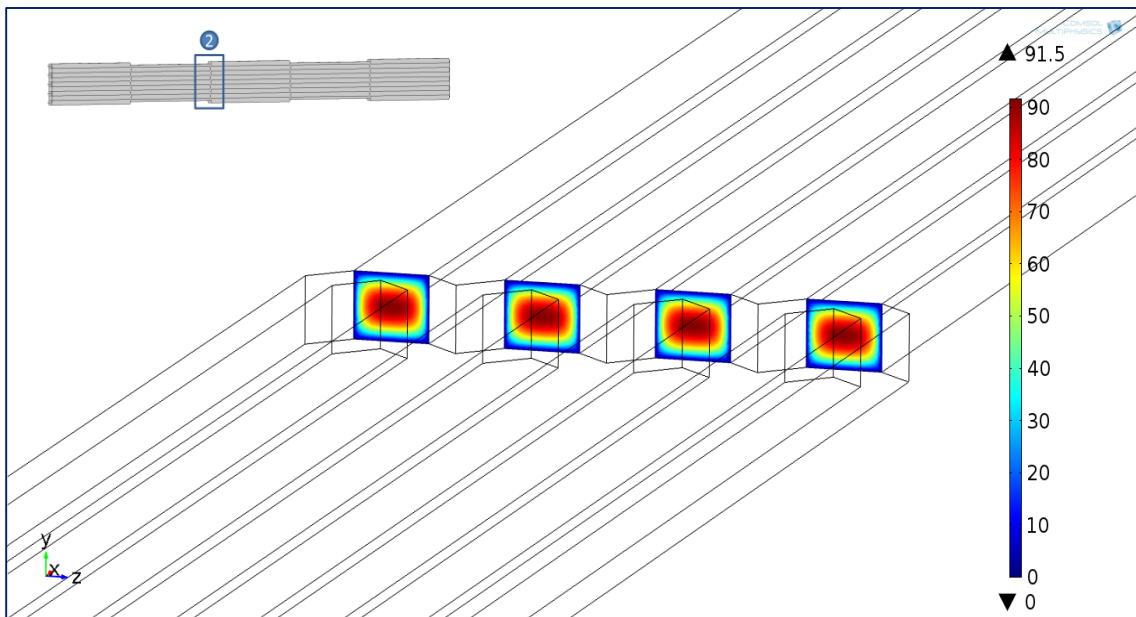
Velocity (cm/s) - 200 μm before 2nd bifurcation



Velocity (cm/s) - Entrance of 2nd bifurcation



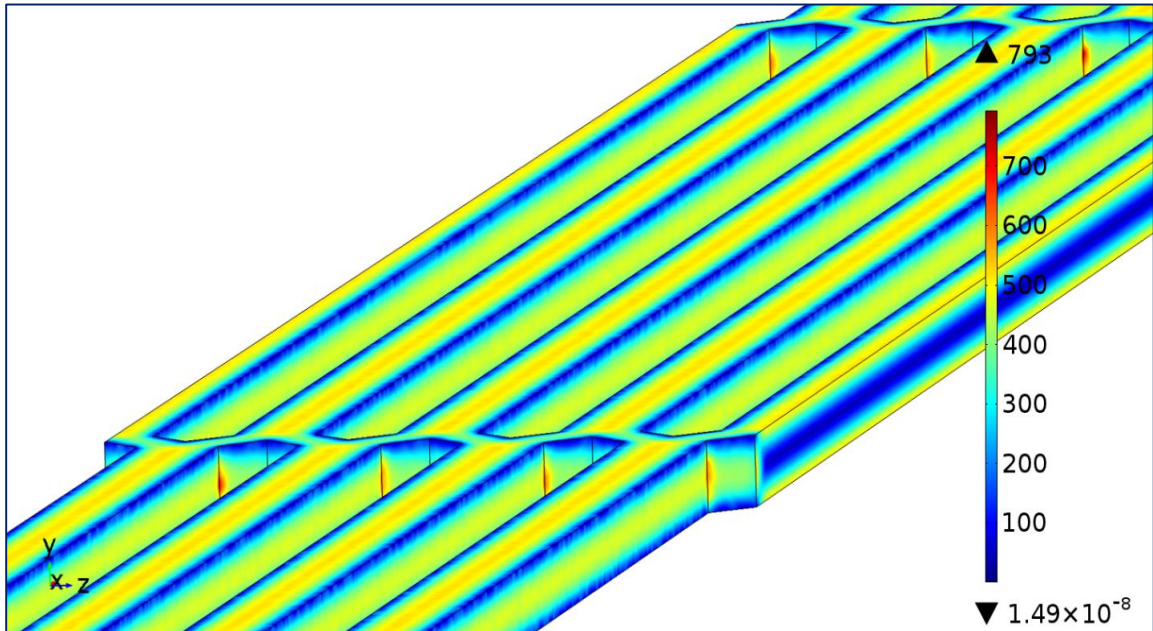
Velocity (cm/s) - Halfway (50 μm) into 2nd bifurcation



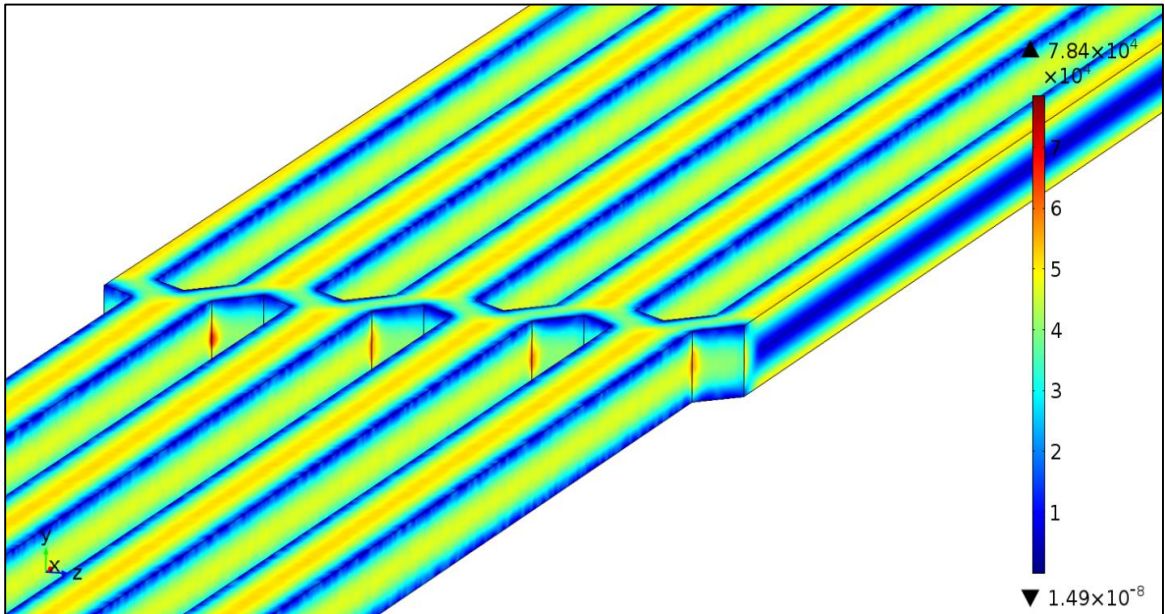
Velocity (cm/s) - End of 2nd bifurcation / Beginning of Next Channel

APPENDIX I: *SURFACE SHEAR RATE DATA*

FLOW RATE = 0.3ML/MIN



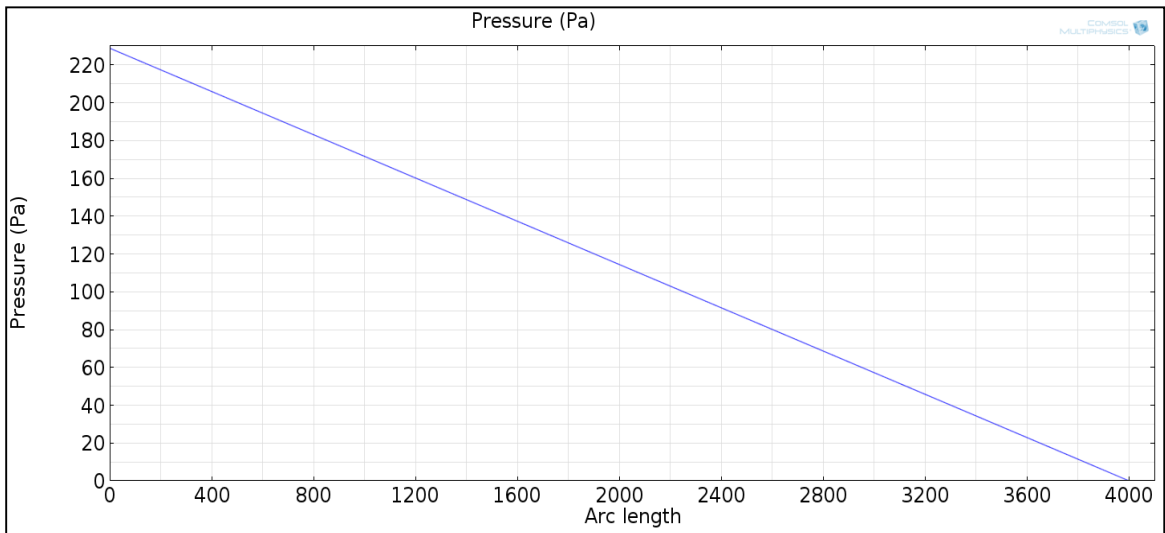
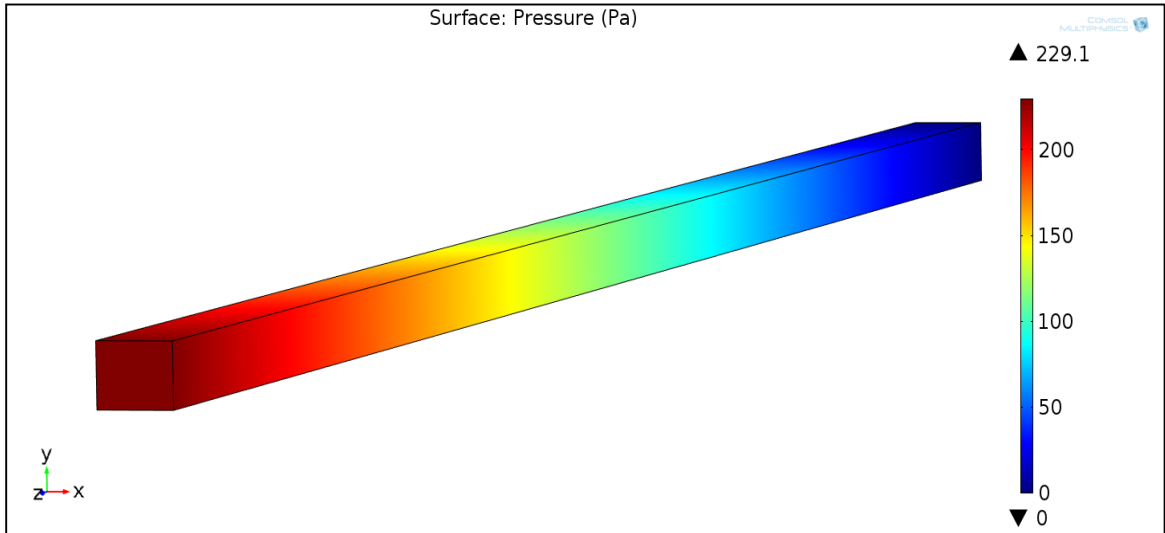
Note: This visualization of shear rate values on the surface of the lamina is good because it shows represents the maximum shear rates that occur along the channel.

APPENDIX J: 100X FLOW RATE***SURFACE SHEAR RATE DATA*****FLOW RATE = 30 mL/MIN**

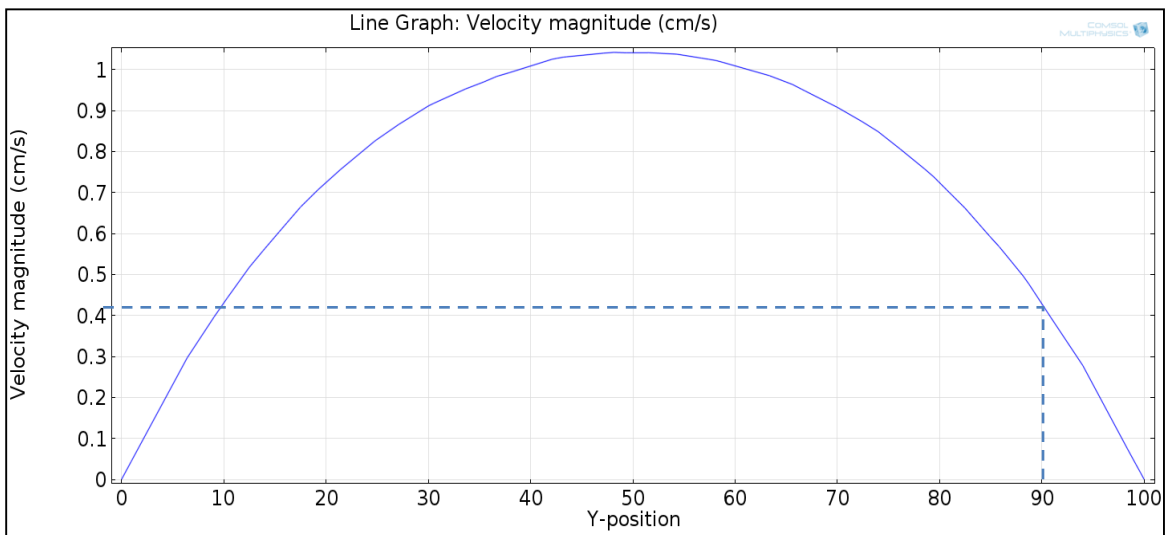
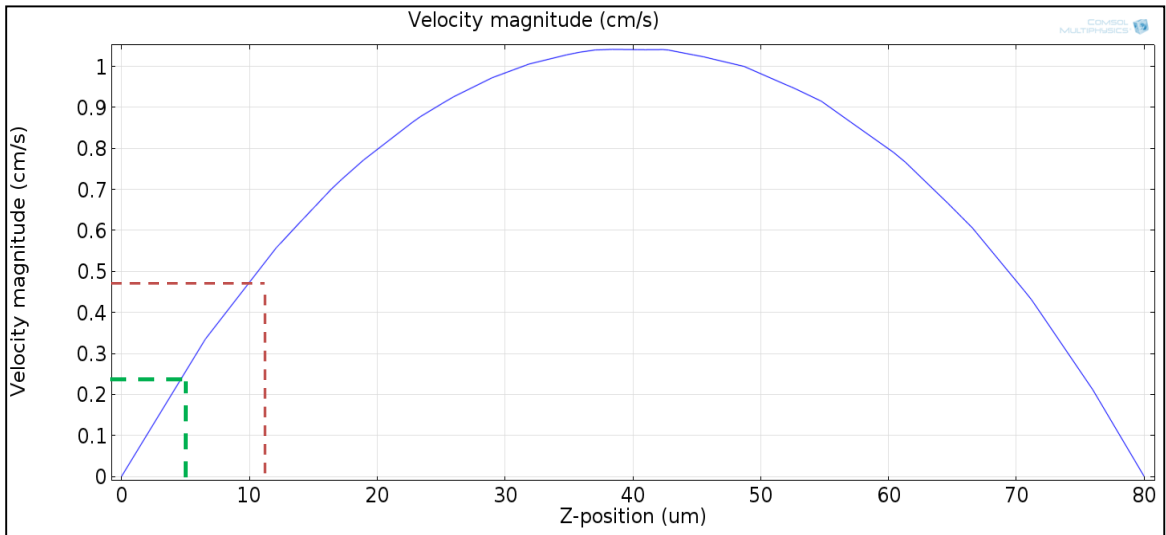
Note: This visualization of shear rate values on the surface of the lamina is good because it shows represents the maximum shear rates that occur along the channel.

APPENDIX K: VALIDATION CHANNEL PRESSURE DROP

FLOW RATE = 0.3ML/MIN

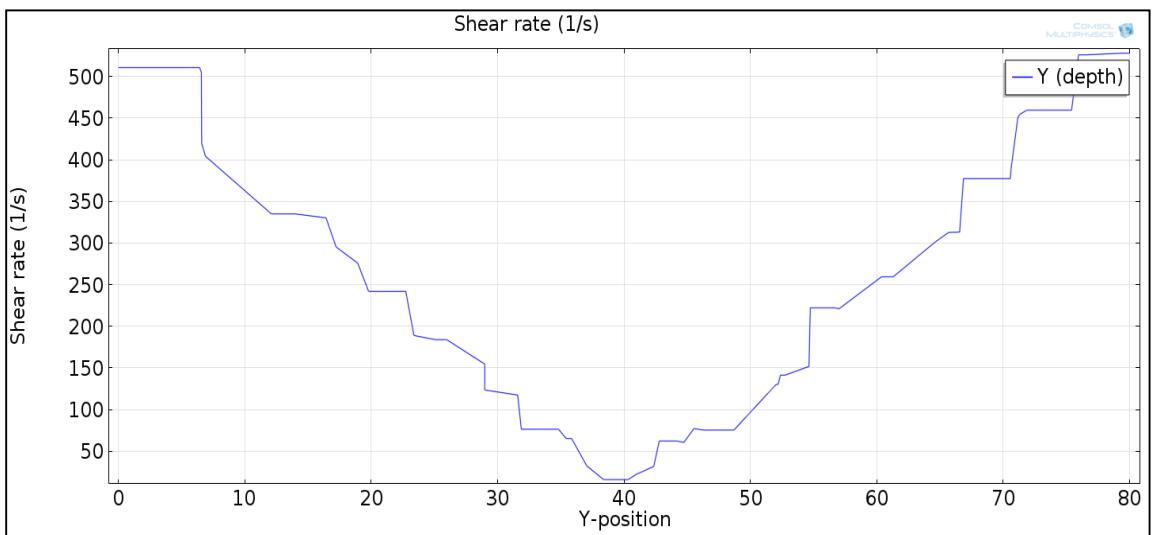
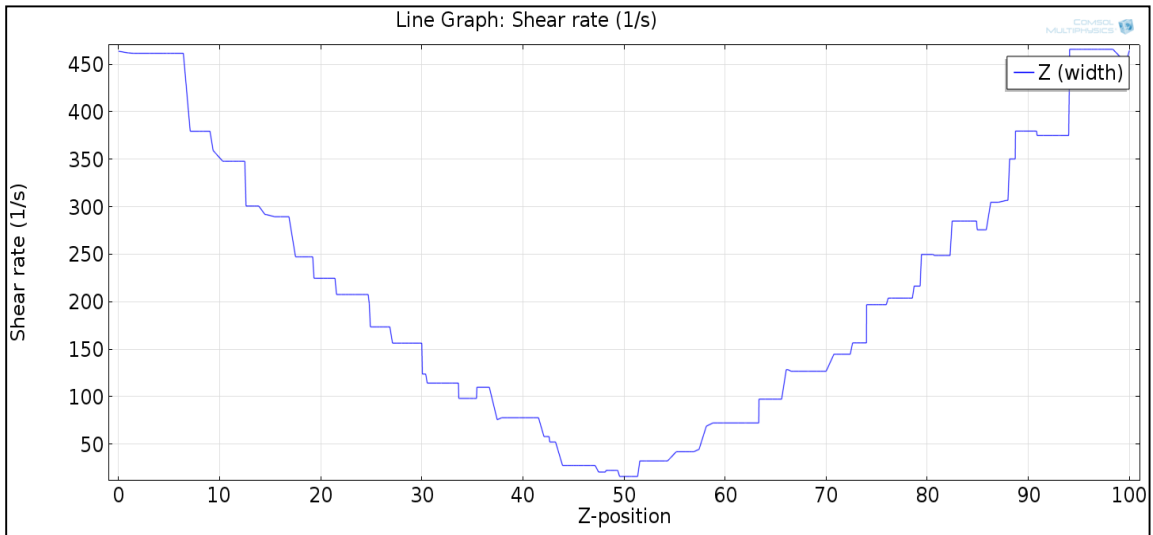


APPENDIX L: VALIDATION CHANNEL VELOCITY PROFILE



Note: In the graphs above, the red and blue lines mark velocities magnitudes relevant for comparing the difference between the COMSOL generated profile and the MATLAB/Analytical Solution generated profile. The green line marks the velocity for fluid 5 μm from the wall, used for the RBC velocity in equation 23 which is equal to 0.23cm/s.

APPENDIX M: VALIDATION CHANNEL SHEAR PROFILE



Note: In the graphs above, the shear rate is taken in the center of the channel length (2 mm). The Z profile scans the Z-profile from the middle of one side wall across the 100 μm width to the other side. Likewise, the Y profile scans the middle of the bottom wall up 80 μm to the center of the top wall.

APPENDIX N: *THEORETICAL VALIDATION OF COMSOL CFD USING MATLAB*

Script #1 - Average Velocity Finder

```

clear
clc

%chamber dimensions in m

width=100*10^-4; %um -> cm
height=80*10^-4; %um -> cm
length=4*10^-1; %mm -> cm

a=width/2;
b=height/2;

%fluid properties
visc=3.12*10^-3; %viscosity (Pa*s)
dp=261.1; %analytical change in pressure (Pa)
dpdx=dp/length; %dp/dx

%enter desired y and z!
y=0;
z=0;

%setup for first iteration
n=1;
epsilon(n)=((-1)^((n-1)/2)/n^3)*(1-
cosh(n*pi/(2*a)*z)/(cosh(n*pi*b/(2*a))))*cos(n*pi/(2*a)*y);
sepsilon(n)=epsilon(n);

flag=1;
while flag==1
    n=n+2;
    epsilon(n)=((-1)^((n-1)/2)/n^3)*(1-
cosh(n*pi/(2*a)*z)/(cosh(n*pi*b/(2*a))))*cos(n*pi/(2*a)*y);
    sepsilon(n)=sepsilon(n-2)+epsilon(n);
    ratio=sepsilon(n)/sepsilon(n-2);

    if ratio > .9999 && ratio <1.0001
        flag=0;
    end
end

umax=16*a^2/(visc*pi^3)*dpdx*sepsilon(n)

```

Output: $u_{\max}=1.1986$

Script #2 - Average Velocity Finder

```

clear all
close all
clc

%coordinate system
z=0; %describing the change in width
y=0; %describing the change in height
%as such x is describing the change in length

%chamber dimensions in m

width=100*10^-4; %um -> cm
height=80*10^-4; %um -> cm
channel_length=0.4; %mm -> cm

a=width/2;
b=height/2;

%fluid properties
visc=3.12*10^-3; %viscosity (Pa*s)
dp=226.1; %analytical change in pressure (Pa)
dpdx=dp/channel_length; %dp/dx

%setup for calculations
n=1; %odd integer counter
nz=1; %z counter
ny=0; %y counter
step=2000; %step size (also set to 10000)

for y=0:b/step:b
    flag=1;
    ny=ny+1
    %reset z
    z=0;
    nz=1;
    while flag==1

        if n==1
            epsilon(n)=((-1)^((n-1)/2)/n^3)*(1-
cosh(n*pi*y/(2*a))/(cosh(n*pi*b/(2*a))))*cos(n*pi*z/(2*a));
            sepsilon(n)=epsilon(n);
        end

        n=n+2;
        epsilon(n)=((-1)^((n-1)/2)/n^3)*(1-
cosh(n*pi*y/(2*a))/(cosh(n*pi*b/(2*a))))*cos(n*pi*z/(2*a));
        sepsilon(n)=sepsilon(n-2)+epsilon(n);
        ratio=sepsilon(n)/sepsilon(n-2);

        if isnan(ratio) || ratio > .9999 && ratio <1.0001
            if isnan(sepsilon(n))
                sepsilon(n)=0;
            end
        end
    end
end

```

```

end
u(nz,ny)=16*a^2/(visc*pi^3)*dpdx*sepsilon(n);
zvalue(nz)=z;
yvalue(ny)=y;
nz=nz+1;
z=z+a/step;
n=1;
if z > a
    flag=0;
end
end
end
end

%reset z and y value
z=0;
y=0;

u_ave=mean2(u) %average velocity

```

Outputs :

2,000 X 2,000 grid u _{ave} = 0.4977 cm/s	10,000 X 10,000 grid u _{ave} = 0.4978 cm/s
<pre> Command Window ny = 2000 ny = 2001 u_ave = 0.4977 fx >> </pre>	<pre> Command Window ny = 10000 ny = 10001 u_ave = 0.4978 fx >> </pre>

This script outputs the ny values to track the progress. The resolution is set such that MATLAB plugs in associated values into Equation 28 to form a 2,000 X 2,000 matrix and then rechecked with a 10,000 X 10,000 grid (terminating at ny=2000+1/10,000+1). In both grids each accepted individual value must pass a ratio test that checks to see if the odd value summation has stopped changing. This ratio expects that $\left| \frac{\sum_{n=1,3,5...n}^{EQ} EQ}{\sum_{n=1,3,5...n-2}^{EQ} EQ} \right|$ is less than 0.0001 and runs the odd summations until this conditions is met.

Note: there is a very small difference between the answers obtained from the two resolutions, such that a much higher resolution must be needed to get a perfect answer of **u_{ave} = 0.5 cm/s**

Script #3 - Velocity Profile Generator

```

clear all
close all
clc

%coordinate system
z=0; %describing the change in width
y=0; %describing the change in height
%as such x is describing the change in length

%chamber dimensions in m

width=100*10^-4; %um -> cm
height=80*10^-4; %um -> cm
channel_length=4*10^-1; %mm -> cm

a=width/2;
b=height/2;

%fluid properties
visc=3.12*10^-3; %viscosity (Pa*s)
dp=261.1; %analytical change in pressure (Pa)
dpdx=dp/channel_length; %dp/dx

%setup for calculations
n=1; %odd integer counter
nz=1; %z counter
ny=1; %y counter
step=2000; %step size

flag=1;
while flag==1

    if n==1
        epsilon(n)=((-1)^( (n-1)/2)/n^3)*(1-
cosh(n*pi*y/(2*a))/(cosh(n*pi*b/(2*a))))*cos(n*pi*z/(2*a));
        sepsilon(n)=epsilon(n);
    end

    n=n+2;
    epsilon(n)=((-1)^( (n-1)/2)/n^3)*(1-
cosh(n*pi*y/(2*a))/(cosh(n*pi*b/(2*a))))*cos(n*pi*z/(2*a));
    sepsilon(n)=sepsilon(n-2)+epsilon(n);
    ratio=sepsilon(n)/sepsilon(n-2);

    if ratio > .9999 && ratio <1.0001
        u_z(nz)=16*a^2/(visc*pi^3)*dpdx*sepsilon(n);
        zvalue(nz)=z;
        nz=nz+1;
        z=z+a/step;
        n=1;
        if z > a
            display('z values calculated')
        end
    end
end

```

```

        flag=0;
    end
end
end

%reset z value
z=0;

flag2=1;
while flag2==1

    if n==1
        epsilon2(n)=((-1)^(n-1)/2)/n^3*(1-
cosh(n*pi*y/(2*a))/(cosh(n*pi*b/(2*a))))*cos(n*pi*z/(2*a));
        sepsilon2(n)=epsilon2(n);
    end

    n=n+2;
    epsilon2(n)=((-1)^(n-1)/2)/n^3*(1-
cosh(n*pi*y/(2*a))/(cosh(n*pi*b/(2*a))))*cos(n*pi*z/(2*a));
    sepsilon2(n)=sepsilon2(n-2)+epsilon2(n);
    ratio=sepsilon2(n)/sepsilon2(n-2);

    if ratio > .9999 && ratio <1.0001
        u_y(ny)=16*a^2/(visc*pi^3)*dpx*sepsilon2(n);
        yvalue(ny)=y;
        ny=ny+1;
        y=y+b/step;
        n=1;
        if y > b
            display('y values calculated')
            flag2=0;
        end
    end
end

%reset y value
y=0;

%one symmetrical line
%because I may have slight OCD

% uzflip=fliplr(u_z);
% uyflip=fliplr(u_y);
% zvalflip=fliplr(zvalue);
% yvalflip=fliplr(yvalue);

uz=[fliplr(u_z) (u_z)];
uy=[fliplr(u_y) (u_y)];
zval=[-fliplr(zvalue) zvalue];
yval=[-fliplr(yvalue) yvalue];

plot(zval,uz)
hold on
plot(yval,uy)

```

```

%title('theoretical velocity profile in a rectangular chamber')
legend('z axis (width)', 'y axis (height)')
xlabel('distance from the center (cm)')
ylabel('velocity (cm/s)')

```

```

%Verification Step

```

```

display(round(min(u_z),10))
display(round(min(u_y),10))
%reasonable rounding to account for floating point phenomena

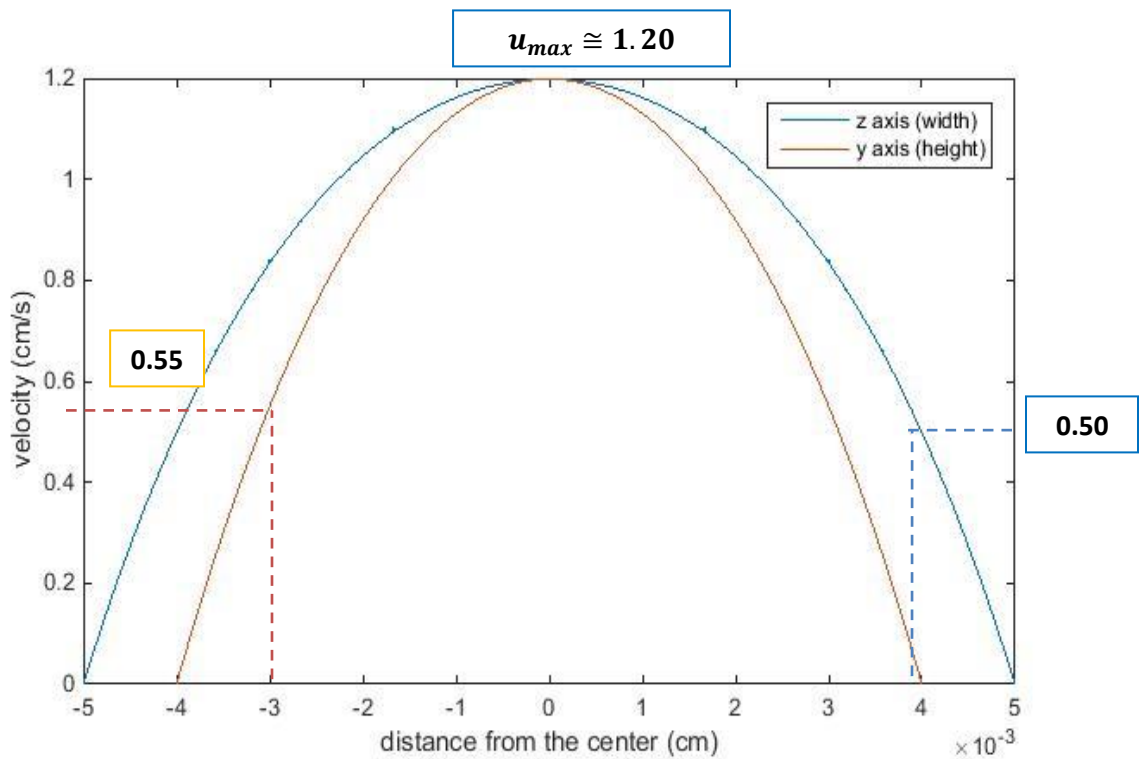
```

```

display(max(u_z))
display(max(u_y))

```

Outputs :



Command Window	Command Window
z values calculated	ans =
y values calculated	1.1986
ans =	
0	
ans =	ans =
0	1.1986
<code>fx</code>	<code>fx >></code>

Note: The velocity profile here can be compared to Appendix I. There are slight, but noticeable

APPENDIX O: TABLE OF USEFUL VALUES

Results of CFD Study of 0.3 mL/min Flow Rate in a Prototype Lamina						
	<i>Maximum</i>		<i>Minimum</i>		<i>Average</i>	
Velocity (cm/s)	1.0537 Center of flow		0 At Walls, No-slip		0.493	
Shear Rate (s ⁻¹)	797 Channel Bifurcation Edge		≅0 Center of flow		249.54	
Shear Stress (Pa)	H ¹ =45% 2.48	H=65% 4.14	0		H=45% 0.779	H=65% 1.30
Shear Stress (Torr)	H=45% 0.0186	H=65% 0.0311	0		H=45% 0.00584	H=65% .00975

Hemolysis Values for 0.3 mL/min Flow Rate								
		<i>Average Shear</i> 0.779 Pa		<i>Highest Normal</i> 1.64 Pa		<i>Max Shear</i> 2.49 Pa		<i>CDL Inflated Shear</i> 2.99 Pa
		H=45%	H=65%	H=45%	H=65%	H=45%	H=65%	H=All
Total Percent Hemolysis	RBC	0.148%	0.0511%	0.0896%	0.308%	0.246%	0.836%	0.382%
	Platelet	0.00122%	0.00591%	0.0121%	0.0581%	0.0436%	0.207%	0.0765%
Percent of Critical Threshold	RBC	2.08%	3.47%	4.38%	7.30%	6.65%	11.1%	7.99%
	Platelet	3.56%	5.92%	7.49%	12.5%	11.4%	18.9%	13.7%
Critical Residence Time	Platelet	39.8 hrs	9.57 hrs	4.99 hrs	1.20 hrs	93.4 min	22.5 min	56.1 min

¹ H refers to hematocrit, which affects the apparent viscosity of blood, which in turn increases the fluidic shear stresses.

Flow Rate Parametric Sweep Results

Flow Rate	Entrance Length (μm)	$\frac{L_e}{L_c}$ Percent	RBC Lysis Percent	Platelet Lysis Percent	Max Shear Stress (Pa)	RBC critical shear stress threshold (Pa)	Platelet critical shear stress threshold (Pa)
1X: 0.3 mL/min	8.05	0.201	0.0148 %	0.00122 %	2.49	37.4	21.9
2X: 0.6 mL/min	16.1	0.403	0.0459 %	0.00605 %	4.97	47.3	28.1
4X: 1.2 mL/min	32.2	0.805	0.142%	0.0299%	9.94	59.7	36.0
20X: 6 mL/min	161	4.01	1.96%	1.22%	49.7	103	64.2
50X: 15 mL/min	402.5	10.1	8.75%	10.1%	124	140	89.1
100X: 30 mL/min	805	20.1	27.1%	49.9%	249	177	114

